MECHANICS-BASED CONTROL OF UNDERACTUATED ROBOTIC WALKING

A Dissertation
Presented to
The Academic Faculty

By

Matthew J. Powell

In Partial Fulfillment
of the Requirements for the Degree
Doctor of Philosophy in the
School of Mechanical Engineering

Georgia Institute of Technology

August 2017

MECHANICS-BASED CONTROL OF UNDERACTUATED ROBOTIC WALKING

Approved by:

Dr. Aaron D. Ames, Advisor
School of Mechanical Engineering
Georgia Institute of Technology

Dr. Daniel Goldman
School of Physics
Georgia Institute of Technology

Dr. Jonathan Rogers
School of Mechanical Engineering
Georgia Institute of Technology

Dr. Patricio A. Vela
School of Electrical and Computer Engineering
Georgia Institute of Technology

Dr. Aaron Young
School of Mechanical Engineering
Georgia Institute of Technology

Date Approved: June 30, 2017

To my Mom and Dad, and brothers Stu and Jason.

TABLE OF CONTENTS

LIST OF TABLES

LIST OF FIGURES

SUMMARY

The proposed research philosophy is to expose the general mechanics of a particular class of bipedal walking robots and then construct controllers which manipulate these mechanics to achieve stable walking. The class of robots is characterized a lack of feet – the robot's lower leg contacts the ground at a single, unactuated pivot point. Stabilizing this type of robot walking can be challenging: underactuation corresponds to nonlinear dynamics that are not affected by the robot's motors and thus not locally controllable. To date, successful methods of stabilizing these robots have leveraged mathematical properties of hybrid walking models to construct nonlinear optimization problems which solve for stable walking gaits. This dissertation builds upon the hybrid control system approaches by illuminating useful properties of the hybrid mechanics of underactuated walking – namely that the underactuated dynamics correspond to the angular momentum about the support pivot and that angular momentum is conserved about the points of impact between the robot and the ground – which can be manipulated to produce stabilizing controllers without use of nonlinear optimization. The Mechanics-Based Control method is implemented in simulation of a planar five-link biped model and is used to design gaits that are implemented in experiments with the AMBER 3M robot. Extensions of the method provide means of stabilizing more complex legged locomotion behaviors in simulation, such as: underactuated 3D robotic walking and planar footed walking under Zero-Moment Point constraints.

CHAPTER 1
INTRODUCTION

To realize the full potential of humanoids robots as valuable tools for the general public, contemporary research is aimed at developing controllers that achieve unassisted walking in unstructured environments. Indeed, a major reason most humanoids robots have not yet been employed to do useful work in society is that making a bipedal machine walk is a difficult task for the current state-of-the-art. Managing the challenges of walking – e.g. intermittent contact between the robot and the ground, transitions between support and swing legs, locally uncontrollable dynamics, actuator power limits, gait efficiency and energy storage, state estimation and sensor fusion – requires tools and methods beyond those provided by the standard continuous-time control literature. This Dissertation focuses on two challenging aspects of locomotion: underactuated dynamics and hybrid state evolution.

Humanoid robots are inherently underactuated: as mechanical systems, these machines have more generalized degrees of freedom than actuated joints. Control can be used to drive humanoids into fully-actuated or over-actuated modes wherein one or both feet sustain planar contact with the walking surface; however, failure of the control system to satisfy dynamic constraints required to maintain these contact conditions results in phases of underactuation and often leads to a fall. A conjecture of this work is that understanding how to stabilize locomotion through phases of underactuation is key to the development of a method that is robust to external disturbances, unstructured terrain and limitations in local controller performance. To study the problem of underactuation, and as is common in the literature, this dissertation considers robots that do not have feet and are therefore always underactuated during phases of single support. The goal is to study and manipulate the mechanics of underactuated walking for this simple system as a step towards understanding and manipulating the general mechanics of legged locomotion.

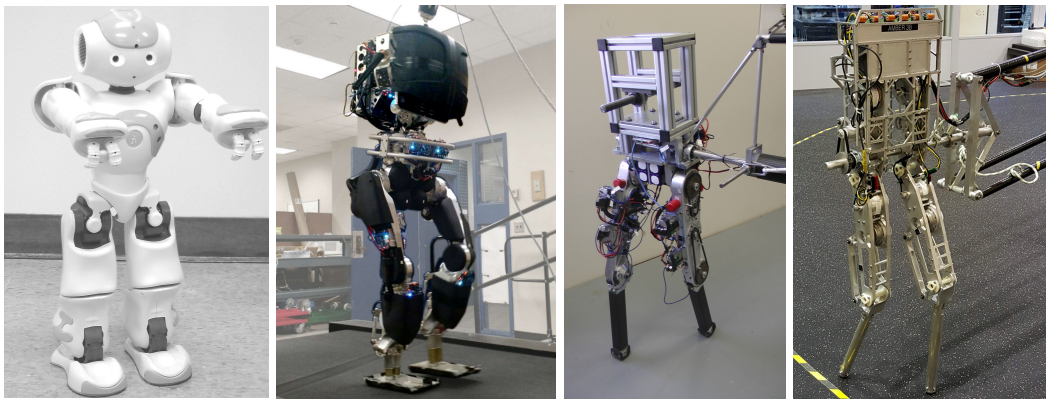

Figure 1.1: (From Left to Right) The humanoid robots NAO and DURUS [39], and the underactuated, point-foot bipeds Proxi and AMBER 3M

1.1 Mechanics-Based Control

Figure 1.1 shows the humanoid robots NAO and DURUS – which have feet and many degrees of freedom – and the bipeds Proxi and AMBER 3 – which do not have feet and have less degrees of freedom. As mentioned, the proposed approach is to study and develop controllers for underactuated walking in the context of the simpler bipeds and then, in future research, translate the lessons learned to more complex humanoid robots.

The five-link, underactuated robot bipeds Proxi and AMBER 3 are characterized by a lack of feet: the robot's lower leg contacts the ground at a single, unactuated point. Achieving stable walking via control of this system is not just a matter of placing one foot in front of the other; the passive interface between the robot and the ground corresponds to one mode of the system that is uncontrollable in continuous-time and impacts between the robot and the ground impart discrete changes in the robot's velocity. To date, successful methods of stabilizing this class of walking robots have leveraged mathematical properties of robot models to construct nonlinear optimization problems which solve for stable gaits, see for example [4, 33, 74, 97]. This Dissertation presents a novel approach built upon the mechanics of underactuated robotic walking – augmented with nonlinear control design – to produce controllers without use of offline gait optimization.

The proposed mechanics-based control approach focuses on the stabilization of the evolution of the angular momentum about the robot's support pivot; this quantity accounts for one of the five degrees of freedom in the planar underactuated biped considered. However, the rate of change of angular momentum about the support pivot in underactuated walking is influenced only by gravity. The robot's actuators can work to manipulate the effect of gravity by modifying the robot's shape and thereby changing the moment-arm by which gravity operates; but the actuators cannot affect the instantaneous rate of change of angular momentum (in mathematical terms, the angular momentum about the support pivot is one of the zero dynamics coordinates [97]). To keep the angular momentum from blowing up and causing instability, the proposed control approach operates on the transfer of angular momentum associated with stepping.

The conjecture of this work is that part of the fundamental mechanics of stable underactuated walking is the stabilization of the transfer of angular momentum from one leg to the next. Indeed, one mathematical criterion for stable walking via Hybrid Zero Dynamics is that the fixed point of the Poincaré map for the HZD of a given continuous-time controller must be exponentially stable (see Theorem 3 of [97]). This statement, together with the fact that part of the zero dynamics of underactuated walking is the rate of change of angular momentum about the support pivot, suggests that walking might be stabilized through regulation of angular momentum in discrete-time. Rather than first constructing parameterized continuous-time controllers and then using optimization to solve for parameters that result in a stable hybrid zero dynamics – as is done in the HZD-based approaches – the present method seeks to directly stabilize the discrete-time angular momentum by manipulating the kinematics of the robot at impact. In particular, the transfer of angular momentum from one leg to the next can be computed exactly as a function of the robot's swing leg position and center of mass velocity. This motivates the design of continuous-time desired trajectories for the swing leg and the vertical center of mass which have endpoints corresponding to a desired transfer of momentum.

The specific choice of desired transfer of angular momentum is obtained through use of the Linear Inverted Pendulum (LIP) model [49], a widely used concept in the contemporary robotic walking community. One of the most successful walking controllers that employs the LIP, the Capture Point [81] method uses the phase space of the LIP to suggest stepping strategies which ensure that the robot is capable of taking another step or stopping. As the LIP is traditionally used in impact-less robot models, the current paper makes modifications to the typical LIP in order to use it for the nonlinear, hybrid model of interest. In particular, the LIP is used in the present paper to predict the evolution of the angular momentum about the support pivot – instead of predicting the center of mass velocity. Consequently, conservation of angular momentum properties of the nonlinear impact model can be used to incorporate (exact) discrete-time effects in this angular momentum variant of the LIP, and thus capture the hybrid nature of the model of interest.

The proposed gait design philosophy is to expose the general mechanics of underactuated walking and then build controllers to manipulate these mechanics. This approach is just one of many usages of Classical Mechanics [30, 62], which has played a large role in the development of several humanoid walking control principles and strategies to-date. The Zero Moment Point concept uses the relationship between the center of mass acceleration and the reaction forces acting on footed robots to establish foot-rotation-stability criteria [95]. Assumptions on the mechanics of the system can be used to reduce the nonlinear rigid-body dynamics into more tractable systems such as the Linear Inverted Pendulum [48], which has seen tremendous success in walking control design [81, 91]. And adding angular momentum feedback to HZD-based virtual constraint optimization results in increased robustness to perturbations in the walking surface [32]. The current paper intends to add to the existing walking mechanics literature by illuminating useful properties of the *hybrid mechanics of underactuated walking*.

1.2 Dissertation Overview

This section provides a brief description of the contents of each chapter in the Dissertation.

Chapter 2: Mechanics-Based Control and the Robotic Walking Literature. This chapter discusses the relationship between Mechanics-Based Control and the greater bipedal robotic walking literature. The constructions in Mechanics-Based Control leverage elements from both the hybrid systems community and from Linear Inverted Pendulum-based walking methods.

Chapter 3: Underactuated Walking Mechanics. This chapter highlights notable properties of the Mechanics of the rigid-body model used to describe underactuated robotic walking. It focuses primarily on the underactuated, planar five-link biped robot which has five degrees of freedom, but only four actuators. The robot is characterized by a lack of feet: its lower leg contacts the ground and rotates freely about a single pivot point. Newton's second law dictates that the instantaneous rate of change of angular momentum about the support pivot is unaffected by the robot's actuators and influenced only by gravity acting at the robot's center of mass. Thus, managing the hybrid evolution of the angular momentum about the support pivot is key to stabilizing underactuated walking.

Chapter 4: Continuous-Time Control. Mechanics-Based Control is a method of embedding constraints needed for stable walking within the design of continuous-time outputs. This chapter presents the construction of the control system for the robot and outlines nonlinear control tools that are used to exponentially stabilize the outputs developed in Mechanics-Based Control.

Chapter 5: Hybrid Systems. Walking consists of intermittent collisions between the robot and the world, and the tools of hybrid systems are useful in modeling this interaction. This dissertation models walking as a hybrid system, as is common in the literature [97]. In this context, walking gaits correspond to periodic solutions of the hybrid system model. The stability of a walking gait corresponds to the stability of a hybrid periodic orbit, which

is often established through Poincaré methods. At the intersection of hybrid systems and control, an extension of the notion of zero dynamics is the Hybrid Zero Dynamics[97], wherein controller outputs are designed to be invariant not only in continuous-time, but also invariant through the reset map of the hybrid system. As in the continuous-time case, the hybrid zero dynamics is a reduced dimensional system. Stability of walking gaits – i.e. periodic orbits in the full-dimensional hybrid system – can be analyzed through analysis of the hybrid zero dynamics.

Chapter 6: Hybrid Walking Mechanics. The main design philosophy of Mechanics-Based Control is to expose the general mechanics of underactuated robotic walking and to build controllers to manipulate these mechanics. This chapter illuminates properties of the general mechanics of underactuated walking – termed the *Hybrid Walking Mechanics* – which emerge from the intersection of Classical Mechanics, Nonlinear Control, and Hybrid Systems. The structure of the resulting hybrid system motivates a novel feedback mechanism for stabilizing walking: regulating the transfer of angular momentum about one support pivot to the next through manipulation of the robot's controllable kinematics.

Chapter 7: Mechanics-Based Control of Planar Underactuated Walking. This chapters outlines the main elements of Mechanics-Based Control and describes how these elements contribute to stable walking. The elements of Mechanics-Based Control are motivated by insights gained from the Hybrid Walking Mechanics, discussed in Chapter 6. In particular, the key contribution of Mechanics-Based Control is a novel mechanism for stabilizing walking gaits – regulating the transfer of angular momentum from one step to the next – which provides a means of creating stable hybrid periodic orbits *by construction*. Mechanics-Based Control is implemented in the form of continuous-time outputs which simultaneously encode a desired continuous-time walking behavior while also encoding a desired discrete-time evolution of the locally uncontrollable modes of the system.

Chapter 8: Mechanics-Based Control Implementation and Extensions. This chapter presents results from experimental implementation of Mechanics-Based Control princi-

ples on the underactuated planar biped AMBER 3M and shows how MBC can be extended to: torque constrained 3D underactuated walking, and planar footed walking under Zero-Moment Point constraints required for balance.

1.3 Contributions

The following four items highlight the primary contributions of this Dissertation.

1. **Structure in the Hybrid Walking Mechanics.** This Dissertation illuminates new properties of underactuated robotic walking that lie at the intersection of Classical Mechanics, Nonlinear Control and Hybrid Systems.

2. **Novel Feedback Mechanism for Stabilizing Underactuated Walking.** In this Dissertation, it is shown that hybrid models of underactuated walking can be stabilized into periodic gaits by regulating the transfer of angular momentum about one support pivot to the next.

3. **Mechanics-Based Control.** This Dissertation presents a method of directly implementing the proposed angular momentum transfer feedback mechanism on the five-link underactuated biped through design of continuous-time outputs. Stabilization of these outputs via standard nonlinear control drives the robot into a stable gait.

4. **Applications and Extensions.** The Mechanics-Based Control philosophy and principles are applied to: experimental underactuated walking in the AMBER 3M robot, 3D underactuated walking under torque constraints, and planar footed walking under Zero-Moment Point constraints.

CHAPTER 2
MECHANICS-BASED CONTROL AND THE ROBOTIC WALKING LITERATURE

Bipedal robotic walking is an extensive field of research; there are nearly as many different walking control methods as there are robots and researchers. Many excellent resources provide an overview the field of robotic walking as a whole, such as [16, 35, 36, 99]. This Chapter focuses on concepts from the literature that motivated Mechanics-Based Control.

2.1 Robot Walking Models

For the purposes of simulation, walking robots are typically modeled as articulated rigid bodies and can be described through kinematics and dynamics calculated via standard methods [26, 69, 89]. In this context, walking models are often delineated by the choice of impact model. Employing rigid-body collisions models, as in [47, 92], results in a hybrid dynamical system model of walking [34, 37]. On the other hand, methods that model the ground as a compliant surface, such as [9], result in a continuous-time model of walking.

For the purposes of control, there is an abundance of "internal models" and "virtual models" used in robot walking controllers [82]. Rigid-body dynamics models describing walking robots are often high-dimensional nonlinear systems whose behavior can only be ascertained through numeric integration. As such, many control methods employ low-dimensional (and sometimes linear) models, or "templates", which attempt to characterize the aggregate behavior of legged locomotion [27]. One of the most widely used models of walking in the contemporary robotics community is the Linear-Inverted Pendulum (LIP) model [49, 50]. The LIP model is obtained through two constraining assumptions: a constant height of the center of mass and zero centroidal angular momentum. Under these conditions, the robot's horizontal and lateral center of mass dynamics become linear and thus,

the tools of linear systems can be used to obtain exact expressions for the modeled robot's behavior. One of the most successful walking controllers that employs the LIP, the Capture Point [81] method uses the phase space of the LIP to suggest stepping strategies which ensure that the robot is capable of taking another step or stopping. Indeed, expressing the COM dynamics as a linear system provides an excellent starting point for the development of many different walking control methods [51, 48, 55, 91]. This Dissertation proposes modifications to the traditional LIP to characterize the evolution of uncontrollable modes – namely the forward center of mass position and angular momentum about the support pivot – in a full-dimensional, nonlinear hybrid model of underactuated walking.

The Spring Loaded Inverted Pendulum (SLIP) [13] is another widely-used model that was developed in the biomechanics community as its solutions correlate with experimental human walking data [29] and it can be used to predict force data in running birds [12]. In the SLIP model, the robot's center of mass dynamics are modeled as if attached to the ground via a massless spring. Stability of SLIP gaits are regulated through control over the angle of the swing leg at the point of impact [94]. As the legs are massless in the SLIP model, the touchdown angle acts as control input in the system. One of the most-successful implementations of SLIP-based control to-date is the unsupported, 3D walking obtained on the ATRIAS robot [46]. Additional implementations of SLIP-based control of legged locomotion include [20, 28, 41, 43, 59, 60, 75, 94].

In addition to these low-dimensional templates used as virtual models for robots, another subset of the legged locomotion community – and the Mechanics-Based Control method presented in this Dissertation – uses the full-dimensional nonlinear rigid-body dynamics in the development of walking controllers. Humanoid robots often have a relatively high number of degrees of freedom (DOF); one such robot, the DURUS robot, has 23 DOF [39] and the well-known ATLAS robot has 28 actuated DOF [56]. For systems of this size, evaluation of the dynamics requires efficient algorithms, such as Spatial Vector Algebra [26], and controller design often leverages nonlinear programming.

2.2 Notions of Stability

The term "stability" can refer to one of many different definitions throughout contemporary and historical robotics walking literature. Often, the employed notion of stability is based on the choice of representation of walking. Mechanics-Based Control uses the notion of stability in the sense of Poincaré, as extended to hybrid systems in [34], wherein stable walking corresponds to stable periodic orbits in a hybrid system model of walking. A perk of this definition of stability is that it is mathematically rigorous and as such, evaluation of the stability of a walking gait can be conducted using precise statements about well-defined mathematical objects, such as hybrid periodic orbits [6, 34, 65, 97]. Stability of a hybrid periodic orbit can be verified through numeric approximation of the Jacobian of the Poincaré map corresponding to the orbit [73].

Another set of useful, yet philosophically different notions of stability are the velocity-based stability margins described in [83]. The work [83] discusses Capture Regions – regions on the walking surface corresponding to viable step locations. Stepping outside the Capture Region will ultimately lead to the robot falling, however, taking steps within the Capture Region will allow the robot to take another step and continue walking. An advantage of this notion of stability is that Capture Regions leverage a low-dimensional approximation of walking, and as such, Capture Regions for high-dimensional, complex 3D humanoid robots can be computed in real-time. Indeed, the Capture-Point method for controlling locomotion employs this notion of stability and has been shown to work reliably on full-scale humanoid robot hardware, such as [84].

Additional notable notions of stability include: Metastability [15] which considers a stochastic model of the walking surface and characterizes the stability of a walking gait through a metric termed the "mean first-passage time" which encodes the expected number of footsteps the robot will take before falling, the gait sensitivity norm [44] and abstraction-based methods for verification of control systems [8, 93, 100].

2.3 Controlling Walking by Stabilizing Hybrid Periodic Orbits

Mechanics-Based Control stabilizes underactuated walking by regulating the transfer of angular momentum from one support pivot to the next and ultimately drives the robot into a stable hybrid periodic orbit. This novel feedback mechanism for stabilizing walking was motivated by a mechanics-based interpretation of existing hybrid walking techniques. The seminal work [34] establishes stability of hybrid periodic orbits under continuous-time control which converges in finite-time. The Hybrid Zero Dynamics framework [97] establishes asymptotically stable hybrid periodic orbits through construction of periodic orbits in a reduced dimensional hybrid system termed the hybrid zero dynamics. Exponential stability was shown in [65]. Also in [65] is the construction of restricted Poincaré map that can be used to determine stability of the full dimensional model. Perhaps a more general proof of stability is presented via use of rapidly exponentially stabilizing control Lyapunov functions (RES-CLFs) in [5, 6]. This motivated the design of a new type of stabilizing controller which uses RES-CLFs to shape the energy of the system to be that of the energy of a desired hybrid periodic orbit [87]. One of the main results in hybrid underactuated walking gait design is that the stability of a walking gait can be determined through stability of the hybrid evolution of the locally uncontrollable modes [34, 65, 97].

A key to Mechanics-Based Control is the connection between these results and the mechanics of underactuated walking. In particular, one of the components of the zero dynamics in underactuated walking is the angular momentum about the support pivot. Using this interpretation, the main theorem of [97] ultimately states the stability of a walking gait in the underactuated biped of interest is related to the stability of the hybrid evolution of the angular momentum about the robot's support pivot. As shown in this Dissertation, properties of the hybrid mechanics of underactauted walking can be used to design a feedback mechanism which stabilizes the hybrid evolution of the angular momentum about the robot's support pivot and thereby drives the system into a stable hybrid periodic orbit.

2.4 Designing Stable Walking Gaits With Nonlinear Programming

Stabilizing underactuated robotic walking has historically required use of nonlinear programming to search for stable hybrid periodic orbits. The recent method of Symmetric Virtual Constraints [85] provides a means of producing stable hybrid periodic orbits without requiring nonlinear programming. One benefit of the proposed Mechanics-Based Control approach to underactuated walking is that it too does not require solution of a nonlinear program. Practically, this saves time in the design and implementation of gaits. Even more important is the fact that, rather than relying on a nonlinear program to search for stabilizing conditions, Mechanics-Based Control encodes stability *by construction* through understanding of the hybrid walking mechanics.

When successful, nonlinear programming is a powerful tool for designing complex and efficient walking gaits and general robot behaviors, as in [21, 22, 96]. Optimization is widely used in contemporary robot walking gait design [52, 68, 74, 78, 80]. Indeed, the Hybrid Zero Dynamics method capable of stabilizing full-dimensional hybrid models of underactuated walking is ultimately implemented through optimization [18, 32, 33, 63, 66, 75, 90]. Extensions of these HZD-based optimization approaches improve robustness through modifications of desired basis functions [14, 32, 38]. Human-Inspired Control builds upon HZD stability guarantees to produce some of the most efficient walking to-date [4, 88]. Recent work has significantly improved the convergence and speed of Human-Inspired Control based optimizations and in doing so, allowed for construction of walking gaits for higher-dimensional, more complex humanoids [39, 40, 42].

One challenge with nonlinear-programming approaches to walking controller design is that conditions required for stability are resolved by an algorithm (which is not guaranteed to converge). The goal of Mechanics-Based Control is to augment the literature by illuminating properties of underactuated mechanics that can be used to design a feedback mechanism for stabilizing underactuated walking directly.

2.5 Controlling Walking through Step Length Regulation

Mechanics-Based Control regulates the transfer of angular momentum from one step to the next through manipulation of the robot's step length and vertical center of mass velocity prior to impact. In the literature, controlling walking through step length regulation is a strategy that has produced numerous experimental walking results. The simple strategies outlined in [45] led to the controller development for PETMAN [70]. As mentioned, at its core the widely-successful Capture-Point method [23, 24, 54, 81] is a means of controlling walking through step length regulation. At a high-level, the length of a step can be adjusted based on a desired change in walking speed; for a fixed walking frequency, longer strides correspond to a decrease in speed while shorter strides provide an increase in walking speed. Moreover, step-length control strategies are often paired with low-dimensional template models, such as the Linear Inverted Pendulum, and therefore do not require as much computation as those controllers which employ the full rigid-body dynamics.

2.6 Controlling Underactuated Walking

This Dissertation focuses on the challenge of stabilizing underactuated walking. In the literature, the Hybrid Zero Dynamics framework [18, 97] is one approach to addressing this challenge. A recent modification [32] of the HZD-based nonlinear programming approach uses nonholonomic [10] virtual constraints – wherein desired functions depend on the angular momentum about the robot's support pivot – to improve robustness of the optimized controller to variations in ground height. Indeed, as mentioned in [17], one component of the underactuated dynamics is the rate of change of angular momentum about the robot's support pivot. The primary contribution of this Dissertation shows how additional properties from Classical Mechanics [30, 62] can be used to directly manipulate the angular momentum to achieve stable underactuated walking.

CHAPTER 3
UNDERACTUATED WALKING MECHANICS

Development of a humanoid robot is an interdisciplinary task: building a walking machine requires tools from electrical, mechanical and computer engineering and designing a control system for the robot draws on even more fields of knowledge. Achieving successful walking with these robots requires harmony across the interdisciplinary components of the machine. Whereas existing motor driver technology is capable of reliably producing desired joint torques and robot operating systems are able to meet strict real-time computation requirements, the challenge of manipulating the general mechanics of locomotion is largely an open problem. Indeed, the failure modes of locomotion – such as loss of balance and falling down – are ultimately described using metrics on the system at a mechanical level. Within the challenge of addressing these failure modes, however, lies information about potential avenues toward a solution: illuminate and exploit useful properties of the mechanics of the system. This Dissertation focuses on the challenge of stabilizing robot locomotion during phases of underactuation, and the main contribution, Mechanics-Based Control, leverages properties of the underlying mechanics to stabilize underactuated walking via a novel feedback mechanism: angular momentum transfer.

As common throughout the literature, this Dissertation models robots as articulated rigid bodies comprised of rigid links that are connected via actuated revolute joints. Choosing this representation endows the overall robot control system with properties of Classical Mechanics. For example, the equations of motion of the robot are obtained through computation of the rigid-body dynamics and correspond to an affine nonlinear control system. This chapter discusses additional properties of the mechanics of walking which contribute to the overall structure of the system and which will be exploited in the development of Mechanics-Based Control.

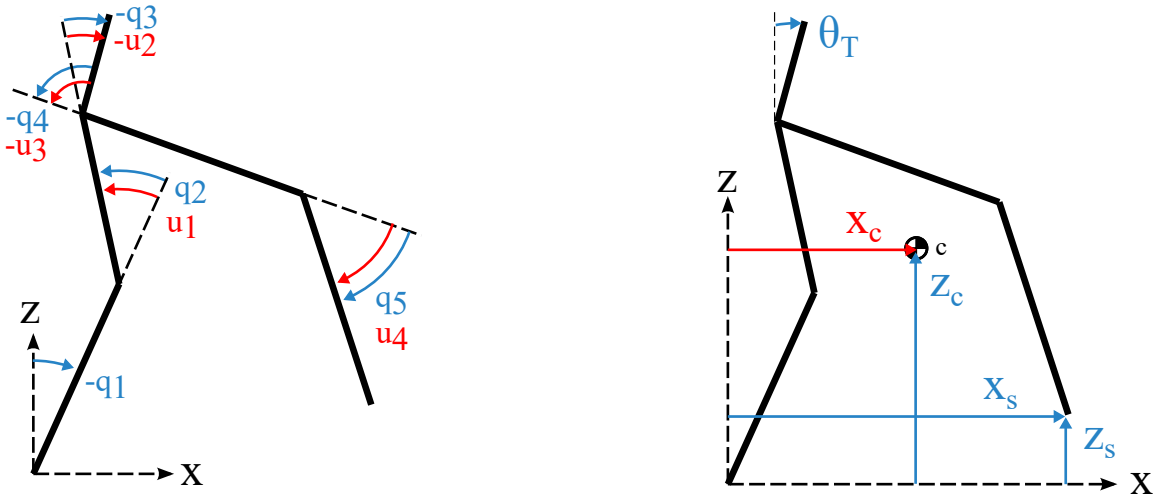

Figure 3.1: (Left) Coordinate conventions for the planar, five-link underactuated biped and (Right) notable kinematic quantities used in this Dissertation

3.1 Articulated Rigid-Body Model: Coordinates and Notation

The robot of interest in this paper is the planar, five-link biped shown in Figure 3.1, which has five degrees of freedom but only four actuators located at the robot's knee and hip joints. As the robot has more degrees of freedom than actuators, it is deemed "underactuated". In this model, the robot's links are treated as rigid bodies and the actuators are modeled as ideal torque sources (with infinite torque bandwidth and zero friction). It is also assumed that sufficient friction prevents the support leg from sliding on the ground and from rotating about the axis perpendicular to the ground (the z axis), and in the context of planar walking, the rotation about the forward axis, the x axis, is also fixed. One unactuated rotation, $\mathbf{q_u} = q_1$, is used to describe the rotation of the support calf about the world y axis; and four relative (intrinsic) rotations, $\mathbf{q_a} = (q_2, q_3, q_4, q_5)^T$, are used to describe the actuated joint angles, which are acted upon by joint torques $\mathbf{u} = (u_1, u_2, u_3, u_4)^T$, in order. The collection of unactuated and actuated angles will often be referred to as a single, "joint angle" vector $\mathbf{q} = (q_1, q_2, \ldots, q_5)^T$. A set of generalized or "extended" coordinates $\mathbf{q_e} = (\mathbf{p_b}^T, \mathbf{q}^T)^T$ is used to construct the collision model for this robot, wherein $\mathbf{p_b} = (x_b, z_b)$ describes the position of the robot's support pivot relative to a fixed world frame.

3.2 Kinematics

The drawing in the right half of Figure 3.1 shows the five components of the robot's kinematics that are used in this Dissertation. As the robot is underactuated, only four of these five quantities can be controlled at any given point in time. Mechanics-Based Control dictates a method of controlling the kinematic functions shown in blue in Figure 3.1 while the quantity shown in red is left uncontrolled in continuous-time. This section defines the notation for – and describes the usage of – each kinematic quantity in the context of the robot model and how each contributes to stable walking via Mechanics-Based Control.

3.2.1 Center of Mass Position

Perhaps the most widely analyzed and manipulated kinematic quantity in the robotics walking community is the robot's center of mass (COM). Let x_c and z_c denote the horizontal and vertical components of the COM relative to the support pivot, and therefore let $\mathbf{p}_c(\mathbf{q})$ denote the position of the robot's center of mass relative to its support pivot in the plane

$$\mathbf{p}_c(\mathbf{q}) := \begin{bmatrix} x_c(\mathbf{q}) \\ z_c(\mathbf{q}) \end{bmatrix}. \tag{3.1}$$

As mentioned, in Mechanics-Based Control the uncontrolled coordinate during underactuated walking is chosen to be the robot's forward component of the center of mass x_c. The vertical component of the COM, z_c, is a crucial component of the proposed control framework: it is used to manipulate the transfer of angular momentum from one support pivot to the next. Indeed, controlling the vertical component of the robot's COM is a common choice made throughout the literature. Driving the COM height to a constant value results in the well-known Linear Inverted Pendulum model [49]; however, studies on human walking data suggest that non-constant COM height can improve efficiency [72]. Alternative strategies use the vertical COM to control balance in humanoid robots [23, 53, 57].

3.2.2 Swing Foot Position

Managing the position of the swing foot – either explicitly or implicitly – is another major aspect of walking control design. Here, let x_s and z_s denote the horizontal and vertical components of swing foot relative to the support pivot, yielding the vector $\mathbf{p}_s$

$$\mathbf{p}_s(\mathbf{q}) := \begin{bmatrix} x_s(\mathbf{q}) \\ z_s(\mathbf{q}) \end{bmatrix}. \tag{3.2}$$

The height of the swing foot above the walking surface characterizes the domain and guard of the hybrid system model of walking presented in Chapter 5. Moreover, Mechanics-Based Control prescribes a method of controlling the height of the swing foot so that impact events occur when uncontrolled states reach desired values.

As discussed in Section 2.5, controlling the robot's step length is a widely used strategy for stabilizing walking. In Mechanics-Based Control, the step length is used to manipulate the post-impact value of one the uncontrolled states – the robot's center of mass position relative to its support pivot – and thereby ensure the hybrid evolution of this state is well-behaved. Among additional strategies, Capture Point [81] is one of the most successful and widely used step-length control method.

3.2.3 Torso Orientation

The final quantity of interest is the orientation of the torso with respect to the world, $\theta_T(\mathbf{q})$, which (because the robot model is planar) can be expressed as the sum

$$\theta_T(\mathbf{q}) := -q_1 - q_2 - q_3. \tag{3.3}$$

In Mechanics-Based Control, this kinematic quantity does not directly contribute to the stability of walking. Instead, the goal is often to drive the torso to an upright configuration to produce "aesthetically normal" walking.

3.2.4 Support and Swing Foot Jacobians

Jacobians of the support and the swing foot are used to construct the equations of motion and impact model used to describe the robot's motion. In particular, the Jacobian, J_b, of the position of the support pivot, $\mathbf{p_b}$, computed using the generalized coordinates, $\mathbf{q_e}$, is given by the partial derivative

$$J_b := \frac{\partial \mathbf{p_b}}{\partial \mathbf{q_e}}. \tag{3.4}$$

One modeling assumption is that the robot's support pivot remains at a fixed position throughout the continuous-time evolution of a single step. This condition can be expressed as a holonomic constraint [36, 69]

$$\dot{\mathbf{p}}_\mathbf{b} = J_b(\mathbf{q_e})\dot{\mathbf{q}}_\mathbf{e} = 0. \tag{3.5}$$

The time-derivative of (3.5) produces a constraint on the robots dynamics

$$J_b(\mathbf{q_e})\ddot{\mathbf{q}}_\mathbf{e} + \dot{J}_b(\mathbf{q_e}, \dot{\mathbf{q}}_\mathbf{e})\dot{\mathbf{q}}_\mathbf{e} = 0, \tag{3.6}$$

which will be used in the following Section to construct a reduced-dimensional dynamical system representing the robot's motion.

Similarly, the Jacobian, J_s, of the position of the swing foot, $\mathbf{p_s}$, computed using the generalized coordinates, $\mathbf{q_e}$, is given by the partial derivative

$$J_s := \frac{\partial \mathbf{p_s}}{\partial \mathbf{q_e}}. \tag{3.7}$$

As described later in this chapter, the swing foot Jacobian (3.7) is used to construct a collision model wherein the impacting foot has zero velocity after impact (i.e. the foot does not bounce after colliding with the ground).

3.3 Rigid Body Dynamics

Letting T and V denote the kinetic and potential energy of the system, the Euler-Lagrange method [30] can be used to obtain the equations of motion for the robot:

$$\frac{d}{dt}\left(\frac{\partial T}{\partial \dot{\mathbf{p}}_\mathbf{b}}\right) - \frac{\partial (T-V)}{\partial \mathbf{p}_\mathbf{b}} = \mathbf{F}, \tag{3.8}$$

$$\frac{d}{dt}\left(\frac{\partial T}{\partial \dot{\mathbf{q}}_\mathbf{u}}\right) - \frac{\partial (T-V)}{\partial \mathbf{q}_\mathbf{u}} = \mathbf{0}, \tag{3.9}$$

$$\frac{d}{dt}\left(\frac{\partial T}{\partial \dot{\mathbf{q}}_\mathbf{a}}\right) - \frac{\partial (T-V)}{\partial \mathbf{q}_\mathbf{a}} = \mathbf{u}, \tag{3.10}$$

where $\mathbf{F} = (F_x, F_z)^T$ are the reaction forces acting on the robot's support pivot. Expressing the Euler-Lagrange equations in this particular representation illuminates useful information about the robot's motion. A subset of the equations of motion (3.10) is affected by the robot's actuators and thus, can be controlled in continuous-time. The subset of motion (3.8) influenced by the reaction forces $\mathbf{F}$ is fully constrained by the fixed support base assumption. However, a component of the robots motion (3.9) is neither affected by the robot's actuators nor by the reaction forces. Stabilization of these modes during walking requires additional tools beyond continuous-time control. This Dissertation proposes a novel stabilization tool which is built using the underlying mechanics of (3.9).

The equations of motion can be used to construct the manipulator dynamics [69, 89]

$$D(\mathbf{q_e})\ddot{\mathbf{q}}_\mathbf{e} + C(\mathbf{q_e}, \dot{\mathbf{q}}_\mathbf{e})\dot{\mathbf{q}}_\mathbf{e} + G(\mathbf{q_e}) = B\mathbf{u} + J_b^T(\mathbf{q_e})\mathbf{F}, \tag{3.11}$$

with inertia, Coriolis and torque distribution matrices, D, C, and B, and gravity vector G. Imposing the constraint (3.6) on (3.11) results in the reduced-dimensional system

$$D(\mathbf{q})\ddot{\mathbf{q}} + C(\mathbf{q}, \dot{\mathbf{q}})\dot{\mathbf{q}} + G(\mathbf{q}) = B\mathbf{u}, \tag{3.12}$$

This form of the robot dynamics (3.12) is used as the control system for the robot.

3.4 Impact Model and Coordinate Relabeling

Impacts between the robot's swing foot and the ground are modeled using the methods prescribed in [36, 47, 92, 98]. In these models, impact events are treated as instantaneous and the impacting leg does not rebound or slip after collision. Quantities just-prior to impact are referred to as "pre-impact" and denoted $\square^-$, post-impact quantities are denoted $\square^+$. The model for the instantaneous change in velocity due to impact is given by:

$$\begin{bmatrix} D(\mathbf{q}_e^-) & -J_s^T(\mathbf{q}_e^-) \\ J_s(\mathbf{q}_e^-) & 0 \end{bmatrix} \begin{bmatrix} \dot{\mathbf{q}}_e^+ \\ F_{imp} \end{bmatrix} = \begin{bmatrix} D(\mathbf{q}_e^-)\dot{\mathbf{q}}_e^- \\ 0 \end{bmatrix}, \tag{3.13}$$

wherein quantities are computed using the extended coordinates and F_{imp} is the impact force. The impact equations (3.13) express conservation of generalized momentum about the point of impact together with the no-rebound nor slip constraint [98]. Letting

$$P(\mathbf{q}^-) := I - D^{-1}(\mathbf{q}_e^-)J_s^T(\mathbf{q}_e^-)(J_s(\mathbf{q}_e^-)D^{-1}(\mathbf{q}_e^-)J_s^T(\mathbf{q}_e^-))^{-1}J(\mathbf{q}_e^-), \tag{3.14}$$

where here $\mathbf{q}_e^- = (0, 0, \mathbf{q}^-)^T$, the post-impact velocities can be obtained via

$$\dot{\mathbf{q}}^+ = P(\mathbf{q}^-)\dot{\mathbf{q}}^-. \tag{3.15}$$

In the model, the velocities undergo an instantaneous jump in value according to (3.15) but the joint angles remain fixed.

To simplify the description of the system, however, the joint angles and velocities are remapped after each impact event to reflect the swapping of the roles of the legs. Assuming the mass and length distribution of the robot's legs is symmetric, one can reduce the analysis of a walking gait by studying the evolution of the "support" and "swing" legs. After an impact event, the support and swing leg swap roles. This reduces the hybrid system representation of the walking model to a single continuous-time phase (whereas using a

"left and right" convention results in a hybrid model with two continuous-time phases). The combined impact model and coordinate relabeling is

$$\mathbf{q}^+ = R\mathbf{q}^- \tag{3.16}$$

$$\dot{\mathbf{q}}^+ = RP(\mathbf{q}^-)\dot{\mathbf{q}}^-, \tag{3.17}$$

where for the planar underactuated model of interest R is a constant matrix given by

$$R := \begin{bmatrix} -1 & -1 & -1 & 1 & 1 \\ 0 & 0 & 0 & 0 & 1 \\ 0 & 0 & 0 & 1 & 0 \\ 0 & 0 & 1 & 0 & 0 \\ 0 & 1 & 0 & 0 & 0 \end{bmatrix}. \tag{3.18}$$

One property due to the coordinate relabeling is that the post-impact kinematics can be expressed in terms of pre-impact kinematics. This means that the post-impact value of one of the uncontrollable modes, the forward center of mass position, x_c, can be expressed as

$$x_c^+ = x_c^- - x_s^-. \tag{3.19}$$

Mechanics-Based Control use this property of the model to design a controller which manipulate the pre-impact step length, x_s^-, to achieve a desired post-impact COM, x_c^+. As discussed in the following section, the coordinate relabeling can also be used to reason about the hybrid evolution of another uncontrollable mode in the system: the angular momentum about the support pivot. It will be shown that the post-impact angular momentum about the support pivot can be expressed in terms of the robot's controllable kinematics; this key insight from the mechanics of the system provides an avenue for regulating the uncontrollable modes during underactuated walking.

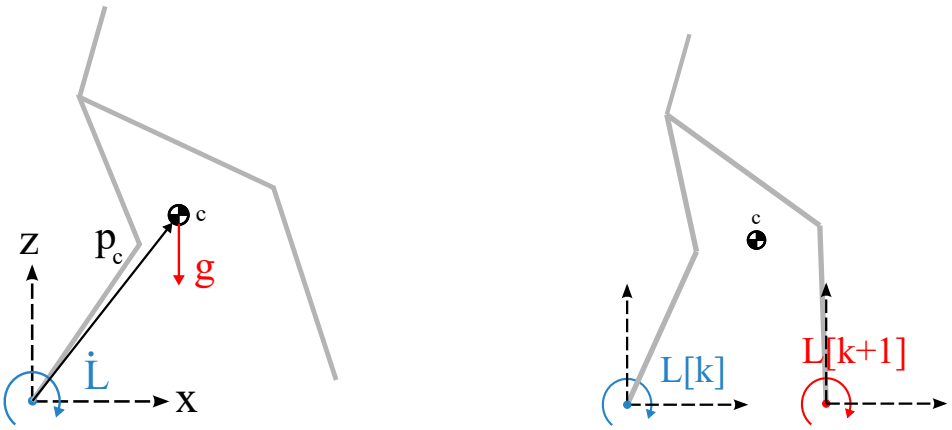

Figure 3.2: Key properties of the articulated rigid-body robot model which Mechanics-Based Control exploits in order to stabilize underactuated walking: (Left) the rate of change of angular momentum about the support pivot is proportional to gravity acting at the robot's COM and (Right) the transfer of angular momentum from one step to the next is a function of the robot's pre-impact kinematics.

3.5 Angular Momentum

The Mechanics-Based Control philosophy is to illuminate characteristics of the mechanics of underactuated walking and to use these insights to design new methods controlling walking. A key component of underactuated mechanics is the (mass-normalized) angular momentum about the support pivot, L, which can be expressed as

$$L = z_c(\mathbf{q})\dot{x}_c(\mathbf{q}, \dot{\mathbf{q}}) - x_c(\mathbf{q})\dot{z}_c(\mathbf{q}, \dot{\mathbf{q}}) + H(\mathbf{q}, \dot{\mathbf{q}}), \tag{3.20}$$

where $H(\mathbf{q}, \dot{\mathbf{q}})$ is the robot's (mass-normalized) centroidal angular momentum [71]. As mentioned, the robot is free to pivot about the support pivot. Application of Newton's second law to this rotation provides the following constraint on the robot's motion:

$$\dot{L} = g x_c(\mathbf{q}). \tag{3.21}$$

Note that (3.21) is equivalent to (3.9). Thus the angular momentum about the robot's support pivot is locally uncontrollable – the instantaneous rate of change of angular momen-

tum about the support pivot is only influenced by gravity. The robot's actuators can work to manipulate the effect of gravity by modifying the robot's shape and thereby changing the moment-arm by which gravity operates; but the actuators cannot affect the instantaneous rate of change of angular momentum (in mathematical terms, the angular momentum about the support pivot is one of the zero dynamics coordinates [97]). To keep the angular momentum from blowing up and causing instability, the Mechanics-Based Control approach operates on the transfer of angular momentum associated with stepping.

3.5.1 Momentum Transfer

When the swing foot impacts the ground, support of the robot transfers from the current support pivot to the point of impact. The corresponding transfer of angular momentum about the current pivot, $L[k]$, $k \in \mathbb{N}_0$, to angular momentum about the next pivot, $L[k+1]$, can be obtained through direct computation

$$L[k+1] = L[k] + x_s[k]\dot{z}_c[k]. \tag{3.22}$$

Furthermore, as angular momentum is conserved about the point of impact in the model of interest, (3.22) can be used to obtain the post-impact angular momentum about the new support pivot as a function of the pre-impact state

$$L^+[k+1] = L^-[k] + x_s^-[k]\dot{z}_c^-[k]. \tag{3.23}$$

While the continuous-time angular momentum is locally uncontrollable, the hybrid evolution of the angular momentum can be regulated through manipulation of the robot's pre-impact kinematics. These insights into the mechanics of the uncontrolled modes of walking provide insights into the design of novel feedback mechanisms for stabilizing walking – a paradigm which is called *Mechanics-Based Control*.

CHAPTER 4
CONTINUOUS-TIME CONTROL

As with any control system, stabilizing robot locomotion requires effective use of the robot's actuators to drive the machine into a desired behavior. Many of the most successful walking strategies to-date aim to use the robot's actuators to satisfy dynamic constraints which provide a stable flat-foot or double-support base throughout walking. While sustaining these "balance constraints" on the dynamics, the resulting motion can be modeled as a fully-controllable system. However, violation of the balance constraints results in phases of underactuation wherein the available control authority does not cover all states of the system. Towards the goal of augmenting understanding of robot locomotion, this Dissertation focuses on the challenge of stabilizing robot locomotion during phases of underactuation and in particular, effectively manipulating underactuated walking mechanics to achieve stability. The proposal is that endowing the robot control system with the ability to handle underactuated dynamics will improve robustness to disturbances that may otherwise destabilize walking by resulting in violations of dynamic balance constraints.

The problem of interest is to design a feedback law – for the controllable degrees of freedom in the underactuated, planar five-link biped of interest – which simultaneously drives the robot into a desired continuous-time walking motion while also ensuring that the hybrid evolution of the locally uncontrollable modes is stable. As noted in the previous section, the uncontrollable modes in the system of interest are the forward COM position and the angular momentum about the robot's support pivot. The main contribution of this work, Mechanics-Based Control, uses properties of the mechanics to encode a desired discrete-time evolution of the COM and angular momentum the design of continuous-time outputs for the robot's controllable kinematics. This chapter discusses the methods used to stabilize these outputs during the continuous-time evolution of the robot's motion.

4.1 Control System

The equations of motion (3.12) used to model the continuous-time evolution of the robot can be expressed as an affine nonlinear control system of the form

$$\dot{\mathbf{x}} = f(\mathbf{x}) + g(\mathbf{x})\mathbf{u}, \tag{4.1}$$

$$\mathbf{y} = h(\mathbf{x}), \tag{4.2}$$

where the states $\mathbf{x} = (\mathbf{q}, \dot{\mathbf{q}}) \in \mathbb{R}^n$ are the joint angles and angular velocities and $\mathbf{u} \in \mathbb{R}^m$ are the torques applied at the joints. In particular, the functions f and g are given by:

$$f(\mathbf{q}, \dot{\mathbf{q}}) = \begin{bmatrix} \dot{\mathbf{q}} \\ -D^{-1}(\mathbf{q})(C(\mathbf{q}, \dot{\mathbf{q}})\dot{\mathbf{q}} + G(\mathbf{q})) \end{bmatrix}, \quad g(\mathbf{q}) = \begin{bmatrix} \mathbf{0} \\ D^{-1}(\mathbf{q})B(\mathbf{q}) \end{bmatrix}, \tag{4.3}$$

where the inertia matrix $D(\mathbf{q})$, Coriolis matrix $C(\mathbf{q}, \dot{\mathbf{q}})$, gravity vector $G(\mathbf{q})$, and torque distribution $B(\mathbf{q})$ matrix are obtained through the rigid-body dynamics model (3.12). The choice of output functions $\mathbf{y} = h(\mathbf{x})$ encodes a walking behavior. Feedback Linearization [86] together with an exponentially stabilizing linear feedback law, such as one produced by a Rapidly Exponentially Stabilizing Control Lyapunov Function (RES-CLF) [5, 6], is used to exponentially stabilize these outputs in continuous-time, and thus drive the robot into the desired walking behavior.

As mentioned in Chapter 3, one component of the rigid-body dynamics model (3.9) is unaffected by the robot's actuators; this corresponds to the rate of change of angular momentum about the robot's support pivot (3.21). Thus, one of the most difficult aspects of designing a control law to stabilize underactuated walking is the fact that the actuator's cannot instantaneously affect the rate of change of angular momentum about the support pivot. The difficulty lies in the design of output functions $\mathbf{y} = h(\mathbf{x})$ which encode a stable hybrid evolution of the uncontrollable modes.

4.2 Outputs

The notation of [4] will be used to described the outputs, namely

$$\mathbf{y} = \mathbf{y}^a(\mathbf{x}) - \mathbf{y}^d(\tau(\mathbf{x}), \alpha), \tag{4.4}$$

where $\mathbf{y}^a(\mathbf{x})$ is a vector of "actual outputs" and $\mathbf{y}^d(\tau(\mathbf{x}), \alpha)$ is a vector of "desired outputs". The actual outputs are functions of the robot's kinematics, e.g. the robot's step length. The desired outputs are typically constructed in the form of basis functions and shaped by a specific choice of controller parameters α. The function $\tau(\mathbf{x})$ is a parameterization of time – used as the independent variable in the basis functions – which renders the closed-loop control system autonomous. One challenging aspect of stabilizing walking in the underactuated, planar five-link biped of interest is that only four outputs can be stabilized and thus, two states in the system are left uncontrolled in continuous-time.

In the original Hybrid Zero Dynamics framework, namely in [97], the actual outputs are chosen to be a linear function of the robot's joint angles. This choice simplifies the inverse kinematics problem of determining joint angle values corresponding to a set of desired output values. The desired basis functions used in [97] are Bézier polynomials which can be used to encode arbitrary continuous behaviors [11]. In the Human-Inspired Control framework, [4], the outputs are designed based on insights gained through analysis of human walking data. In particular, it was found that a subset of human locomotion kinematics can be represented with high correlation by a single function, termed the *canonical walking function*. Human-Inspired Control drives the actual robot kinematics to desired values encoded through the canonical walking function with optimized parameters, resulting in stable and efficient walking. Mechanics-Based Control provides a novel output design paradigm through the use of simple basis functions which manipulate the robot's mechanics to encode stable walking.

4.3 Partial Feedback Linearization

In Hybrid Zero Dynamics, Human-Inspired Control and Mechanics-Based Control outputs are designed so as to have relative degree two [86] along the rigid body dynamics. The corresponding (partial) feedback linearization control law is given by

$$\mathbf{u}(\mathbf{q}, \dot{\mathbf{q}}) = L_g L_f \mathbf{y}^{-1}(\mathbf{q}, \dot{\mathbf{q}}) \left(-L_f^2 \mathbf{y}(\mathbf{q}, \dot{\mathbf{q}}) + \mu \right), \tag{4.5}$$

where $L_g L_f \mathbf{y}$ and $L_f^2 \mathbf{y}$ are Lie derivatives of the (relative degree two) outputs along the rigid body dynamics and care has to be made to ensure that $L_g L_f \mathbf{y}$ is invertible over the domain of interest. Applying (4.5) to (4.1) and defining coordinates $\eta = (\mathbf{y}^T, \dot{\mathbf{y}}^T)^T$ transforms the closed-loop dynamics into the following system

$$\dot{\eta} = \begin{bmatrix} 0 & I \\ 0 & 0 \end{bmatrix} \eta + \begin{bmatrix} 0 \\ I \end{bmatrix} \mu, \tag{4.6}$$

$$\dot{\xi} = f_Z(\eta, \xi). \tag{4.7}$$

Note that (4.6) is a linear control system on the outputs, and as such, standard linear feedback methods can be used to design control law μ to stabilize the outputs η to the origin. However, due to the presence of underactuation in the system, a subset of the the closed-loop system, namely the coordinates ξ in (4.7), under partial feedback linearization is locally uncontrollable. As noted throughout the literature and as discussed in the following sections, the key to stabilizing walking is to properly manage the hybrid evolution of the locally uncontrollable states, ξ. Mechanics-Based Control leverages insights provided by the mechanics of the robot – namely that the angular momentum about the support pivot is one of the uncontrollable states ξ – to design outputs which simultaneously encode a desired walking motion while also encoding a desired hybrid evolution of ξ. Using feedback linearization with a properly designed μ to stabilize MBC outputs results in stable walking.

4.4 Rapidly Exponentially Stabilizing Control Lyapunov Functions

A general method for producing a μ to exponentially stabilize the outputs is the construction of rapidly exponentially stabilizing control Lyapunov function (RES-CLF); the following definition of a RES-CLF can be found in [5, 6] (with a modification $\varepsilon > 0$)

Definition 1. *For the system* (4.6)–(4.7)*, a continuously differentiable function* $V_\varepsilon : X \to \mathbb{R}$ *is a* **rapidly exponentially stabilizing control Lyapunov function (RES-CLF)** *if there exist positive constants* $c_1, c_2, c_3 > 0$ *such that for all* $\varepsilon > 0$*,*

$$c_1\|\eta\|^2 \leq V_\varepsilon(\eta) \leq \varepsilon^2 c_2\|\eta\|^2, \tag{4.8}$$

$$\inf_{\mu\in U}\left[L_f V_\varepsilon(\eta) + L_g V_\varepsilon(\eta)\mu + \varepsilon c_3 V(\eta)\right] \leq 0, \tag{4.9}$$

for all $\eta \in X$.

Recall that the control objective is to stabilize the outputs to the origin, i.e. drive $\eta \to 0$ (rapidly). It has been shown [5, 6], that by using a RES-CLF, the outputs can be stabilized to the origin at a rate proportional to a tunable-parameter, $\varepsilon > 0$. In particular, consider the set of inputs μ such that $\dot{V}_\varepsilon(\eta, \mu) \leq -\varepsilon c_3 V_\varepsilon(\eta)$; this set is denoted $K_\varepsilon(\eta)$ and is given by:

$$K_\varepsilon(\eta) := \{\mu : L_F V_\varepsilon(\eta) + L_G V_\varepsilon(\eta)\mu + \varepsilon c_3 V_\varepsilon(\eta_x) \leq 0\}.$$

Applying control inputs $\mu \in K_\varepsilon(\eta)$ to the output dynamics (4.6), with initial condition $\eta(0)$, results in an exponential bound on the norm of the outputs:

$$\|\eta(t)\| \leq \varepsilon\sqrt{\frac{c_2}{c_1}}e^{-\frac{c_3}{2}\varepsilon t}\|\eta(0)\|. \tag{4.10}$$

The combination of this property of nonlinear control together with the properties of the underactuated mechanics fully characterizes the continuous-time evolution of the system.

4.5 Zero Dynamics

Feedback Linearization together with a stabilizing linear feedback is used to exponentially zero the control system's outputs, and thus, in the context of walking, drive the robot into a prescribed gait. The set of states wherein the outputs are identically zero is known as a zero dynamics surface [86]. In the case of relative-degree two outputs, the zero dynamics surface, denoted Z, is given by

$$Z = \{\mathbf{x} \in \mathbb{R}^n : \mathbf{y}(\mathbf{x}) = 0,\ \dot{\mathbf{y}}(\mathbf{x}) = 0\}. \tag{4.11}$$

The rigid-body model of the five-link, underactuated biped of interest has ten states (five joint angles and five velocities). Due to underactuation, the robot's four actuators can only exponentially zero four outputs and four derivatives – resulting in a two-dimensional zero dynamics surface.

One useful property is that the zero dynamics surface is invariant along the flow of the closed-loop system under exponentially stabilizing feedback. Thus, flows which start on the zero dynamics surface remain on the zero dynamics surface for the duration of the continuous-time phase. As a result, the full robot state vector, $(\mathbf{q}, \dot{\mathbf{q}}) \in Z$, can be obtained through just the values of the zero dynamics coordinates $\xi \in \mathbb{R}^2$, at any point in time, through the coordinate transformation [97]. Moreover, analysis of the evolution of the robot's full-dimensional state vector can be determined through analysis of the evolution of two-dimensional zero dynamics coordinates, as dictated by

$$\dot{\xi} = f_Z(0, \xi). \tag{4.12}$$

As mentioned, Newton's second law dictates that one of the zero dynamics coordinates in the underactuated biped of interest is proportional to the angular momentum about the support pivot. There is freedom in the design of the other zero dynamics coordinate through

design of the outputs $\mathbf{y}$. In the context of Mechanics-Based Control, these outputs are designed so that the forward component of the center of mass relative to the support pivot is the other zero dynamics coordinate. This design choice is motivated through insights gained through examination of properties of the hybrid mechanics of walking.

A key to controlling walking is proper management of the evolution of the zero dynamics coordinates. By definition, these coordinates are locally uncontrollable in continuous-time, and hence, the only means to regulate their continuous-time behavior is through manipulation of the initial conditions. In the context of walking, the initial conditions are the values of the robot's state at the beginning of a continuous-time phase. And as discussed in the following section, these initial conditions are determined through the reset map of a hybrid model of walking, which encodes both an impact model and a model of the change of support from one leg to the next. Mechanics-Based Control proposes a method of managing the hybrid evolution of the zero dynamics coordinates through manipulation of the reset map of the hybrid model of walking based on insights gained from the properties of the mechanics of the system.

CHAPTER 5
HYBRID SYSTEMS

Walking consists of intermittent collisions between the robot and the world. Therefore, as is common in the literature [36], this dissertation models walking as a hybrid dynamical system. In this context, walking gaits correspond to periodic solutions of the hybrid system model and stability of these walking gaits is often established through Poincaré methods [34]. At the intersection of hybrid systems and control, an extension of the notion of zero dynamics is the Hybrid Zero Dynamics [97], wherein controller outputs are designed to be invariant not only in continuous-time, but also invariant through the reset map of the hybrid system. One of the most widely employed results in the context of the hybrid systems approach to robotic walking is that the stability of walking gaits – i.e. periodic orbits in the full-dimensional hybrid system – can be determined through stabilize of periodic orbits in the reduced-dimensional hybrid zero dynamics [34, 65, 97].

Designing a controller to drive a hybrid model of underactuated walking into a stable periodic orbit is a difficult task and often requires use of nonlinear programming to search for controller parameters corresponding to a stable periodic orbit. To augment existing understanding of underactuated walking provided by the literature, this Dissertation highlights a useful connection between mechanics, control and hybrid systems. As mentioned in Chapter 4, one component of the zero dynamics in the underactuated robot of interest is the angular momentum about the robot's support pivot. This is, again, due to the property from underactuated rigid-body mechanics that the robot's actuators do not influence the rate of change of angular momentum about the robot's support pivot. By extension, the angular momentum is one of the hybrid zero dynamics coordinates and as such, properties of the angular momentum mechanics can be used to gain insight into the structure of the Poincaré map for the hybrid zero dynamics. Because the stability of the full di-

mensional system can be determined through the stability of the hybrid zero dynamics, the properties of the hybrid mechanics can be used to reveal a novel feedback mechanisms for stabilizing underactuated walking. This is a key observation that leads to the development of Mechanics-Based Control which stabilizes walking by regulating the transfer of angular momentum about one support pivot to the next. This chapter presents the particular hybrid system model used to represent walking gaits in the planar underactuated biped of interest.

5.1 Hybrid Model of Walking

Following the presentation in [6], a hybrid control system, $\mathscr{HC}$, of the five-link biped of interested can be expressed as

$$\mathscr{HC} = \begin{cases} \dot{\mathbf{x}} = f(\mathbf{x}) + g(\mathbf{x})\mathbf{u} & \mathbf{x}^- \notin S \\ \mathbf{x}^+ = \Delta(\mathbf{x}^-) & \mathbf{x}^- \in S \end{cases}, \tag{5.1}$$

where the states $\mathbf{x} = (\mathbf{q}, \dot{\mathbf{q}}) \in \mathbb{R}^{10}$ are the joint angles and angular velocities, $\mathbf{u} \in \mathbb{R}^4$ are the torques applied at the joints and the control system (f, g) is obtained through computation of the rigid-body dynamics as in (4.1). The guard S of the hybrid system is characterized by the set of states for which the robot's swing leg impacts the ground (from above),

$$S = \{(\mathbf{q}, \dot{\mathbf{q}}) \in \mathbb{R}^{10} \ : \ z_s(\mathbf{q}) = 0, \ \dot{z}_s(\mathbf{q}, \dot{\mathbf{q}}) < 0\}. \tag{5.2}$$

Figure 5.1 provides a visual depiction of the domain of the hybrid system, which is characterized by the states wherein the height of the robot's swing foot $z_s(\mathbf{q})$ is above the ground. When the state in $\mathscr{HC}$ reaches the guard S, i.e. when the robot's swing foot impacts the ground, the robot's state undergoes a discrete change dictated by the reset map, $\Delta(\mathbf{x}^-)$, of the hybrid system. The reset map models the instantaneous change in joint velocities due to a rigid-body collision (3.13), as well as the relabeling of the states to reflect the swapping of the roles of the "support" and "swing" legs, as discussed in Section 3.4.

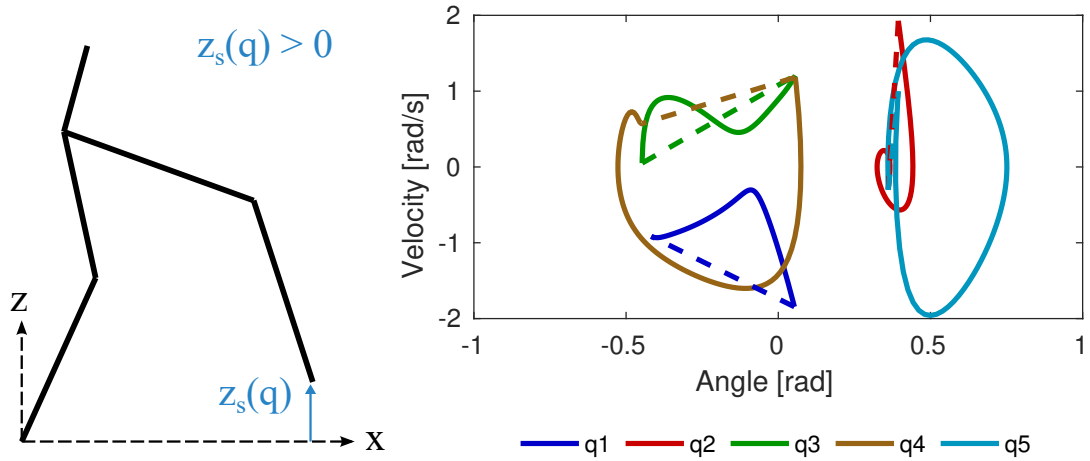

Figure 5.1: (Left) The domain and guard of the hybrid system model for underactuated walking are characterized by the height of the swing foot above ground. (Right) In hybrid models of walking, gaits correspond to hybrid periodic orbits.

The reset map of the hybrid system is given by

$$\Delta(\mathbf{q}^-, \dot{\mathbf{q}}^-) = \begin{bmatrix} R\mathbf{q}^- \\ RP(\mathbf{q}^-)\dot{\mathbf{q}}^- \end{bmatrix}. \tag{5.3}$$

where R is the relabeling matrix (3.18) and $P(\mathbf{q}^-)$ models the rigid-body collision (3.14).

When feedback control of the form $\mathbf{u} = \mathbf{u}(\mathbf{x})$ is applied to the control system (f, g), the result is a closed-loop dynamical system, $f_{cl}(\mathbf{x})$, given by

$$f_{cl}(\mathbf{x}) = f(\mathbf{x}) + g(\mathbf{x})\mathbf{u}(\mathbf{x}), \tag{5.4}$$

and a corresponding (closed-loop) hybrid system, $\mathscr{H}$, given by

$$\mathscr{H} = \begin{cases} \dot{\mathbf{x}} = f_{cl}(\mathbf{x}) & \mathbf{x}^- \notin S \\ \mathbf{x}^+ = \Delta(\mathbf{x}^-) & \mathbf{x}^- \in S \end{cases}. \tag{5.5}$$

As mentioned, walking gaits correspond to periodic orbits – such as the one shown in Figure 5.1 – in the hybrid system $\mathscr{H}$ and therefore, the goal is to design feedback control laws which drive the hybrid system into a stable periodic orbit.

5.2 Walking Gaits, Periodic Orbits and Stability

In the context of the hybrid system representation of walking, the robot's behavior will be described using the notation and definitions in [6] (one modification, however, is that fixed-points will be assumed to be post-impact states rather than pre-impact states). During the continuous-time evolution of the system, i.e. when the robot rotates freely about one support pivot while its other leg swings through the air, the motion of the system is described as a solution of the closed-loop dynamics. In particular, let $\phi_t(\mathbf{x}_0)$ be the solution of the closed-loop dynamics of the hybrid system (5.5), starting from an initial condition $\mathbf{x}_0 \in \Delta(S)$. The solution ϕ_t is called *hybrid periodic* with period $T > 0$ if $\Delta(\phi_T(\mathbf{x}_0)) = \mathbf{x}_0$. Thus a hybrid periodic solution is one wherein the robot's state always returns to the same value – in this context, the initial state $\mathbf{x}_0$ or "fixed-point"– after each time the robot's swing leg impacts the ground. A walking gait is a *hybrid periodic orbit* denoted by the set

$$\mathscr{O} = \{\phi_t(\mathbf{x}_0) \in \mathbb{R}^{10} : 0 \leq t \leq T\} \tag{5.6}$$

for a hybrid periodic solution $\phi_t(\mathbf{x}_0)$ with initial condition $\mathbf{x}_0 \in \Delta(S)$. Note that the period T of a walking gait characterizes the amount of time between impact events, i.e. the time it takes the continuous-time evolution of the system to reach the guard S when starting from the fixed-point of the orbit. Similarly, when analyzing the general behavior of the hybrid system, one is often interested in the time-to-impact function $T_I : \Delta(S) \to \mathbb{R}_{\geq 0}$ defined by

$$T_I(\mathbf{x}_0) = \inf\{t \geq 0 : \phi_t(\mathbf{x}_0) \in S\}. \tag{5.7}$$

Note that the time-to-impact is a function of the robot's state (in fact, it is a continuous-function of the state [6]). Thus, for non-periodic motions or while the hybrid system converges to a periodic orbit, the time between impact events varies from step to step.

While (5.7) is a partial function (theoretically, the hybrid system could encounter situations wherein it never reaches the guard), this Dissertation will restrict the scope of analysis to domains where the time-to-impact is finite. This is only a mild restriction for the under-actuated biped of interest, as the rate-of-change of angular momentum about the robot's support pivot is only zero when the robot's center of mass is above the support pivot and so long as the forward COM velocity is nonzero in this configuration, the robot will either fall forward or backward.

Representing walking gaits as hybrid periodic orbits allows for use of tools – such as the method of Poincaré [34] – to make precise mathematical statements regarding the stability of a gait. Following the methodology in [65], define the distance from a point $\mathbf{x} \in \mathbb{R}^{10}$ to a periodic orbit $\mathscr{O}$ to be $\mathrm{dist}(\mathbf{x}, \mathscr{O}) := \inf_{\mathbf{y} \in \mathscr{O}} \|\mathbf{x} - \mathbf{y}\|$. Furthermore, denote a ball of radius $\delta > 0$ around a periodic orbit by the set $B_\delta(\mathscr{O}) = \{\mathbf{x} \in \mathbb{R}^{10} : \mathrm{dist}(\mathbf{x}, \mathscr{O}) < \delta\}$. A periodic orbit is *locally exponentially stable* if there exist $\delta, M, \beta > 0$ such that it $\mathbf{x}_0 \in B_\delta(\mathscr{O})$ if follows that $\mathrm{dist}(\phi_t(\mathbf{x}_0), \mathscr{O}) \leq M e^{-\beta t} \mathrm{dist}(\mathbf{x}_0, \mathscr{O})$.

Following [6], stability analysis of a hybrid periodic orbit $\mathcal{O}$ via the method of Poincaré involves analysis of the corresponding Poincaré map $P : \Delta(S) \to \Delta(S)$

$$P(\mathbf{x}_0) = \Delta(\phi_{T_I(\mathbf{x}_0)}(\mathbf{x}_0)). \tag{5.8}$$

Exponentially stable fixed points of P correspond to exponentially stable hybrid periodic orbits [34, 65, 97]. One method of determining the (local) exponential stability of a fixed-point of the Poincaré map is through computation of eigenvalues of the Jacobian of the Poincaré map, DP, at the fixed-point of given hybrid periodic orbit. One eigenvalue of DP will always be unity; and a hybrid periodic orbit is locally exponentially stable if the remaining eigenvalues of DP have magnitude less than one. In practice, verification of the stability of a hybrid periodic orbit (and thus stability of a walking gait) is checked through a numeric approximation of the eigenvalues of the corresponding Poincaré map [73].

5.3 Hybrid Executions

Solutions of hybrid systems of the form (5.5) are often expressed as *hybrid executions*. In this Dissertation, the notation of [7] will be used to discuss hybrid executions.

Definition 2. *From Definition 2 of [7], an execution of a (simple) hybrid system $\mathscr{H}$ is a tuple $\chi = (\Lambda, \mathcal{I}, \mathcal{C})$, where*

- $\Lambda = \{0, 1, 2, \dots\} \subseteq \mathbb{N}$ *is a finite or infinite indexing set,*
- $\mathcal{I} = \{I_i\}_{i \in \Lambda}$ *where for each $i \in \Lambda$, I_i is defined as follows: $I_i = [t_i, t_{i+1}]$ if $i, i+1 \in \Lambda$ and $I_{N-1} = [t_{N-1}, t_N]$ or $[t_{N-1}, t_N)$ or $[t_{N-1}, \infty)$ if $|\Lambda| = N$, N finite. Here, for all $i, i+1 \in \Lambda$, $t_i \leq t_{i+1}$ with $t_i, t_{i+1} \in \mathbb{R}$, and $t_{N-1} \leq t_N$ with $t_{N-1}, t_N \in \mathbb{R}$.*
- $\mathcal{C} = \{c_i\}_{i \in \Lambda}$ *is a set of continuous trajectories, and they must be consistent with the closed-loop dynamics of $\mathscr{H}$, i.e. they must satisfy $\dot{c}_i(t) = f_{\text{cl}}(c_i(t))$ for $t \in I_i$.*

We require that when $i, i+1 \in \Lambda$,

1. $c_i(t) \in D \; \forall t \in I_i$,
2. $c_i(t_{i+1}) \in S$,
3. $\Delta(c_i(t_{i+1})) = c_{i+1}(t_{i+1})$,

were D is the domain of $\mathscr{H}$. The initial condition for the hybrid execution is $c_0(t_0) \in D$.

Hybrid executions provide a useful means of succinctly describing the behavior of the hybrid system representation of underactuated robotic walking. The indexing set Λ provides an index for each of the N individual strides the robot takes over the course of a particular experiment. Associated with each $i \in \Lambda$ stride is the solution of the closed-loop dynamics, $c_i \in \mathcal{C}$, and corresponding interval of time $I_i \in \mathcal{I}$ between takeoff and impact of the swing leg. The conditions (1)-(3) in Definition 2 capture the discrete mechanics of walking. Hybrid executions are used in Theorems 2 and 3 of this Dissertation.

5.4 Hybrid Zero Dynamics

Recall that in this Dissertation the control system for robot walking (4.1) is expressed as

$$\dot{\mathbf{x}} = f(\mathbf{x}) + g(\mathbf{x})\mathbf{u} \tag{5.9}$$

$$\mathbf{y} = \mathbf{y}^a(\mathbf{x}) - \mathbf{y}^d(\tau(\mathbf{x}), \alpha), \tag{5.10}$$

and that associated with a set of outputs is the zero dynamics surface (4.11)

$$Z = \{\mathbf{x} \in \mathbb{R}^{10} : \mathbf{y}(\mathbf{x}) = 0,\ \dot{\mathbf{y}}(\mathbf{x}) = 0\}. \tag{5.11}$$

In the Hybrid Zero Dynamics framework [97], nonlinear programming is used to determine parameters α of the desired functions which correspond to an orbit that satisfies

$$\Delta(S \cap Z) \subset Z. \tag{5.12}$$

Outputs that satisfy (5.12) are called "hybrid invariant", in that the zero dynamics surface associated with the outputs is invariant in continuous-time and across impact events. Moreover, analysis of closed-loop hybrid systems with hybrid invariant outputs can be reduced to the analysis of a two-dimensional hybrid system termed the *Hybrid Zero Dynamics*

$$\mathscr{H}_Z = \begin{cases} \dot{\xi} = f_Z(\xi) & \xi^- \notin S \cap Z \\ \xi^+ = \Delta_Z(\xi^-) & \xi^- \in S \cap Z \end{cases}, \tag{5.13}$$

wherein ξ are zero dynamics coordinates associated with the choice of outputs and $f_Z(\xi) = f_Z(0, \xi)$ are the zero-dynamics of the closed-loop system (4.12). Using the connection between the uncontrollable modes and the mechanics of walking allows provides insight into the behavior of the corresponding reduced dimensional hybrid system and by extension, insight into the evolution states in the full-dimensional hybrid model of walking.

As mentioned, in the context of hybrid system models, stable walking gaits correspond to stable hybrid periodic orbits. Moreover, stable hybrid periodic orbits in the full-dimensional hybrid model of walking can be produced through construction of a hybrid zero dynamics (5.13), by designing outputs that satisfy (5.12), and by enforcing additional constraints which ensure that the hybrid zero dynamics has a stable periodic orbit [6, 34, 65, 97]. Thus, the stability of an underactuated walking gait is ultimately determined by the stability of the hybrid evolution of the locally uncontrollable modes in the system. One contribution of this Dissertation, as presented in the next Chapter, is to expose the properties of the hybrid mechanics of these uncontrollable modes. Illumination of these Hybrid Walking Mechanics provides insights into a new feedback mechanism for stabilizing the hybrid evolution of the uncontrolled modes, and thereby drive the robot into a stable gait.

It will be shown that the hybrid evolution of the locally uncontrollable modes can be modeled as a hybrid control system wherein the control inputs act on the reset map. To distinguish between representations, hybrid control systems with reset map inputs are denoted calligraphic symbol $\mathcal{HC}$. These alternate hybrid control systems take the form

$$\mathcal{HC} = \begin{cases} \dot{\xi} = f_Z(\xi) & \xi^- \notin S_Z \\ \xi^+ = \Delta_Z(\xi^-) + u_\Delta & \xi^- \in S_Z \end{cases}. \tag{5.14}$$

Mechanics-Based Control dictates a method of designing a feedback law $u_\Delta = u_\Delta(\xi^-)$ which ensures that the hybrid evolution of the locally uncontrollable states is stable. This feedback mechanism is directly encoded in the design of continuous-time outputs, and as such, control of this form does not rely on nonlinear programming to search for stable periodic orbits. As mentioned in the next Chapter, this control authority over the reset map is a powerful tool for shaping the evolution of the hybrid system and it is ultimately the properties of the mechanics of the uncontrolled modes system which reveal how to arrive at this hybrid control system representation.

CHAPTER 6
HYBRID WALKING MECHANICS

The main design philosophy of Mechanics-Based Control is to expose the general mechanics of underactuated robotic walking and to build controllers to manipulate these mechanics. To this end, this chapter illuminates properties of the general mechanics of underactuated walking – termed the *Hybrid Walking Mechanics* – which emerge from the intersection of Classical Mechanics, Nonlinear Control, and Hybrid Systems.

In underactuated walking, the passive interface between the robot and the ground corresponds to two modes of the system that are uncontrollable in continuous-time and impacts between the robot and the ground can be destabilizing if not addressed properly. Characterizing and subsequently managing the hybrid evolution of these "locally uncontrollable modes" is the key to controlling underactuated walking. Indeed, in existing results, the stability of a walking gait is determined by a reduced dimensional hybrid system – termed the Hybrid Zero Dynamics – wherein the states are the locally uncontrollable modes due to underactuation. The original HZD framework characterizes the hybrid evolution of the uncontrollable modes using abstract coordinate definitions which allow for the most generally applicable statements on stability; however, this abstract characterization results in an obscure nonlinear hybrid system whose solutions are difficult to ascertain without numeric integration. As such, the tools of nonlinear programming are typically required to "search for" and construct stabilizing walking controllers.

The Hybrid Walking Mechanics proposed in this chapter is an alternative, mechanics-based representation of the hybrid evolution of the uncontrollable modes in underactuated walking. As discussed in the next sections, this representation provides tangible insight into the behavior of the uncontrolled modes in underactuated walking and illuminates a novel feedback mechanism for stabilizing walking.

6.1 Continuous-Time Walking Mechanics

This section presents a mechanics-based characterization of the continuous-time dynamics in underactuated robotic walking. A key property of the robot model due to Classical Mechanics is that one of the uncontrollable modes in underactuated walking is the angular momentum about the robot's support pivot. As discussed in Section 3.5, the rate of change of angular momentum about the support pivot in underactuated walking is influenced only by gravity. The robot's actuators can work to manipulate the effect of gravity by modifying the robot's shape and thereby changing the moment-arm by which gravity operates; but the actuators cannot affect the instantaneous rate of change of angular momentum. It follows that in an underactuated robot subject to nonlinear control as outlined in Section 4.3, one component of the zero dynamics is necessarily proportional to the rate of change of angular momentum about the support pivot *for all choices of continuous-time control*.

This Dissertation considers bipedal robot walking models with one degree of underactuation which, under continuous-time control, corresponds to a zero dynamics surface with at least two coordinates. While one of the zero dynamics coordinates is always proportional to the angular momentum about the support pivot, there is freedom in the choice of the other zero dynamics coordinate. In the original HZD formulation, the other zero dynamics coordinate was expressed generally as an abstract, monotonically increasing function of the robot's joint angles. Concrete HZD implementations have used various monotonically increasing kinematic quantities, such as the angle of a virtual line connecting the robot's hip and support pivot in [97] and the position of the hip relative to the support pivot in [4].

Analysis of the continuous and discrete mechanics of walking motivates the choice of an alternative choice of monotonically increasing zero dynamics coordinate: the forward position of the robot's center of mass relative to the support pivot. This section constructs the zero dynamics – termed the Zero Mechanics – for this coordinate choice and leverages tools from walking mechanics literature to characterize the behavior of the Zero Mechanics.

6.1.1 The Zero Mechanics of Walking

The Zero Mechanics of Walking is a set of two ordinary differential equations describing motion of the uncontrolled states – i.e. the zero dynamics – in closed-loop underactuated walking under a particular choice of control. As will be discussed throughout the Dissertation, making the connection between the Mechanics and the Zero Dynamics of underactuated walking allows for useful characterization of the uncontrolled states and ultimately provides insight into novel feedback principles that result in stable walking. This section outlines the derivation of the Zero Mechanics of closed-loop underactuated walking.

Consider the rigid-body dynamics of the five-link biped as described in Section 3.3, wherein the continuous-time dynamics are obtained through the Euler-Lagrange method. As noted in Chapter 4, specifically (4.1) and (4.3), the rigid-body dynamics can be expressed as a system of first-order nonlinear differential equations. These equations of motion, together with a choice of outputs encoding a desired walking motion, comprises a control system for the robot, which takes the form:

$$\dot{\mathbf{x}} = f(\mathbf{x}) + g(\mathbf{x})\mathbf{u}, \tag{6.1}$$

$$\mathbf{y}(\mathbf{x}) = \mathbf{y}^a(\mathbf{x}) - \mathbf{y}^d(\mathbf{x}, \alpha). \tag{6.2}$$

Here, $\mathbf{x} = (\mathbf{q}, \dot{\mathbf{q}})$ is a vector of joint angles $\mathbf{q}$ and joint velocities $\dot{\mathbf{q}}$. The outputs $\mathbf{y}$ encode the behavior of the robot through a vector of actual, $\mathbf{y}^a$, and desired functions, $\mathbf{y}^d$, parameterized by controller coefficients α. The goal of continuous-time control is to drive $\mathbf{y}(\mathbf{x}) \to 0$ and thus drive the robot into the behavior prescribed by $\mathbf{y}^d$.

As the robot is underactuated, the system is only partially feedback linearizable: the five-link biped robot of interest has five degrees of freedom and one degree of underactuation, hence the maximum number of outputs that can be simultaneously stabilized through control is four. Thus, the behavior of the robot can be *partially prescribed* through design of four-dimensional, linearly-independent actual $\mathbf{y}^a$ and desired $\mathbf{y}^d$ output functions. As in the

original HZD formulation, this Dissertation considers outputs which have relative-degree two along the continuous-time dynamics (6.1), thus the behavior of the robot is partially encoded by the outputs and their derivatives, the collection of which will be denoted

$$\eta(\mathbf{x}) = \begin{bmatrix} \mathbf{y}(\mathbf{x}) \\ \dot{\mathbf{y}}(\mathbf{x}) \end{bmatrix}. \tag{6.3}$$

The feedback linearization law corresponding to this class of outputs takes the form

$$\mathbf{u} = L_g L_f \mathbf{y}(\mathbf{x})^{-1}(-L_f L_f \mathbf{y}(\mathbf{x}) + \mu). \tag{6.4}$$

Applying (6.4) to (6.1) results in the following transformed control system

$$\dot{\eta} = F\eta + G\mu, \tag{6.5}$$

$$\dot{\xi} = f_Z(\eta, \xi), \tag{6.6}$$

which is comprised of the linearized output dynamics (6.5) and locally uncontrollable, non-linear dynamics (6.6) whose coordinates $\xi = (\xi_1, \xi_2)$ are typically referred to as the "zero dynamics coordinates". The outputs, derivatives of the outputs, and the zero dynamics fully encode the behavior of the robot through the coordinate transformation

$$\Phi : x \mapsto \begin{pmatrix} \eta(\mathbf{x}) \\ \xi(\mathbf{x}) \end{pmatrix}, \tag{6.7}$$

and its inverse. In practice, obtaining the states $\mathbf{x}$ from the outputs, $\eta(\mathbf{x})$, and zero dynamics coordinates, $\xi(\mathbf{x})$, is done by solving an inverse kinematics problem. In this system, there is control authority to explicitly prescribe a subset of the robot's behavior through design of $\eta(\mathbf{x})$, but there will always be at least a two-dimensional subset, $\xi(\mathbf{x})$, of the robot's behavior that cannot be explicitly prescribed.

The goal of this section is to characterize the zero dynamics coordinates $\xi(\mathbf{x})$ in terms of the mechanics of the system. As noted in Section 3.5, a key property of the underactuated, rigid-body dynamics model is that the rate of change of angular momentum about the robot's support pivot, $L(\mathbf{q}, \dot{\mathbf{q}})$, is independent of the robot's joint torques. Letting $x_c(\mathbf{q})$ denote the horizontal component of the vector from the support pivot to the robot's center of mass, Newton's second law dictates that the rate of change of the (mass-normalized) angular momentum about the support pivot, $\dot{L}$, is proportional to $x_c(\mathbf{q})$; specifically,

$$\dot{L} = g x_c(\mathbf{q}) \tag{6.8}$$

wher g is the gravity constant. It follows that for all choices of controller outputs, one element of the corresponding zero dynamics is proportional to the rate of change of angular momentum about the support pivot. In the hybrid robotic walking literature, the angular momentum about the support pivot is typically chosen to be the "second" zero dynamics coordinate, ξ_2; and consequently,

$$\xi_2 = L(\mathbf{q}, \dot{\mathbf{q}}), \tag{6.9}$$

$$\dot{\xi}_2 = g x_c(\mathbf{q}). \tag{6.10}$$

Note that in the original HZD notation, specifically in equation (23) of [97], the second zero dynamics coordinate is defined to be $\xi_2 = \gamma(\mathbf{q}, \dot{\mathbf{q}})$ where $\gamma(\mathbf{q}, \dot{\mathbf{q}})$ is equivalent to the angular momentum about the support pivot.

While the second zero dynamics coordinate is always proportional to the angular momentum about the support pivot, there is flexibility in choosing the "first" zero dynamics coordinate, ξ_1. The original HZD framework [97] specifies a monotonically increasing function of only the configuration variables and specific implementations have used the position of the robot's hip or the angle of a virtual line connecting the hip to the support pivot. Analysis of the hybrid mechanics of walking motivates an alternative, explicit choice

for this coordinate: the forward center of mass relative to the support pivot, $\xi_1 = x_c(\mathbf{q})$. As will be seen in the following sections, choosing the first zero dynamics coordinate to be x_c results in a useful interpretation of the zero dynamics and ultimately illuminates a novel mechanism for stabilizing walking. In the context of continuous-time mechanics, a motivation for choosing $\xi_1 = x_c(\mathbf{q})$ is that the second component of the zero dynamics becomes a linear differential equation, i.e. under this choice of coordinates (6.10) becomes $\dot{\xi}_2 = g\xi_1$.

In the primary contribution of this Dissertation, Mechanics-Based Control, the outputs η are designed so that the collection of zero dynamics coordinates $\xi = (x_c, L)$ and outputs *fully encodes* the behavior of the robot, i.e. so that

$$\begin{aligned} \eta_1 &= \mathbf{y}(\mathbf{q}, \dot{\mathbf{q}}), \quad \eta_2 = \dot{\mathbf{y}}(\mathbf{q}, \dot{\mathbf{q}}), \\ \xi_1 &= x_c(\mathbf{q}), \qquad \xi_2 = L(\mathbf{q}, \dot{\mathbf{q}}), \end{aligned} \tag{6.11}$$

is a valid coordinate transformation. Thus, given values for the outputs, the center of mass and the angular momentum, the states of the robot can be obtained by solving the inverse kinematics problem

$$\mathbf{x} = \Phi^{-1}(\eta, x_c, L). \tag{6.12}$$

In practice, to ensure that the inverse kinematics problem (6.12) is well-posed and that (6.11) is a valid choice of coordinates, the outputs η will be constructed so that the matrix

$$d\Phi = \begin{bmatrix} d\eta \\ dx_c \\ dL \end{bmatrix} \tag{6.13}$$

has full rank. This can be achieved by designing the kinematic quantities to be controlled, $\mathbf{y}^a(\mathbf{q})$, to be independent of one another and independent of $x_c(\mathbf{q})$.

Following the Hybrid Zero Dynamics framework, for outputs that satisfy the above conditions, analysis of the evolution of the robot's state can be reduced to analysis of only the center of mass and angular momentum when $\eta \equiv 0$, i.e. when the robot's actual motion is equal to the desired motion as prescribed through the design of the outputs. Under this constraint, the states can be obtained by solving the inverse kinematics problem

$$\mathbf{x} = (\mathbf{q}, \dot{\mathbf{q}}) = \Phi^{-1}(0, x_c, L). \tag{6.14}$$

As will be seen in future sections, the stability of a walking gait can be determined through the stability of the hybrid evolution of x_c and L. The continuous-time component of this hybrid evolution will be referred to as the Zero Mechanics, and is defined as follows.

Definition 3. *For outputs η constructed so that* (6.11) *is a valid coordinate transform on a domain of interest, the Zero Mechanics is a two-dimensional system given by*

$$\dot{x}_c = \kappa(x_c, L) \tag{6.15}$$

$$\dot{L} = g x_c \tag{6.16}$$

where x_c and L are the forward component of the robot's COM relative to the support pivot and the angular momentum about the support pivot, and where $\kappa(x_c, L)$ is given by

$$\kappa(x_c, L) = \frac{1}{z_c(\vartheta)}(L + x_c \dot{z}_c(\vartheta, \dot{\vartheta}) - H(\vartheta, \dot{\vartheta})) \tag{6.17}$$

with $z_c(\vartheta)$ the height of the COM and $H(\vartheta, \dot{\vartheta})$ the centroidal angular momentum computed using states obtained through the inverse coordinate transform (6.14)*, i.e. states obtained on the corresponding zero dynamics surface via $(\vartheta, \dot{\vartheta}) = \Phi^{-1}(0, x_c, L)$.*

This mechanics-based interpretation of the zero dynamics of underactuated walking yields a dynamical system that can be qualitatively characterized by comparing it with the well-known Linear Inverted Pendulum model, as described in the following Section.

6.1.2 Zero Mechanics and the Linear Inverted Pendulum

In the original Hybrid Zero Dynamics framework, stability of walking is determined through stability of periodic orbits in the hybrid zero dynamics. Thus, one must evaluate the exact solution of a particular zero dynamics to determine stability of walking. As the zero dynamics is nonlinear, the corresponding solution and thus contribution to stability historically have been determined through numeric integration. In this section, we show that the mechanics-based interpretation of the zero dynamics, the Zero Mechanics proposed in (6.15) – (6.16), is similar in form to a well-known linear system known as the Linear Inverted Pendulum [49]. In fact, the LIP is a special case of the Zero Mechanics and it can be derived through a particular choice of controller outputs. The LIP is perhaps the most widely used model of robot walking and this Section will show how to use the LIP to characterize the qualitative behavior of the Zero Mechanics.

Consider the zero mechanics given in (6.15) – (6.16). For outputs chosen such that the height of the center of mass is a constant $z_c \equiv z_0 > 0$, i.e. $\dot{z}_c = 0$, and that the centroidal angular momentum, H, is zero, it follows that $\kappa(x_c, L) \equiv \frac{1}{z_0} L$ and the corresponding zero mechanics are linear. In fact, under this specific choice of outputs, the Zero Mechanics becomes an angular momentum variant of the Linear Inverted Pendulum. The following equation array shows the general Zero Mechanics and the angular momentum variant of the Linear Inverted Pendulum side-by-side:

$$\begin{array}{ll} \overbrace{\dot{x}_c = \kappa(x_c, L)}^{\text{Zero Mechanics}} & \overbrace{\dot{x}_c = \dfrac{1}{z_0} L,}^{\text{LIP}} \\ \dot{L} = g x_c & \dot{L} = g x_c. \end{array} \tag{6.18}$$

Note that both models have linear angular momentum dynamics, and the only nonlinearity appears in the velocity of the forward component of the COM.

In the Zero Mechanics, the height of the center of mass and the centroidal angular

momentum need not (and realistically, should not) be constant. However, for outputs in which the magnitude of the vertical COM velocity and centroidal angular momentum are relatively small, i.e. for outputs that satisfy

$$\|x\dot{z}_c - H\| << L, \tag{6.19}$$

over a domain of interest, it follows that

$$\kappa(x_c, L) \approx \frac{1}{z_c} L \tag{6.20}$$

and thus the Zero Mechanics and the Linear Inverted Pendulum are similar. Mechanics-Based Control exploits this similarity to estimate the behavior of Nonlinear Zero mechanics through use of tools from linear systems.

One linear systems tool, the phase space, allows for a characterization of the global behavior of the LIP which, through the similarity between the LIP and the Zero Mechanics, will serve as an approximate characterization of the global behavior of the Zero Mechanics. The phase space of the angular momentum variant of the LIP, shown in Figure 6.1, is partitioned into four quadrants by a saddle at the origin with asymptotes

$$L = \pm z_c \sqrt{\frac{g}{z_c}} x. \tag{6.21}$$

Note that in the angular momentum variant of the LIP in (6.18), the velocity of the horizontal component of the COM is proportional to the angular momentum. It follows that the top half of the LIP phase plane corresponds to forward motion, i.e. $\dot{x}_c > 0$ when $L > 0$. Moreover, solutions that begin in the top quadrant of the phase space – as delineated by the asymptotes (6.21) – have the property that $\dot{x}_c(t) > 0$ over all t. Solutions that begin in any of the other three quadrants ultimately reach a time in which $\dot{x}_c(t) < 0$. Thus, for the LIP model, forward walking is achieved by ensuring that the state (x_c, L) lies within the top

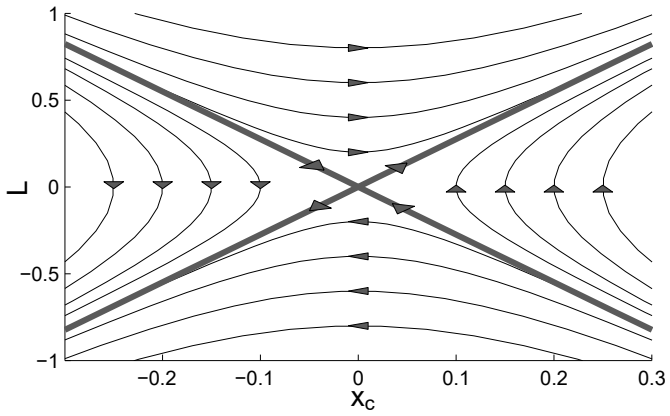

Figure 6.1: A variant of the Linear Inverted Pendulum phase space, for $z_0 = 0.7$m and $m = 1$kg, is used to characterize the evolution of the forward angular momentum and the relative horizontal center of mass in underactuated walking. The goal of the Mechanics-Based Control implementation is to ensure that the transfer of momentum due to stepping returns the angular momentum and COM to the top (forward walking) quadrant.

quadrant of the phase space at all times – even after impact and application of the reset map. Moreover a hypothesis in this Dissertation is that, for outputs in which the Zero Mechanics and the LIP are similar, the phase space of the Zero Mechanics is qualitatively similar to that of the LIP. In this context, the notion of "qualitative similarity" is taken to mean that the top quadrant of the LIP phase space serves as an approximation of the forward walking region of the nonlinear Zero Mechanics state space. Thus the goal of Mechanics-Based Control will be to ensure that the states (x_c, L) in the nonlinear Zero Mechanics remain within the top quadrant of the LIP phase space – even through impact and application of the reset map.

Another linear systems tool that will be exploited is the exact solution of the dynamics. Let $x_L(t)$ denote the solution of the LIP dynamics (6.18)

$$x_L(t) = c_1 e^{\lambda t} + c_2 e^{-\lambda t}, \tag{6.22}$$

where $\lambda = \sqrt{g/z_0}$ and c_1 and c_2 are functions of the initial condition. In traditional usage of the LIP model, c_1 and c_2 are functions of the initial position $x_c(0)$ and velocity $\dot{x}_c(0)$; however, in this Dissertation, c_1 and c_2 are designed using the initial center of mass position

and the angular momentum about the support pivot

$$c_2 = \frac{1}{2}x_c - \frac{L}{2\lambda z_0}, \tag{6.23}$$

$$c_1 = x_c - c_2, \tag{6.24}$$

through the relationship between velocity and angular momentum $L = z_0 \dot{x}_c$. The derivative of (6.22) provides an estimate of the evolution of the angular momentum in the system

$$L(t) = z_0 \lambda \left(c_1 e^{\lambda t} - c_2 e^{-\lambda t} \right). \tag{6.25}$$

Furthermore, given an initial condition $(x_c(0), L(0))$ one can show that solutions $(x_L(t), L(t))$ of the linear system satisfy the following constraint

$$x_L(t) = \sqrt{\frac{L^2(t)}{g z_0} - \frac{L^2(0)}{g_z 0} + x_c^2(0)}. \tag{6.26}$$

As discussed in later sections, Mechanics-Based Control will use the LIP solution (6.26) to construct an estimate the future value of the COM, $\hat{x}_c$, corresponding to a specified value of the angular momentum, $L = \omega$, based on the current measurement of the robots state $(\mathbf{q}, \dot{\mathbf{q}})$. The estimate $\hat{x}_c(\mathbf{q}, \dot{\mathbf{q}})$ takes the form

$$\hat{x}_c(\mathbf{q}, \dot{\mathbf{q}}) = \sqrt{\frac{\omega^2}{g z_0} - \frac{L^2(\mathbf{q}, \dot{\mathbf{q}})}{g z_0} + x_c^2(\mathbf{q})} \tag{6.27}$$

This estimate is continuously updated based on current measurements of the robot's state $(\mathbf{q}, \dot{\mathbf{q}})$ and converges to the actual value of the COM when the angular momentum reaches ω. Mechanics-Based Control employs this estimate of the zero dynamics to ultimately encode stability of the Hybrid Walking Mechanics in the construction of continuous-time outputs. The following section illuminates properties of the Hybrid Walking Mechanics that motivate the Mechanics-Based Control constructions.

6.2 Hybrid Walking Mechanics

This section presents a mechanics-based characterization – termed the Hybrid Walking Mechanics – of the hybrid evolution of the locally uncontrollable modes in underactuated walking. The Hybrid Walking Mechanics is a two-dimensional hybrid system wherein the states are the forward component of the center of mass position relative to the support pivot and the angular momentum about the support pivot. Applying the standard HZD line of reasoning, it follows that the stability of periodic orbits within a full dimensional hybrid walking model of the form (5.1) can be determined through stability of periodic orbits within the Hybrid Mechanics. Moreover, as discussed in the following sections, imposing a mechanics-based interpretation of the Hybrid Zero Dynamics yields a hybrid system whose elements suggest novel mechanisms for stabilizing locomotion.

6.2.1 Derivation of the Hybrid Walking Mechanics

The Hybrid Walking Mechanics proposed in this section is a hybrid system comprised of the continuous-time, Zero Mechanics, discussed in Section 6.1.1 and the discrete-time mechanics discussed in Sections 3.4 and 3.5.1. The coordinates in this hybrid system are the forward center of mass relative to the support pivot, x_c and the angular momentum about the support pivot, L. In this hybrid system, the dynamical system is the Zero Mechanics (6.15) – (6.16), stated again for reference

$$\dot{x}_c = \kappa(x_c, L) \tag{6.28}$$

$$\dot{L} = g x_c. \tag{6.29}$$

where κ is defined in (6.17). In the traditional HZD constructions, the guard of a Hybrid Zero Dynamics is typically defined in terms of the first zero dynamics coordinate. However, for the Hybrid Walking Mechanics, we will consider a guard that encodes states wherein the angular momentum has reached a particular value $\omega > 0$. In particular, the guard S_ω

corresponding to a choice of ω is given by

$$S_\omega = \{(x_c, L) : x_c > 0, L = \omega\}. \tag{6.30}$$

The reset map is obtained through the COM transfer equation (3.19) and the momentum transfer equation (3.22), described in Section 3.4, and stated again for reference

$$x_c^+ = x_c^- - x_s^-, \tag{6.31}$$

$$L^+ = L^- + x_s^- \dot{z}_c^-. \tag{6.32}$$

Recall that on a Zero Mechanics surface, the joint angles and velocities can be expressed through the diffeomorphism (6.14). As the step length and vertical center of mass are functions of the joint angles and velocities, i.e. $x_s = x_s(\mathbf{q})$ and $\dot{z}_c = \dot{z}_c(\mathbf{q}, \dot{\mathbf{q}})$, on a Zero Mechanics surface we can use (6.14) to express these quantities as functions of x_c and L,

$$x_s = x_s(x_c, L), \tag{6.33}$$

$$\dot{z}_c = \dot{z}_c^-(x_c, L). \tag{6.34}$$

With these constructs in hand, we can now define the Hybrid Walking Mechanics.

Definition 4. *For $\omega > 0$, the **Hybrid Walking Mechanics** is a hybrid system, $\mathscr{H}_\omega$, given by*

$$\mathscr{H}_\omega = \begin{cases} \dot{x}_c = \kappa(x_c, L) \\ \dot{L} = g x_c \end{cases} \quad (x_c, L) \notin S_\omega$$
$$\begin{cases} x_c^+ = x_c^- - x_s^-(x_c, L) \\ L^+ = L^- + x_s^- \dot{z}_c^-(x_c, L) \end{cases} \quad (x_c, L) \in S_\omega \tag{6.35}$$

with κ as defined in (6.17)*, guard S_ω as defined in* (6.30)*, and reset map obtained by applying* (6.33)–(6.34) *to the discrete mechanics* (6.31)–(6.32)*.*

6.2.2 Hybrid Walking Mechanics and Stability

In the context of hybrid walking models, a well-established and oft-exploited result is that the stability of an underactuated walking gait is determined by the stability of a periodic orbit in the Hybrid Zero Dynamics of the gait's controller. Applying this line of reasoning to controllers which satisfy assumptions outlined in the previous section, it follows that stability of walking can be established by stabilizing a periodic orbit in a Hybrid Walking Mechanics – this is precisely what Mechanics-Based Control is designed to accomplish.

Expressing the Hybrid Zero Dynamics in terms of the Mechanics provides physical insights into the conditions required for stability of hybrid periodic orbits under traditional HZD-based control, as outlined in the original HZD stability theorem, Theorem 3 of [97]. In this theorem, the Poincaré map which determines stability of walking is one-dimensional and the coordinate of this map is proportional to the square of the angular momentum about the robot's support pivot. Thus, a stable fixed point of the Poincaré map corresponds to a particular value of the angular momentum about the support pivot. In the original HZD context, stability of the fixed point is determined through the term δ_{zero} (defined in the text following equation (45) of [97]) which is a constant function of the configuration of the robot just prior to impact. Under this interpretation, the stability of the fixed point of the Poincaré map of the hybrid zero dynamics can be manipulated by manipulating the configuration of the robot just prior to impact. Indeed, in the original HZD framework, optimization is used to find a fixed configuration that corresponds to a stable fixed point.

Interestingly, this mechanics-based interpretation of the conditions required for hybrid stability illuminates an alternative strategy for stabilizing walking: dynamically manipulating the configuration of the robot to directly regulate the transfer of angular momentum from one step to the next. Instead of relying on the robot to return to a fixed configuration which results in a locally exponentially stable fixed point of the Poincaré map, the proposed Mechanics-Based Control strategy is to explicitly control the Poincaré map through dynamic manipulation of the robot's configuration, as described in the following section.

6.3 Controlling the Hybrid Walking Mechanics

As the stability of a hybrid periodic orbit (i.e. a walking gait) can be determined through stability of the fixed-point of the corresponding Poincaré return map, Mechanics-Based Control seeks to create a stable walking gait by driving the Poincaré map of the Hybrid Walking Mechanics – the discrete-time evolution of the forward center of mass and angular momentum – to a stable fixed point. The structure of the Hybrid Walking Mechanics (6.35) illuminates a means of controlling the Poincaré map through manipulation of the robot's kinematics prior to impact. In particular, the transfer of the forward COM position and angular momentum from one step to the next (i.e. the reset map) is a function of controllable kinematic quantities, the step length and vertical COM velocity, prior to impact. The main contribution of this Dissertation, Mechanics-Based Control, exploits this structure in the design continuous-time outputs for the step length and vertical center of mass position that simultaneously encode desired continuous-time evolution of these kinematics – swinging the leg forward and maintaining a nominal height of the center of mass – while also encoding a desired post-impact forward COM and angular momentum. This section proposes a simplified hybrid control system which models the macroscopic elements of the Hybrid Walking Mechanics and which provides a platform for developing this novel strategy of manipulating the Poincaré map through manipulation of the robot's kinematics. Moreover, the strategy used to determine viable fixed points corresponding to stable periodic orbits in this simplified hybrid control system will be directly translated to the strategy prescribed in Mechanics-Based Control to stabilize the full-dimensional hybrid model.

6.3.1 Representative Hybrid Mechanical Control System

Consider the following hybrid control system,

$$\mathcal{HC}_\omega = \begin{cases} \begin{aligned} \dot{x}_c &= \frac{1}{z} L \\ \dot{L} &= g x_c \end{aligned} & (x_c, L) \notin S_\omega \\ \begin{aligned} x_c^+ &= x_c^- + u_x \\ L^+ &= L^- + u_L \end{aligned} & (x_c, L) \in S_\omega \end{cases} \tag{6.36}$$

wherein the states are the position of the forward center of mass relative to the support pivot, x_c, and the (mass normalized) angular momentum about the support pivot L. Here $\omega > 0$ and the guard S_ω is as defined in (6.30). The continuous-time dynamics in (6.36) are those of the Linear Inverted Pendulum, with constant height of the center of mass $z_c > 0$. Recall from Section 6.1.2 that for continuous-time outputs that satisfy $\|x\dot{z} - H\| << L$, the LIP dynamics and the nonlinear dynamics are qualitatively similar. In addition, the reset map of the proposed hybrid system is fully controllable, with admissible inputs $(u_x, u_L) \in \mathbb{R}^2$. This reset map is meant to highlight the control authority over the reset map in the Hybrid Walking Mechanics (6.35) through the ability to design continuous-time outputs for the robot's step length and vertical center of mass position such that

$$x_s^- = -u_x \tag{6.37}$$

$$\dot{z}_c^- = \frac{u_L}{x_s^-}. \tag{6.38}$$

Note that many characteristics of the proposed hybrid control system (6.36) are equivalent to those of the general Hybrid Walking Mechanics (6.35). The angular momentum dynamics are equivalent. Under continuous-time control with outputs that satisfy (6.37)–(6.38), the reset map is equivalent. The only difference between this model and the general hybrid system is the forward COM dynamics. That is to say, the COM component of the

zero dynamics of a set of Mechanics-Based Control outputs is in general not equivalent to the Linear Inverted Pendulum dynamics. However, we continue our analysis under the assumption that the LIP can act as a proxy for the full nonlinear dynamics. This model allows us to use the tools of linear systems to analyze the LIP dynamics and reason about the whole state space of the proposed hybrid control system, and ultimately to determine the set of periodic orbits that exist in a hybrid control system of this form for a given $\omega > 0$.

6.3.2 Explicit Hybrid Periodic Orbit Construction via Control

A challenging aspect of underactuated control design is that, in general, the zero dynamics of a set of walking outputs is nonlinear. As a result, production of stable hybrid periodic orbits has historically required nonlinear optimization to numerically integrate the zero dynamics and to search for a fixed point corresponding to a periodic orbit. One benefit of the representative hybrid system (6.36) is that the dynamics are linear and thus we can use the tools of linear systems to characterize the entire state space of hybrid systems of this form. Another benefit is that the reset map of the representative hybrid system is fully controllable; this allows us to design controllers that *generate hybrid periodic orbits by construction*. And most importantly, *we can use the same methods to construct periodic orbits in the nonlinear Hybrid Walking Mechanics*, as discussed in the next Chapter on Mechanics-Based Control.

We propose the following control inputs, with parameters x_c^* and L^* to be determined, to the reset map of the representative hybrid system (6.36),

$$u_x(x_c^-, x_c^*) = x_c^* - x_c^-, \tag{6.39}$$

$$u_L(L^-, L^*) = L^* - L^-. \tag{6.40}$$

Recall again that in the general Hybrid Walking Mechanics these control inputs correspond to desired pre-impact kinematics, as described in (6.37) – (6.38) and that Mechanics-Based

Control will encode these "reset map controllers" in the full Hybrid Walking Mechanics through design of continuous-time outputs. Applying (6.39)–(6.40), with controller parameters x_c^* and L^*, to (6.36) results in the closed-loop hybrid system

$$\mathcal{H}_\omega(x_c^*, L^*) = \begin{cases} \dot{x}_c = \dfrac{1}{z}L \\ \dot{L} = g x_c \end{cases} \quad (x_c, L) \notin S_\omega \qquad . \qquad (6.41)$$
$$\begin{cases} x_c^+ = x_c^* \\ L^+ = L^* \end{cases} \quad (x_c, L) \in S_\omega$$

In this section, we will show conditions under which the controller parameters x_c^* and L^* correspond to the fixed point of a hybrid periodic orbit in $\mathcal{H}_\omega(x_c^*, L^*)$. Moreover, we will characterize the entire set of parameters x_c^* and L^* that generate periodic orbits in the corresponding hybrid system $\mathcal{H}_\omega(x_c^*, L^*)$. Points in this set are post-impact center of mass and angular momentum values that correspond to forward walking in the representative hybrid system; thus, this set serves as a suggestion for how to control the center of mass and angular momentum in the nonlinear Hybrid Walking Mechanics in order to produce a forward walking gait. In the next chapter, we present Mechanics-Based Control wherein outputs will be designed to drive the nonlinear Hybrid Walking Mechanics into points within the set constructed in this section.

Figure 6.2 shows the phase space of the linear inverted pendulum dynamics. Overlayed in this figure is the guard, S_ω, given again for reference:

$$S_\omega = \{(x_c, L) : x_c > 0, L = \omega\}, \qquad (6.42)$$

where $\omega > 0$ specifies the desired value of the angular momentum about the support pivot at impact events. Note that under COM and momentum transfer control of the form (6.39)–(6.40), any state that reaches the guard is mapped to the desired point (x_c^*, L^*) through the reset map. Thus, we can calculate the set of periodic orbits in the hybrid system $\mathcal{H}_\omega(x_c^*, L^*)$

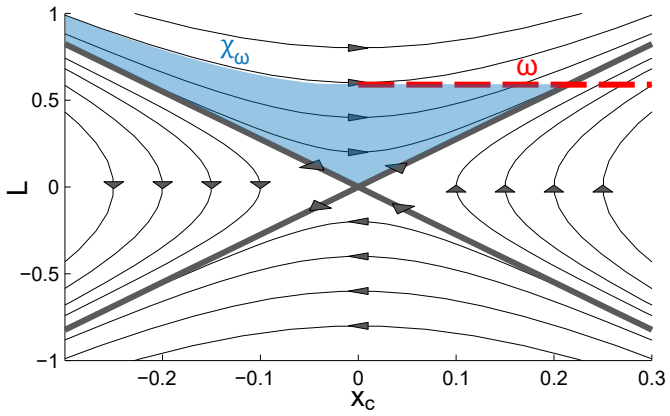

Figure 6.2: The set of states $\mathcal{X}_\omega$ which reach the guard in the Hybrid Zero Mechanics is shown in blue and overlayed on the phase space of the angular momentum variant of the Linear Inverted Pendulum.

by calculating the set of initial conditions which reach the guard in finite time. To construct this set, note that the minimum angular momentum along solutions of the LIP dynamics (6.25), starting from initial condition (x_c^+, L^+), occurs at $x_c = 0$ and is given by

$$L_{\min}(x_c^+, L^+) = \sqrt{(L^+)^2 - g z_0 (x_c^+)^2}. \tag{6.43}$$

This function can be used to describe the set $\mathcal{X}_\omega$ of initial conditions which reach the guard in finite time. In particular, for $\omega > 0$ the set $\mathcal{X}_\omega$ is given by

$$\begin{aligned} \mathcal{X}_\omega = \{\, (x_c, L) : (\, (0 < L_{\min}(x_c, L)) \cap (L > 0)\,) \cap \\ (\, (\, (L_{\min}(x_c, L) < \omega) \cap (x_c \leq 0)\,) \cup (\, (L < \omega) \cap (x_c > 0)\,)\,)\,\}. \end{aligned} \tag{6.44}$$

This set, shown in blue in Figure 6.2, is a connected subspace encompassed by: the two asymptotes of the LIP phase space, the guard, and the constraint on the minimum angular momentum. Intuitively, this set describes the initial conditions which have enough energy to complete a step, but less energy than the maximum the robot is capable of recovering from. Given the definition of the set $\mathcal{X}_\omega$, we now present the main result of this chapter: conditions on the existence of periodic orbits in the proposed closed-loop hybrid system.

Theorem 1. *Let $\mathcal{H}_\omega(x_c^*, L^*)$ be a closed-loop hybrid system under Mechanics-Based Control of the form* (6.41)*, with $\omega > 0$ and guard S_ω as defined in* (6.42)*. Let $\mathcal{X}_\omega$ be the set defined in* (6.44)*. If $(x_c^*, L^*) \in \mathcal{X}_\omega$, then $\mathcal{H}_\omega(x_c^*, L^*)$ has an exponentially stable hybrid periodic orbit $\mathcal{O}$ with fixed point $(\bar{x}_c, \bar{L}) \in S_\omega$, given by*

$$\begin{pmatrix} \bar{x}_c \\ \bar{L} \end{pmatrix} = \begin{pmatrix} \sqrt{\omega^2 - (L^*)^2 + g z_0 (x_c^*)^2} \\ \omega \end{pmatrix}. \tag{6.45}$$

Furthermore, all flows of the continuous dynamics of $\mathcal{H}_\omega(x_c^*, L^*)$ that start in $\mathcal{X}_\omega$ converge to $\mathcal{O}$ in one hybrid execution.

Proof. The point on the guard (6.45) is computed using the solution to the Linear Inverted Pendulum dynamics (6.26). As the reset map of $\mathcal{H}_\omega(x_c^*, L^*)$ maps points on the guard S_ω to the point (x_c^*, L^*), the only step required in the proof is to show that all points in $\mathcal{X}_\omega$ reach the guard. Here, the proof will reason about the phase space of the (linear) dynamics of $\mathcal{H}_\omega(x_c^*, L^*)$, as shown in Figure 6.2. This phases space is partitioned into four quadrants by the eigenvectors $L = \pm z\sqrt{g/z}x_c$. The top quadrant of the phase space – corresponding to forward motion – can be defined using the constraints $(0 < L_{\min}(x_c, L)) \cap (L > 0)$. Flows in this quadrant of the phase reach the guard so long as $L < \omega$ when $x_c = 0$; this condition is ensured by the constraint $((L_{\min}(x_c, L) < \omega) \cap (x_c \leq 0)) \cup ((L < \omega) \cap (x_c > 0))$. □

Theorem 1 illustrates the power of having full control authority over the reset map in the representative hybrid control system for underactuated walking. In particular, this control authority allows for design of control inputs which drive the system to a desired state (x_c^*, L^*) *in one hybrid execution*. Moreover, through use of tools from linear systems, we can compute the entire set of states for which $\mathcal{H}_\omega(x_c^*, L^*)$ has a periodic orbit. And as mentioned, the primary difference between $\mathcal{H}_\omega(x_c^*, L^*)$ and the full Hybrid Walking Mechanics $\mathscr{H}_\omega$, is nonlinearity in the forward COM dynamics. Thus, the analysis and results on $\mathcal{H}_\omega(x_c^*, L^*)$ will be used to suggest control strategies for the full nonlinear model.

CHAPTER 7
MECHANICS-BASED CONTROL OF PLANAR UNDERACTUATED WALKING

This chapter compiles the contents of previous chapters – notable properties of mechanics, control and hybrid systems – to construct the main contribution of this Dissertation: Mechanics-Based Control. This controller is a novel method of stabilizing hybrid models of underactuated walking by leveraging properties of the mechanics of the robot. At its core, the controller stabilizes the transfer of angular momentum from one leg to the next through continuous-time control coupled with hybrid system models that capture impacts that occur at foot strike. In particular, conservation of angular momentum at impact allows for computation of the exact transfer of momentum as a function of the robot's step length and vertical center of mass velocity just prior to foot impact. This motivates the construction of continuous-time reference trajectories for the robot's step length and vertical center of mass with endpoints corresponding to a desired transfer of angular momentum. Driving the robot to these trajectories results in stable underactuated walking.

7.1 Overview

This section outlines the main elements of Mechanics-Based Control and describes how these elements contribute to stable walking. The elements of Mechanics-Based Control are motivated by insights gained from the Hybrid Walking Mechanics, discussed in Chapter 6. In particular, the key contribution of Mechanics-Based Control is a novel mechanism for stabilizing walking gaits – regulating the transfer of angular momentum from one step to the next – which provides a means of creating stable hybrid periodic orbits *by construction*. Mechanics-Based Control is implemented in the form of continuous-time outputs which simultaneously encode a desired continuous-time walking behavior while also encoding a desired discrete-time evolution of the locally uncontrollable modes of the system.

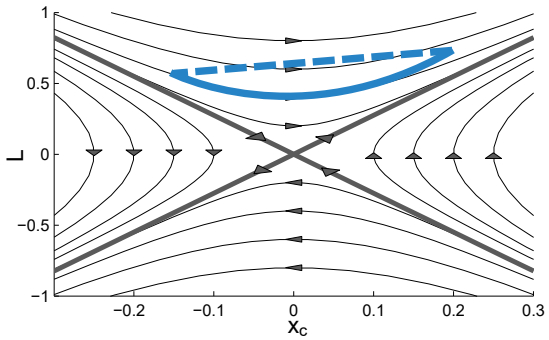

Figure 7.1: An example hybrid periodic orbit in the Hybrid Walking Mechanics

7.1.1 Novel Walking Feedback Mechanism: Regulating Angular Momentum Transfer

Mechanics-Based Control stabilizes underactuated robotic walking through a novel feedback mechanism: regulating the transfer of COM position and angular momentum about one support pivot to the next. In MBC, continuous-time outputs are designed so that a valid choice of the corresponding zero dynamics coordinates is the forward COM position and angular momentum about the support pivot. Applying standard results in hybrid walking literature, it follows that the stability of a walking gait can be related to the stability of the hybrid evolution of these coordinates. Whereas creating stable periodic orbits in the hybrid zero dynamics has historically required use of nonlinear programming to search for fixed points, Mechanics-Based Control provides a means of *directly encoding the fixed point of the hybrid zero mechanics* and thus creating hybrid periodic orbits by construction. Figure 7.1 shows an example of one such periodic orbit in the Hybrid Walking Mechanics. To create this orbit, Mechanics-Based Control leverages properties of the Hybrid Walking Mechanics, as discussed in Chapter 6. In particular, Mechanics-Based Control uses the controllable kinematics to regulate the hybrid evolution of the uncontrollable state through manipulation of the reset map. This provides a means of directly driving the post-impact state – the forward component of the COM and the angular momentum about the support pivot after impact – to a specified fixed point, and by doing so, create a stable periodic orbit in the Hybrid Walking Mechanics by construction.

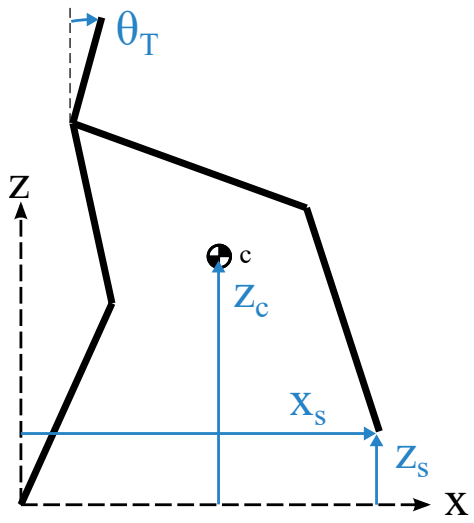

Figure 7.2: Controlled kinematic quantities in Mechanics-Based Control

7.1.2 Mechanics-Based Control Outputs

Mechanics-Based Control uses the "controllable kinematics" to regulate the hybrid evolution of the uncontrollable states – the transfer of COM and angular momentum from one support pivot to the next. For the planar five-link biped, Mechanics-Based Control is ultimately manifested in the construction of desired outputs for the robot's foot position, vertical center of mass and torso orientation – kinematic quantities which are shown in Figure 7.2. In particular, as discussed in Section 6.3, the post-impact values of the horizontal COM position and angular momentum can be manipulated by controlling the pre-impact step length and vertical center of mass velocity according to the discrete mechanics (3.22). These impact mechanics provide a set of "boundary conditions" on the endpoints of the desired trajectories for the swing foot and vertical center of mass. Mechanics-Based Control prescribes a means of designing parameterized basis functions for the controllable kinematics whose coefficients encode the goal of simultaneously swinging the leg forward while also ensuring that the uncontrolled coordinates are regulated in the hybrid evolution of the system. In this design the coefficients of the desired functions are dynamically updated during the continuous-time phase based on a dynamically updating, forward horizon estimate of the pre-impact zero mechanics.

7.1.3 Forward Horizon Estimate of the Zero Mechanics

A challenge with underactuated walking is that the robot control system is only *partially feedback linearizable* – meaning that the robot's behavior can only be *partially encoded* through output design. In the specific robot of interest, underactuation results in two uncontrolled states – the forward COM and angular momentum about the support pivot – whose evolution is *implicitly designed* through choice of initial condition and design of the continuous-time outputs. Guaranteeing the behavior of this system traditionally requires use of nonlinear programming wherein the nonlinear zero dynamics are numerically integrated for each "guess" of controller parameters. However, the mechanics-based interpretation of the zero dynamics of walking allows one to approximate the behavior of the nonlinear system with the Linear Inverted Pendulum, as discussed in section 6.1.2. This allows provides a means of, at every time-step, recalculating a forward horizon estimate of the zero mechanics coordinates using the exact solution of the linear system. While this estimate is only an approximation of the behavior of the nonlinear system, it becomes increasingly accurate as the time-horizon shrinks.

7.1.4 Implementation via Continuous-Time Control

The outputs for the robot's foot position, vertical center of mass and torso orientation, designed with the forward horizon estimate of the Zero Mechanics, simultaneously encode the desired continuous-time and the desired discrete-time evolution of the system. Using standard nonlinear control – such as Feedback Linearization [86] – to stabilize outputs of this form results in stable periodic walking in simulation for a range of controller parameters. Continuous-time control methods, such as pole-placement or Rapidly Exponentially Stabilizing Control Lyapunov functions, can be used to exponentially stabilize the MBC outputs. Alternatively, Model Predictive Control can be used to produce a stabilizing output dynamics consistent with torque limits and momentum transfer constraints. This alternative is discussed in greater detail in Section 8.2.

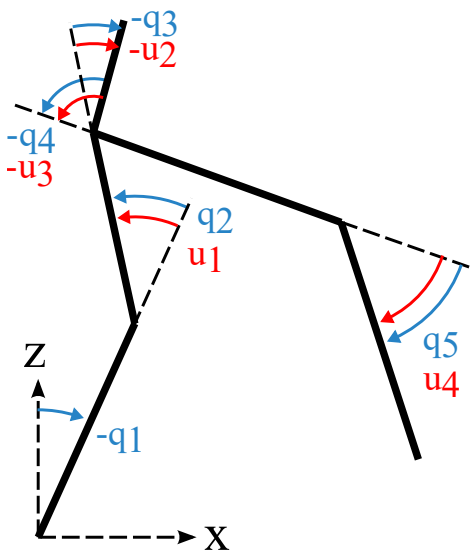

Figure 7.3: Degrees of freedom and actuator input coordinate definitions for the five-link biped

7.2 Internal Model

The methods described in Chapter 3 are used to construct the model of the five-link underactuated biped that is used as the internal model in Mechanics-Based Control. The robot, shown in Fig. 7.3, is modeled as a rigid-body tree comprised of five links and four actuators, as in [97]. The base of the tree is located at the bottom of the support leg; it is assumed that sufficient friction prevents the support leg from sliding on the ground and from rotating about the axis perpendicular to the ground (the $\hat{z}$ axis), and in the context of planar walking, the rotation about the forward axis, $\hat{x}$, is also fixed. One unactuated rotation, $\mathbf{q_u} = q_1$, is used to describe the rotation of the support calf about the world $\hat{y}$ axis; and four relative (intrinsic) rotations, $\mathbf{q_a} = (q_2, q_3, q_4, q_5)^T$, are used to describe the actuated joint angles, which are acted upon by joint torques $\mathbf{u} = (u_1, u_2, u_3, u_4)^T$, in order. The collection of unactuated and actuated angles will often be referred to as a single, "joint angle' vector $\mathbf{q} = (q_1, q_2, \ldots, q_5)^T$. This section discusses properties of the model that will be used in the construction of the proposed mechanics-based control approach to walking.

7.2.1 Equations of motion

As in [36], the equations of motion for this system are obtained through the Euler-Langrange method. Letting T denote the kinetic energy and V denote the potential energy in the system, the Euler-Lagrange equations take the form

$$\frac{d}{dt}\left(\frac{\partial T}{\partial \dot{\mathbf{q}}_\mathbf{u}}\right) - \frac{\partial (T-V)}{\partial \mathbf{q}_\mathbf{u}} = \mathbf{0}, \tag{7.1}$$

$$\frac{d}{dt}\left(\frac{\partial T}{\partial \dot{\mathbf{q}}_\mathbf{a}}\right) - \frac{\partial (T-V)}{\partial \mathbf{q}_\mathbf{a}} = \mathbf{u}, \tag{7.2}$$

and can be rearranged to the "standard" matrix form

$$D(\mathbf{q}) \begin{bmatrix} \ddot{\mathbf{q}}_\mathbf{u} \\ \ddot{\mathbf{q}}_\mathbf{a} \end{bmatrix} + CG(\mathbf{q}, \dot{\mathbf{q}}) = \begin{bmatrix} \mathbf{0} \\ \mathbf{u} \end{bmatrix}, \tag{7.3}$$

where $D(\mathbf{q})$ is often termed the generalized inertia matrix and $CG(\mathbf{q}, \dot{\mathbf{q}})$ is a vector of Coriolis and Gravity effects, and $\mathbf{u}$ is a vector of joint torques. Letting $\mathbf{x} = (\mathbf{q}, \dot{\mathbf{q}})$, the equations of motion can be written $\dot{\mathbf{x}} = f(\mathbf{x}) + g(\mathbf{x})\mathbf{u}$.

7.2.2 Impact Model and Coordinate Relabeling

In the model considered, impacts between the robot and the ground cause discrete changes in the robot's linear momentum and joint velocities, resulting in a hybrid system model. This section employs the impact model presented in [36] and described in Section 3.4, wherein impacts are assumed to be perfectly inelastic and to occur over an infinitesimal time. Quantities just-prior to impact are referred to as "pre-impact" and denoted $\square^-$, post-impact quantities are denoted $\square^+$. The discrete change in joint-angle velocities due to impact takes the form

$$\dot{\mathbf{q}}^+ = \Delta(\mathbf{q}^-)\dot{\mathbf{q}}^-, \tag{7.4}$$

see Section 3.4 for the derivation of $\Delta(\mathbf{q}^-)$. As the base of the kinematic chain is located at the support foot, a relabeling procedure is used to "re-base" the coordinates when the robot takes a step. In particular, the joint angles are relabeled according to

$$\mathbf{q}^+ = R\mathbf{q}^- \tag{7.5}$$

where $R \in \mathbb{R}^{5\times 5}$ is the constant matrix defined in (3.18). A key property of this impact model is that the angular momentum about the point of impact is conserved. This fact is exploited in the proposed mechanics-based walking controller.

7.2.3 Hybrid System Model and Walking Gaits

The evolution of the states in this hybrid system can be compactly represented using Poincaré map techniques. In particular, the state of the robot just-prior to impact in the end of the $k+1$th step, $\mathbf{x}^-[k+1]$, is given by

$$\mathbf{x}^-[k+1] = \Delta\left(\mathbf{x}^-[k]\right) + \int_0^{T[k+1]} f(\mathbf{x}(t))dt \tag{7.6}$$

where $T[k+1] = T(\Delta(\mathbf{x}^-[k]))$. In this paper, walking gaits correspond to periodic solutions of the hybrid system which further correspond to fixed points of (7.6); i.e. $\mathbf{x}^-[k+1] = \mathbf{x}^-[k] = \mathbf{x}^*$, for $k = 1, 2, \ldots$ Numeric Poincaré analysis is often used to verify the local stability of a walking gait [34]. As the particular robot considered is underactuated, creating stable walking gaits can be challenging: underactuation corresponds to nonlinear dynamics that are not affected by the robot's motors and thus not locally controllable. A key observation, however, is that one of the components of the underactuated dynamics corresponds to the rate of change of angular momentum about the robot's support pivot. This fact motivates the proposed mechanics-based strategies for designing controller outputs which leverage properties of the angular momentum about the stance pivot in order to stabilize walking as discussed in the following sections.

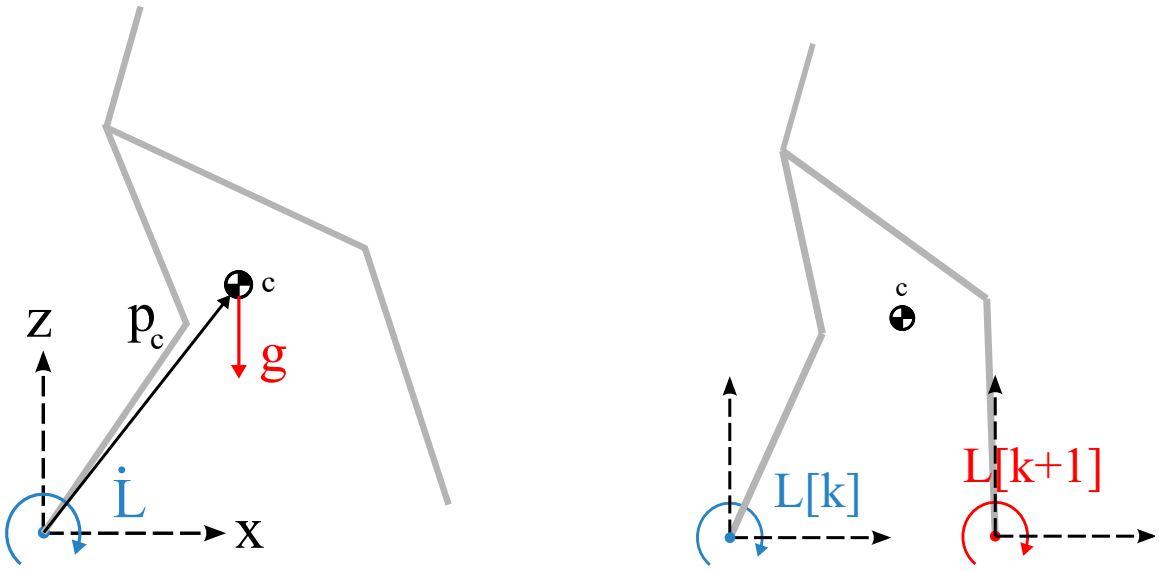

Figure 7.4: (Left) In the continuous-time walking mechanics, Newton's second law dictates that the rate of change of angular momentum about the support pivot in underactuated walking is only influenced by gravity acting at the robot's center of mass and hence, it is locally uncontrollable. The key to stabilizing walking through Mechanics-Based Control is by regulating the transfer of angular momentum from one support pivot to the next (Right).

7.3 Underactuated Hybrid Walking Mechanics

The robot model of interest is a nonlinear hybrid system. Producing walking controllers for this type of system has historically required use of nonlinear optimization; however, this Dissertation leverages properties of the mechanics of the model to construct walking gaits and stabilizing controllers without the use of (offline) optimization. In Chapter 6, is shown that a modification of the Linear Inverted Pendulum can be used to characterize the evolution of the forward COM position and angular momentum about the support pivot in the (nonlinear) underactuated walking model. Additionally, as discussed in Chapter 3, conservation of angular momentum is used to derive an exact expression for the transfer of angular momentum from one leg to the next. These properties are used in the construction of the proposed Mechanics-Based Control method.

7.3.1 Angular Momentum

In the planar model of walking, the rotations about the forward, x, and the vertical, z, axes are constrained to be constant. However, the robot is free to pivot about the lateral, y, axis. The (mass-normalized) angular momentum, L, corresponding to this rotation is

$$L = z_c \dot{x}_c - x_c \dot{z}_c + H, \tag{7.7}$$

where x_c and z_c are the forward and vertical components of the robot's center of mass relative to the support pivot and H is the (mass-normalized) centroidal angular momentum. Application of Newton's second law dictates that the instantaneous rate of change of angular momentum about the support pivot point is a passive quantity given by

$$\dot{L} = g x_c \tag{7.8}$$

where g is the constant acceleration due to gravity. This fact plays a large role in the proposed mechanics-based controller.

7.3.2 Momentum Transfer

Let x_s denote the horizontal position of the swing foot relative to the support pivot. When the swing foot impacts the ground, support of the robot transfers from the current support pivot to the point of impact. The corresponding transfer of angular momentum about the current pivot, $L[k]$, $k \in \mathbb{N}_0$, to angular momentum about the next pivot point, $L[k+1]$, can be obtained through direct computation

$$L[k+1] = L[k] + x_s[k] s \dot{z}_c[k]. \tag{7.9}$$

Furthermore, as angular momentum is conserved about the point of impact in the model of interest, (7.9) can be used to obtain the post-impact angular momentum about the new

pivot as a function of the pre-impact state

$$L^+[k+1] = L^-[k] + x_s^-[k]\dot{z}_c^-[k]. \tag{7.10}$$

Similarly, the center of mass relative to the support foot undergoes a discrete change at impact due to support change:

$$x_c^+[k+1] = x_c^-[k] - x_s^-[k]. \tag{7.11}$$

Continuous-time controllers for x_s and z_c will be designed to achieve pre-impact values, $x_s^-[k]$ and $\dot{z}_c^-[k]$, corresponding to desired $(x_c^+[k+1], L_y^+[k+1])$ using (7.10) and (7.11). An output for z_s will ensure the swing foot hits the ground according to the desired transfer of forward momentum.

It is important to reiterate that the rate of change of angular momentum about the stance pivot is *independent* of the torques applied by the robot's actuators; thus, (7.8) and (7.10) are a key components of *all underactuated walking behaviors*. While the continuous-time evolution of L is uncontrollable, the hybrid evolution of L can be controlled through control of x_n and $\dot{z}_c$ using (7.10), (7.11) and the following qualitative characterization of the continuous-time angular momentum.

7.3.3 Continuous-Time Angular Momentum Characterization

The Linear Inverted Pendulum is traditionally used to estimate the evolution of the robot's forward COM velocity; however, this Dissertation presents a variation of the LIP which instead predicts the evolution of the angular momentum about the support pivot. Recall that in the underactuated robot model, the rate of change of angular momentum (7.1) is a nonlinear expression given by

$$z_c\ddot{x}_c - x_c\ddot{z}_c + \dot{H} = gx_c. \tag{7.12}$$

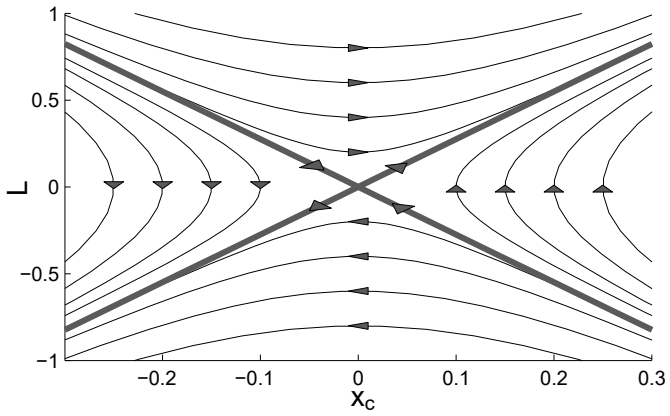

Figure 7.5: Phase space of the angular momentum variant of the Linear Inverted Pendulum

An angular momentum variant of the Linear Inverted Pendulum model can be obtained from (7.12) by setting the vertical height of the center of mass to a constant $z_c \equiv z_0$, thus $\ddot{z}_c \equiv 0$, and by setting $\dot{H}_y = 0$. These constraints yield the following linear system

$$L = z_0 \dot{x}_c, \tag{7.13}$$

$$\dot{L} = g x_c, \tag{7.14}$$

The phase space of the angular momentum LIP – shown in Fig. 7.5 – provides a qualitative characterization of the evolution of L and x_c in the nonlinear system for $z_c \dot{x}_c >> -x_c \dot{z}_c + H_c$. Note that the asymptotes $L = \pm z_0 \sqrt{g/z_0} x_c$ divide the phase space into four quadrants, and that the top quadrant corresponds to forward walking. This characterization suggests that in order to ensure forward walking in the nonlinear hybrid system model (7.6), the post-impact x_c^+ and L^+ should always take values in the top quadrant of the LIP phase space. The proposed mechanics-based control method for walking will leverage this characterization by ensuring that the initial condition (post-impact center of mass and angular momentum) is always within the region of the phase space corresponding to forward walking – this will be achieved through use of the momentum transfer equation (7.10) and (7.11) which provides a means of manipulating the post-impact center of mass and angular momentum as a function of the robot's step length and vertical COM velocity.

7.4 Mechanics-Based Output Design

This section presents the main contribution of the paper: a controller which stabilizes underactuated robotic walking by operating on the transfer of angular momentum from one leg to the next. The goal will be to construct continuous-time desired trajectories for the robot's swing leg and vertical center of mass – which update continuously as the center of mass and angular momentum evolve – to effect a desired transfer of angular momentum through foot impact and then stabilize to these trajectories via nonlinear control. The final form of the outputs to be constructed is

$$\mathbf{y}(\mathbf{q}, \dot{\mathbf{q}}) = \begin{bmatrix} x_s(\mathbf{q}) \\ z_s(\mathbf{q}) \\ z_c(\mathbf{q}) \\ \theta_T(\mathbf{q}) \end{bmatrix} - \begin{bmatrix} x_s^d(x_c(\mathbf{q}), \mathbf{k_x}(\mathbf{q}, \dot{\mathbf{q}})) \\ z_s^d(x_c(\mathbf{q}), \mathbf{k_z}(\mathbf{q}, \dot{\mathbf{q}})) \\ z_c^d(x_c(\mathbf{q}), \mathbf{k_c}(\mathbf{q}, \dot{\mathbf{q}})) \\ 0 \end{bmatrix} \tag{7.15}$$

where $x_s^d(x_c, \mathbf{k_x})$ and $z_s^d(x_c, \mathbf{k_z})$ are desired trajectories for the horizontal and vertical components of the swing foot, and $z_c^d(x_c, \mathbf{k_c})$ is a desired trajectory for the vertical center of mass. Coefficients $\mathbf{k}_\square(\mathbf{q}, \dot{\mathbf{q}})$ of the desired trajectories in (7.15) will be designed to connect initial values for the swing leg and vertical center of mass to desired pre-impact values of these quantities corresponding to a prescribed transfer of angular momentum using the COM and momentum transfer equations. These coefficients are continuously updated based on a running estimate of the pre-impact COM and momentum. The last output encodes the auxiliary goal of keeping an upright torso by driving θ_T to zero. Figure 7.2 shows the kinematic quantities controlled in continuous-time under Mechanics-Based Control.

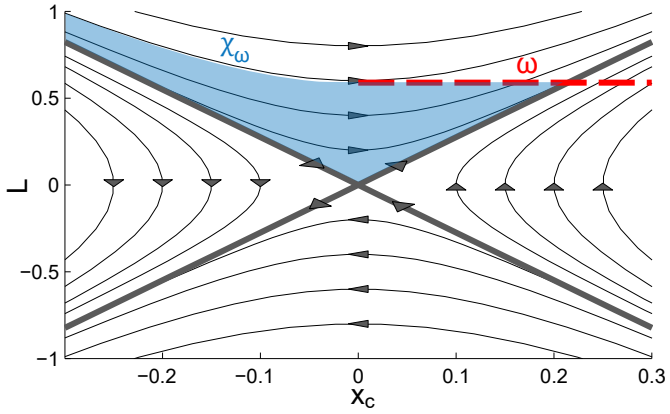

Figure 7.6: The set of states corresponding to forward walking in the representative hybrid system for the forward COM and angular momentum about the robot's support pivot

7.4.1 Desired Momentum Transfer and Pre-Impact Kinematics

To stabilize walking, the proposed mechanics-based control approach dictates desired values for the post-impact horizontal component of the center of mass, $x_c^+[k+1] = x_c^*$, and the angular momentum about the support pivot, $L[k+1] = L^*$. The desired x_c^* is realized through the use of (7.11) in the construction of desired trajectories for the swing leg that satisfy the following conditions when the robot's COM reaches a pre-impact value x_c^-

$$x_s^d(x_c^-, \mathbf{k_x}(\mathbf{q}^-, \dot{\mathbf{q}}^-)) = x_c^- - x_c^*, \tag{7.16}$$

$$z_s^d(x_c^-, \mathbf{k_z}(\mathbf{q}^-, \dot{\mathbf{q}}^-)) = 0. \tag{7.17}$$

Similarly, a desired transfer of forward momentum from a pre-impact value L^- to the desired post-impact value L^* is realized using (7.10) via the following condition

$$\dot{z}_c^d(x_c^-, \mathbf{k_c}(\mathbf{q}^-, \dot{\mathbf{q}}^-)) = \frac{L^* - L^-}{x_c^- - x_c^*}. \tag{7.18}$$

Note that these "boundary conditions" are functions of (x_c^-, L^-), which are unknown in general; however, the following section describes a method of continuously estimating x_c^- for a fixed value of L^- using the Linear Inverted Pendulum.

7.4.2 Forward Horizon Estimate of the Zero Mechanics

Note that the boundary conditions outlined in the previous section are functions of the pre-impact values x_c^- and L^-, which are generally unknown during the continuous-time evolution of the controller. However, by making – and enforcing – the design choice that continuous-time phase of the gait will end when the angular momentum reaches a a particular value, $L^- = \omega$, where $\omega > 0$ is a design variable, we can use the solution to the LIP dynamics (7.13)–(7.14) to calculate a running estimate $\hat{x}_c^-$ of the corresponding value of the horizontal center of mass at the end of the continuous-time phase, x_c^-, based on the current measurements of $x_c(\mathbf{q})$ and $L(\mathbf{q}, \dot{\mathbf{q}})$. In particular, $\hat{x}_c^-(\mathbf{q}, \dot{\mathbf{q}})$ is given by

$$\hat{x}_c^-(\mathbf{q}, \dot{\mathbf{q}}) = \sqrt{\frac{\omega^2}{gz_0} - \frac{L^2(\mathbf{q}, \dot{\mathbf{q}})}{gz_0} + x_c^2(\mathbf{q})}. \tag{7.19}$$

This value is estimated continuously throughout the step, and converges to the value of $x_c(\mathbf{q})$ in the nonlinear system as $L(\mathbf{q}, \dot{\mathbf{q}})$ approaches ω.

To reiterate a key property of this running estimate: while the forward evolution of x_c in the nonlinear system will differ from the solution to the corresponding LIP dynamics, if the robot reaches a state where $L(\mathbf{q}, \dot{\mathbf{q}}) = \omega$, *the proposed estimate will be equal to the true value in the nonlinear system*, i.e. $\hat{x}_c^-(\mathbf{q}, \dot{\mathbf{q}}) = x_c(\mathbf{q})$. As discussed in the next section, the desired output for the height of the swing foot is designed so that the robot's swing foot impacts the ground when $L(\mathbf{q}, \dot{\mathbf{q}}) = \omega$. Hence, the running estimate $\hat{x}_c^-(\mathbf{q}, \dot{\mathbf{q}})$ can be substituted for x_c^- in the boundary conditions (7.16), (7.17) and (7.18) and used, in conjunction with additional boundary constraints, to dynamically calculate the coefficients $\mathbf{k_x}$, $\mathbf{k_z}$, and $\mathbf{k_c}$ to simultaneously encode a desired continuous-time walking behavior and a desired transfer of COM and angular momentum.

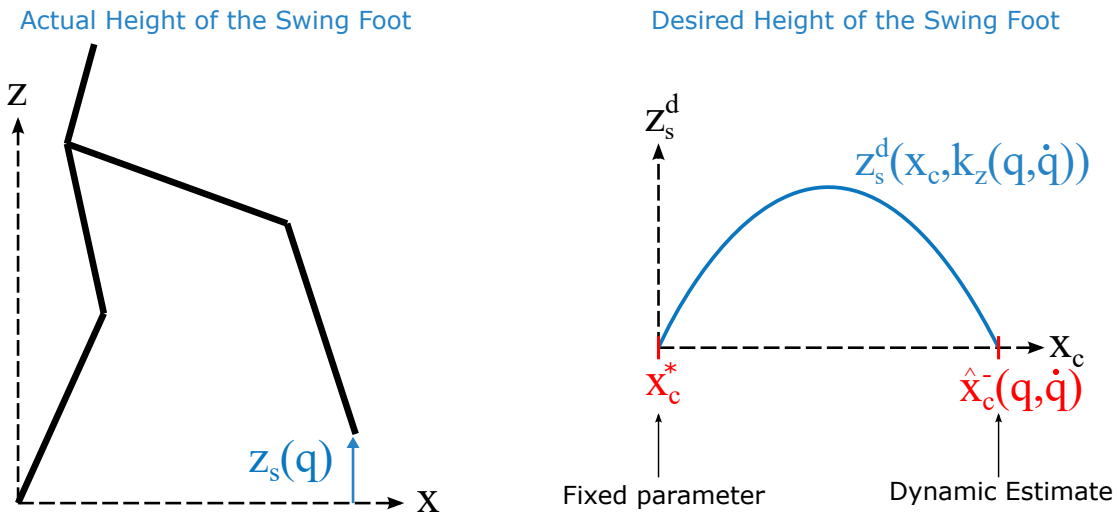

Figure 7.7: (Left) Actual height of the swing foot output and (Right) properties of the desired height of the swing foot output

7.4.3 Height of the Swing Foot Output Constraints

The output for the height of the swing foot is given by

$$y_z = z_s(\mathbf{q}) - z_s^d(x_c(\mathbf{q}), \mathbf{k_z}(\mathbf{q}, \dot{\mathbf{q}})). \tag{7.20}$$

There is freedom in the choice of basis function used to encode the desired swing height behavior, $z_s^d(x_c(\mathbf{q}), \mathbf{k_z}(\mathbf{q}, \dot{\mathbf{q}}))$. Suitable choices include the quadratic and the sine function. This section presents constraints on z_s^d that are necessary in Mechanics-Based Control and which can be implemented through any suitable basis function.

In Mechanics-Based Control, a desired trajectory for the height of the swing foot is designed to keep the foot above the ground until the angular momentum reaches a specified value, $L = \omega > 0$, at which point the foot is forced to impact the ground. This prescribed behavior is implemented through a set of constraints on the desired output which use the forward horizon estimate of the center of mass, (7.19), proposed in the previous section. In particular, coefficients $\mathbf{k_z}(\mathbf{q}, \dot{\mathbf{q}})$ of the desired swing height function must satisfy the

following boundary constraints at each $(\mathbf{q}, \dot{\mathbf{q}})$ along the continuous-time flow of the system:

$$z_s^d(x_c^+, \mathbf{k_z}(\mathbf{q}, \dot{\mathbf{q}})) = 0, \tag{7.21}$$

$$z_s^d(\hat{x}_c^-(\mathbf{q}, \dot{\mathbf{q}}), \mathbf{k_z}(\mathbf{q}, \dot{\mathbf{q}})) = 0. \tag{7.22}$$

The constraint (7.21) corresponds to the desired swing foot being zero at the beginning of a step, and the constraint (7.22) corresponds to the desired swing foot impacting the ground when the COM reaches the running estimate $\hat{x}_c^-(\mathbf{q}, \dot{\mathbf{q}})$. As mentioned in the previous section, the latter constraint corresponds to a pre-impact state wherein the angular momentum reaches the desired value $L^- = \omega$. In addition to these boundary conditions, the desired function must also be designed so that the foot does not impact the ground early, i.e. $\mathbf{k_z}(\mathbf{q}, \dot{\mathbf{q}})$ must also satisfy following constraint

$$z_s^d(x_c, \mathbf{k_z}(\mathbf{q}, \dot{\mathbf{q}})) > 0, \qquad x_c^+ < x_c < \hat{x}_c^-(\mathbf{q}, \dot{\mathbf{q}}) \tag{7.23}$$

Note that these constraints (7.21)–(7.23) on the desired swing foot height can be encoded in closed-form through simple basis functions, such as a quadratic function of the center of mass or through use of a sine function.

Using continuous-time control to exponentially stabilize a swing foot height output of the form (7.20) wherein the desired foot height satisfies (7.21)–(7.23) ensures that the robot's foot strikes the ground when $L^- = \omega$. Under these conditions, the function $\hat{x}_c^-(\mathbf{q}, \dot{\mathbf{q}})$ can be similarly used to construct constraints on the robot's step length and vertical center of mass outputs which encode a desired transfer of COM and angular momentum – and ultimately stabilize walking – as described in the following sections.

7.4.4 Step Length Output Constraints: Encoding COM Transfer

Mechanics-Based Control stabilizes walking by driving the post-impact COM position relative to the support pivot and the angular momentum about the support pivot to desired values. In particular, the robot's post-impact COM position relative to the support pivot is manipulated through design of an output for the robot's step length

$$y_x = x_s(\mathbf{q}) - x_s^d(x_c(\mathbf{q}), \mathbf{k_x}(\mathbf{q}, \dot{\mathbf{q}})). \tag{7.24}$$

As in the swing foot height output construction, there is freedom in the choice of basis function used to encode the desired step length behavior, $x_s^d(x_c(\mathbf{q}), \mathbf{k_x}(\mathbf{q}, \dot{\mathbf{q}}))$. Suitable choices for the step length include linear and cubic functions of x_c. This section presents constraints on x_s^d that encode a desired transfer of COM from one step to the next.

Given a desired value for the post-impact COM, x_c^*, the corresponding pre-impact step length can be calculated using the boundary condition (7.16). Substituting the estimate of the pre-impact COM in (7.16), together with a constraint on the step length at the beginning of the step, yields constraints on the desired step length output:

$$x_s^d(x_c^+, \mathbf{k_x}(\mathbf{q}, \dot{\mathbf{q}})) = x_s^+, \tag{7.25}$$

$$x_s^d(\hat{x}_c^-(\mathbf{q}, \dot{\mathbf{q}}), \mathbf{k_x}(\mathbf{q}, \dot{\mathbf{q}})) = x_c^- - x_c^*, \tag{7.26}$$

where x_c^+ and x_s^+ are fixed measurements of the robot's COM and step length at the beginning of a step. Note that these constraints can be encoded in closed form through use of linear or cubic basis functions for the desired step length. As mentioned in Section 7.4.1, the desired post-impact x_c^* and angular momentum L^* are chosen to be in the quadrant of the LIP phase space corresponding to forward walking. Exponentially stabilizing a step length output which satisfies (7.26) ultimately drives the system to a post-impact state wherein the center of mass achieves the prescribed value $x_c^+ = x_c^*$.

7.4.5 Height of the COM Output Constraints: Encoding Angular Momentum Transfer

The angular momentum about the support pivot in underactuated walking is locally uncontrollable. Thus, in order to stabilize walking, one must ensure that the hybrid evolution of the angular momentum is well behaved. Towards this end, Mechanics-Based Control regulates the transfer of angular momentum about one support pivot to the next by manipulating the velocity of the vertical component of the COM prior to impact. This section outlines a constraint on the vertical COM output which encodes a desired transfer of angular momentum. The output for the height of the COM is given by

$$y_c = z_c(\mathbf{q}) - z_c^d(x_c(\mathbf{q}), \mathbf{k_c}(\mathbf{q}, \dot{\mathbf{q}})). \tag{7.27}$$

As in the swing foot outputs, there is freedom in the choice of basis function used to construct $z_c^d(x_c(\mathbf{q}), \mathbf{k_c}(\mathbf{q}, \dot{\mathbf{q}}))$. Choosing to drive the COM to a constant height results in Linear Inverted Pendulum behavior, however, simulation results suggest that adding oscillation to a nominally constant COM height can greatly reduce the torque requirements of the gait.

Recall that the height of the swing foot is designed to cross zero when the angular momentum reaches a specified pre-impact value $L^- = \omega > 0$, and at this point, the estimate $\hat{x}_c^-(\mathbf{q}, \dot{\mathbf{q}})$ and the actual forward COM position, x_c^-, are equivalent. Substituting these two conditions into (7.18), and choosing a desired post-impact COM and angular momentum (x_c^*, L^*), yields the following constraint on the vertical COM output

$$\dot{z}_c^d(\hat{x}_c^-(\mathbf{q}, \dot{\mathbf{q}}), \mathbf{k_c}(\mathbf{q}, \dot{\mathbf{q}})) = \frac{L^* - \omega}{\hat{x}_c^-(\mathbf{q}, \dot{\mathbf{q}}) - x_c^*}. \tag{7.28}$$

Exponentially stabilizing a vertical COM output (7.27) that satisfies (7.28) ultimately regulates the transfer of angular momentum from one support pivot to the next. Moreover, this condition – and hence hybrid stability – can be encoded *in closed form* through use of a suitable basis function, such as a sine function with a constant offset.

7.4.6 Torso Output Construction

In the context of this Dissertation, the torso is an "auxiliary" degree of freedom which does not directly influence the stability of a walking gait. As such, consider the simplest choice of torso output is given by

$$y_T = \theta_T(\mathbf{q}) - 0, \tag{7.29}$$

where $\theta_T = -q_1 - q_2 - q_3$ describes the orientation of the robot's torso with respect to the fixed world frame. The output (7.29) encodes the goal of maintaining an upright torso – a suitable condition on the nominal forward walking gaits considered in this Dissertation.

A goal of future work is to investigate how to utilize the torso output to manipulate the centroidal angular momentum. Indeed, one hypothesis is that for many robots the torso output may be a dominant component of the centroidal angular momentum. Thus, the choice of maintaining an upright torso corresponds to a relatively small magnitude of the centroidal angular momentum – which coupled with a nominally constant height of the center of mass – corresponds to dynamics that are qualitatively similar to the Linear Inverted Pendulum. Further understanding of the continuous-time mechanics may provide information about how to use the torso to manipulate the centroidal angular momentum to achieve dynamics that are qualitatively different from the Linear Inverted Pendulum.

7.5 Properties of Closed-Loop Mechanics-Based Control

The goal of this section is to analyze the behavior of the planar, five-link underactuated biped under Mechanics-Based Control. As mentioned in Chapters 3 and 5, the robot is modeled as an articulated rigid body whose motion can be represented via a hybrid control system $\mathscr{HC}$ of the form

$$\mathscr{HC} = \begin{cases} \dot{\mathbf{x}} = f(\mathbf{x}) + g(\mathbf{x})\mathbf{u} & \mathbf{x}^- \notin S \\ \mathbf{x}^+ = \Delta(\mathbf{x}^-) & \mathbf{x}^- \in S \end{cases}, \tag{7.30}$$

wherein the states $\mathbf{x} = (\mathbf{q}, \dot{\mathbf{q}}) \in \mathbb{R}^{10}$ are the joint angles and angular velocities, $\mathbf{u} \in \mathbb{R}^4$ are the torques applied at the joints and the control system (f, g) is obtained through computation of the rigid-body dynamics as in (4.1). The guard S and reset map Δ of $\mathscr{HC}$ model the collisions between the robot and the walking surface, as described in Chapter 5.

The robot of interest has five degrees of freedom but only four actuators and as such, it is underactuated. As a result, two of the ten states are locally uncontrollable in the control system $\dot{\mathbf{x}} = f(\mathbf{x}) + g(\mathbf{x})\mathbf{u}$ of the hybrid model $\mathscr{HC}$. It follows that to stabilize the hybrid model of underactuated walking, continuous-time controllers of the form $\mathbf{u}(x)$ must regulate the hybrid evolution of the locally uncontrollable modes while also driving the controllable modes into a desired walking motion. Designing controllers to simultaneously meet these two specifications has historically required using nonlinear programming to search for viable controller parameters; however, by expressing the uncontrollable modes in terms of the mechanics of the system, as discussed in Chapter 6, a new strategy for stabilizing this system (one that does not require solution of a nonlinear program) emerges: regulate the transfer of angular momentum and forward center of mass position from one support pivot to the next. Properties of the rigid-body collision model and reset map illuminate a means of manipulating the transfer of angular momentum and center of mass position from one step to the next by manipulating the robot's controllable kinematics just prior to impact

events. Section 7.4 shows how to use this relationship between the controllable kinematics and momentum transfer to construct Mechanics-Based Control outputs $\mathbf{y}_{\mathrm{MBC}}(\mathbf{q}, \dot{\mathbf{q}})$ of the form (7.15), stated again for reference:

$$\mathbf{y}_{\mathrm{MBC}}(\mathbf{q}, \dot{\mathbf{q}}) = \begin{bmatrix} x_s(\mathbf{q}) \\ z_s(\mathbf{q}) \\ z_c(\mathbf{q}) \\ \theta_T(\mathbf{q}) \end{bmatrix} - \begin{bmatrix} x_s^d(x_c(\mathbf{q}), \mathbf{k_x}(\mathbf{q}, \dot{\mathbf{q}})) \\ z_s^d(x_c(\mathbf{q}), \mathbf{k_z}(\mathbf{q}, \dot{\mathbf{q}})) \\ z_c^d(x_c(\mathbf{q}), \mathbf{k_c}(\mathbf{q}, \dot{\mathbf{q}})) \\ 0 \end{bmatrix}. \tag{7.31}$$

The outputs $\mathbf{y}_{\mathrm{MBC}}(\mathbf{q}, \dot{\mathbf{q}})$ simultaneously encode the continuous-time controlled behavior and a desired hybrid evolution of the locally uncontrollable modes in the system – the forward position of the center of mass x_c and the angular momentum about the support pivot L. To achieve a specified transfer of angular momentum and center of mass, the desired functions and their coefficients must satisfy the boundary conditions (7.21)–(7.23), (7.25)–(7.26), and (7.28). Feedback Linearization [86] is used to enforce the behavior prescribed by the outputs on the control system of $\mathscr{HC}$. The MBC output vector (7.31) has relative degree two [86] along the rigid body dynamics, as the dependence on $\dot{\mathbf{q}}$ appears via the angular momentum and the time-derivative of the angular momentum is independent of the joint torques. As such, the (partial) Feedback Linearization control law $\mathbf{u}_{\mathrm{MBC}}$ corresponding to $\mathbf{y}_{\mathrm{MBC}}(\mathbf{q}, \dot{\mathbf{q}})$ is

$$\mathbf{u}_{\mathrm{MBC}}(\mathbf{q}, \dot{\mathbf{q}}) = L_g L_f \mathbf{y}_{\mathrm{MBC}}^{-1}(\mathbf{q}, \dot{\mathbf{q}}) \left(-L_f^2 \mathbf{y}_{\mathrm{MBC}}(\mathbf{q}, \dot{\mathbf{q}}) + \mu \right), \tag{7.32}$$

where $L_g L_f \mathbf{y}_{\mathrm{MBC}}$ and $L_f^2 \mathbf{y}_{\mathrm{MBC}}$ are Lie derivatives of the (relative degree two) outputs along the rigid body dynamics and care has to be made to ensure that $L_g L_f \mathbf{y}_{\mathrm{MBC}}$ is invertible. In this section, we assume that the stabilizing linear feedback μ in (7.32) is obtained through construction of a RES-CLF, V_ε, as discussed in Section 4.4. Thus, an exponentially

stabilizing μ is selected from the set $K_\varepsilon(\eta)$, stated again for reference

$$K_\varepsilon(\eta) := \{\mu : L_F V_\varepsilon(\eta) + L_G V_\varepsilon(\eta)\mu + \varepsilon c_3 V_\varepsilon(\eta_x) \leq 0\}, \tag{7.33}$$

where $\eta = (\mathbf{y}_{\text{MBC}}, \dot{\mathbf{y}}_{\text{MBC}})^T$. Applying (7.32) with $\mu \in K_\varepsilon(\eta)$ to the control system in (7.30) results in the closed-loop dynamics, $f_{\text{MBC}}(\mathbf{x})$, given by

$$f_{\text{MBC}}(\mathbf{x}) := f(\mathbf{x}) + g(\mathbf{x})\mathbf{u}_{\text{MBC}}(\mathbf{x}), \tag{7.34}$$

and corresponding closed-loop hybrid system, $\mathscr{H}_{\text{MBC}}$, given by

$$\mathscr{H}_{\text{MBC}} = \begin{cases} \dot{\mathbf{x}} = f_{\text{MBC}}(\mathbf{x}) & \mathbf{x}^- \notin S \\ \mathbf{x}^+ = \Delta(\mathbf{x}^-) & \mathbf{x}^- \in S \end{cases}. \tag{7.35}$$

As discussed in Chapter 5, associated with $\mathscr{H}_{\text{MBC}}$ is the Time-to-Impact (partial) function

$$T_I(\mathbf{x}_0) = \inf\{t \geq 0 : \phi_t(\mathbf{x}_0) \in S\}. \tag{7.36}$$

The goal of this section is to establish conditions under which $\mathscr{H}_{\text{MBC}}$ has a stable periodic orbit (i.e. conditions for stable walking under Mechanics-Based Control). Lemmas 1 and 2 show that, due to the construction of the outputs in Mechanics-Based Control, the norm of the error between desired and actual pre-impact and post-impact values of the unactuated states is proportional to the norm of the pre-impact value of the outputs. Theorems 2 and 3 uses the results of Lemmas 1 and 2 to reason about hybrid executions in the system under the assumption that the robot's forward velocity is always positive. In practice, this condition is often met by choosing the desired post-impact point $(x_c^*, L^*) \in \mathcal{X}_\omega$, where $\mathcal{X}_\omega$ is the set of points that generate periodic orbits (i.e. correspond to forward walking) in the Hybrid Zero Mechanics, as described in Chapter 6.

7.5.1 Pre-Impact Properties of Closed-Loop Mechanics-Based Control

The following Lemma describes bounds on the pre-impact values of the uncontrolled modes (the forward center of mass position and the angular momentum about the support pivot) which result from the construction of the Mechanics-Based Control output for the height of the swing foot, as described in Section 7.4.3. In particular, it is shown that in pre-impact states under Mechanics-Based Control, the error in the COM estimate and the error between the desired and actual pre-impact angular momentum are both proportional to the error in the controlled outputs. These properties, together with properties of exponentially stabilizing nonlinear control, will be used to construct statements regarding the stability of walking gaits under Mechanics-Based Control.

Lemma 1. *Consider a closed-loop hybrid system under Mechanics-Based Control, $\mathscr{H}_{\mathrm{MBC}}$, of the form* (7.35) *with design parameter $\omega > 0$. Let $\mathbf{x}^+ = (\mathbf{q}^+, \dot{\mathbf{q}}^+)$ be an initial condition for this system such that the time-to-impact* (7.36) *– computed on the flow $\phi_t(\mathbf{x}^+)$ of the dynamical system in $\mathscr{H}_{\mathrm{MBC}}$ – is finite, i.e. $T_I(\mathbf{x}^+) < \infty$. Let $\mathbf{x}^- = \phi_{T_I(\mathbf{x}^+)}(\mathbf{x}^+) \in S$ denote the "pre-impact" state at the end of the continuous-time phase starting from $\mathbf{x}^+$. At this pre-impact state, the dynamic estimate of the COM $\hat{x}_c^-$, computed via* (7.19)*, satisfies*

$$\|\hat{x}_c^- - x_c^-\| \leq \frac{1}{L_{z_s}} \|\eta^-\|, \tag{7.37}$$

where $x_c^- = x_c(\mathbf{q}^-)$ and $\eta^- = \eta(\mathbf{q}^-, \dot{\mathbf{q}}^-)$ and L_{z_s} is the Lipschitz constant of the desired swing height function. Additionally, the error between the pre-impact angular momentum $L^- = L(\mathbf{q}^-, \dot{\mathbf{q}}^-)$ and the specified termination value ω satisfies

$$\|L^- - \omega\| \leq \frac{1}{L_{\hat{x}}} \frac{1}{L_{z_s}} \|\eta^-\|, \tag{7.38}$$

where $L_{\hat{x}}$ is the Lipschitz constant of the forward COM estimate. ⌟

Proof. Rearranging the terms in the output for the height of the swing foot (7.20) yields an expression for the actual height of the swing foot z_s as a function of the output error y_z and the desired height of the swing foot, z_s^d, as follows

$$z_s(\mathbf{q}) = y_z + z_s^d(x_c(\mathbf{q}), \mathbf{k_z}(\mathbf{q}, \dot{\mathbf{q}})). \tag{7.39}$$

At a pre-impact state, $\mathbf{x}^- = (\mathbf{q}^-, \dot{\mathbf{q}}^-)$, the height of the swing foot is zero, $z_s(\mathbf{q}^-) = 0$, and

$$z_s^d(x_c(\mathbf{q}^-), \mathbf{k_z}(\mathbf{q}^-, \dot{\mathbf{q}}^-)) = -y_z^-. \tag{7.40}$$

Subtracting (7.22) from both sides of (7.40) and taking the norm gives

$$\|z_s^d(x_c^-, \mathbf{k_z}(\mathbf{q}^-, \dot{\mathbf{q}}^-)) - z_s^d(\hat{x}_c^-, \mathbf{k_z}(\mathbf{q}^-, \dot{\mathbf{q}}^-))\| = \|y_z^-\|. \tag{7.41}$$

Assuming the desired swing height function is bi-Lipschitz in a neighborhood of $(\mathbf{q}^-, \dot{\mathbf{q}}^-)$ with associated Lipschitz constant $L_{z_s^d}$ results in

$$\|\hat{x}_c^- - x_c^-\| \leq \frac{1}{L_{z_s^d}} \|z_s^d(x_c^-, \mathbf{k_z}(\mathbf{q}^-, \dot{\mathbf{q}}^-)) - z_s^d(\hat{x}_c^-, \mathbf{k_z}(\mathbf{q}^-, \dot{\mathbf{q}}^-))\| \leq \frac{1}{L_{z_s^d}} \|y_z^-\|. \tag{7.42}$$

Noting that $\|y_z^-\| \leq \|\eta^-\|$, gives the first property (7.37) of the Lemma

$$\|\hat{x}_c^- - x_c^-\| \leq \frac{1}{L_{z_s^d}} \|\eta^-\|. \tag{7.43}$$

Combining (7.43) with (7.19) gives the second property (7.38) of the Lemma

$$\|L^- - \omega\| \leq \frac{1}{L_{\hat{x}_c^-}} \frac{1}{L_{z_s^d}} \|\eta^-\|, \tag{7.44}$$

where $L_{\hat{x}_c^-}$ is the assumed bi-Lipschitz constant of the forward horizon estimate of the center of mass. □

7.5.2 Post-Impact Properties of Closed-Loop Mechanics-Based Control

The Mechanics-Based Control strategy for stabilizing walking is to regulate the hybrid evolution of the uncontrolled states, i.e. to regulate the transfer of the robot's center of mass position and angular momentum from one support pivot to the next. To this end, outputs for the step-length and vertical center of mass position are designed to drive the post-impact COM to a desired value, $x_c^+ \to x_c^*$, and similarly, to drive the post-impact angular momentum to a desired value $L^+ \to L^*$. The following Lemma uses properties of the discrete mechanics (7.10)–(7.11) together with the results from Lemma 1 to establish bounds on the error between the actual and desired post-impact COM and angular momentum values.

Lemma 2. *Consider a closed-loop hybrid system under Mechanics-Based Control, $\mathscr{H}_{\mathrm{MBC}}$, of the form* (7.35) *with design parameter $\omega > 0$ and desired post-impact center of mass $x_c^* < 0$ and angular momentum $L^* > 0$ values. Let $\mathbf{x}_0 = (\mathbf{q}_0, \dot{\mathbf{q}}_0)$ be an initial condition for this system such that the time-to-impact* (7.36) *– computed on the flow $\phi_t(\mathbf{x}_0)$ of the dynamical system in $\mathscr{H}_{\mathrm{MBC}}$ – is finite, i.e. $T_I(\mathbf{x}_0) < \infty$. Let $\mathbf{x}^- = \phi_{T_I(\mathbf{x}_0)}(\mathbf{x}_0) \in S$ denote the "pre-impact" state at the end of the continuous-time phase starting from $\mathbf{x}_0$ and let $\mathbf{x}^+$ denote the "post-impact state" obtained after application of the reset map to $\mathbf{x}^-$, i.e. $\mathbf{x}^+ = \Delta(\mathbf{x}^-)$. If the pre-impact state is bounded, i.e. if there exists an $M > 0$ such that*

$$\max\left(\|x_c^* - x_c^-\|, \left\|\frac{L^* - \omega}{x_c^- - x_c^*}\right\|\right) \leq M, \tag{7.45}$$

where x_c^- and L^- are computed using $\mathbf{x}^-$, then the post-impact center of mass $x_c^+ = x_c(\mathbf{q}^+)$ and angular momentum about the support pivot $L^+ = L(\mathbf{q}^+, \dot{\mathbf{q}}^+)$ satisfy

$$\|x_c^+ - x_c^*\| \leq \left(1 + \frac{1 + L_x}{L_{z_s}}\right)\|\eta^-\|, \tag{7.46}$$

$$\|L^+ - L^*\| \leq \left(3M + \frac{L_c M + L_x M}{L_{z_s}}\right)\|\eta^-\|, \tag{7.47}$$

where $\eta^- = \eta(\mathbf{q}^-, \dot{\mathbf{q}}^-)$ and L_x, L_{z_s}, and L_c are Lipschitz constants for x_s^d, z_s^d and z_c^d. ⌟

Proof. Rearranging the terms in the output for the step-length (7.24) yields

$$x_s(\mathbf{q}) = y_s + x_s^d(x_c(\mathbf{q}), \mathbf{k_x}(\mathbf{q}, \dot{\mathbf{q}})). \tag{7.48}$$

Combining (7.48) with the reset map (7.11) for x_c gives the expression $x_c^+ = x_c^- - y_s^- - x_s^{d-}$, wherein pre-impact quantities $\square^-$ are computed using the pre-impact state, i.e. $x_c^- = x_c(\mathbf{q}^-)$. Rearranging terms in this expression gives

$$x_c^+ - x_c^- + x_s^d(x_c^-, \mathbf{k_x}(\mathbf{q}^-, \dot{\mathbf{q}}^-)) = y_s^-. \tag{7.49}$$

Recall from (7.16) that the desired output for the step length is designed using the forward horizon estimate of the center of mass so that at pre-impact states

$$x_s^d(\hat{x}_c^-, \mathbf{k_x}(\mathbf{q}^-, \dot{\mathbf{q}}^-)) = \hat{x}_c^- - x^*. \tag{7.50}$$

Moreover, assume that x_s^d is Lipschitz continuous with constant L_x so that

$$\|x_s^d(x_c^-, \mathbf{k_x}(\mathbf{q}^-, \dot{\mathbf{q}}^-)) - x_s^d(\hat{x}_c^-, \mathbf{k_x}(\mathbf{q}^-, \dot{\mathbf{q}}^-))\| \leq L_x \|x_c^- - \hat{x}_c^-\|. \tag{7.51}$$

Combining (7.51) with (7.49) and using the triangle inequality yields

$$\left\|x_c^+ - x^*\right\| \leq \|y_s^-\| + (1 + L_x)\|x_c^- - \hat{x}_c^-\| \tag{7.52}$$

Noting that $\|y_s^-\| \leq \|\eta^-\|$ and using Lemma 1 gives the first property of Lemma 2. The second property of Lemma 2 is similarly constructed by assuming Lipschitz continuous $\dot{z}_c^d$, and by using the momentum transfer condition on the desired COM velocity (7.18), using the bound (7.45) assumed in the Lemma, and using the results from Lemma 1. $\square$

7.5.3 Structure of the Hybrid Evolution Under Mechanics-Based Control

The goal of this section is to employ the results of Lemmas 1 and 2 to expose structure in Hybrid Executions of the closed-loop hybrid system under Mechanics-Based Control. The following analysis is based on the assumption that the robot's forward center of mass velocity is positive throughout the steps in the execution. In practice, this condition is often met by choosing the desired post-impact point $(x_c^*, L^*) \in \mathcal{X}_\omega$, where $\mathcal{X}_\omega$ is the set of points that generate periodic orbits (i.e. correspond to forward walking) in the Hybrid Zero Mechanics, as described in Chapter 6. The analysis will assume executions start on the zero dynamics surface associated with the Mechanics-Based Control outputs.

Towards this end, consider a closed-loop hybrid system under Mechanics-Based Control, $\mathscr{H}_{\text{MBC}}$, of the form (7.35) with design parameter $\omega > 0$ and desired post-impact center of mass $x_c^* < 0$ and angular momentum $L^* > 0$ values, and outputs $\mathbf{y}_{\text{MBC}}$. Let $\mathbf{x}_0^+$ be an initial condition for this system on the zero dynamics surface Z_{MBC} associated with $\mathbf{y}_{\text{MBC}}$, i.e. let $\mathbf{x}_0^+ = (\mathbf{q}_0, \dot{\mathbf{q}}_0) \in Z_{\text{MBC}}$ so that

$$\mathbf{y}_{\text{MBC}}(\mathbf{x}_0^+) = \dot{\mathbf{y}}_{\text{MBC}}(\mathbf{x}_0^+) = 0, \tag{7.53}$$

$$x_c(\mathbf{x}_0^+) = x_c^*, \tag{7.54}$$

$$L(\mathbf{x}_0^+) = L^*. \tag{7.55}$$

Under the assumption of positive forward center of mass velocity, it follows that the corresponding time-to-impact (7.36) – computed on the flow $\phi_t(\mathbf{x}_0^+)$ of the dynamical system in $\mathscr{H}_{\text{MBC}}$ – is finite, i.e. $T_I\left(\mathbf{x}_0^+\right) < \infty$. Let $\mathbf{x}_0^- = \phi_{T_I\left(\mathbf{x}_0^+\right)}(\mathbf{x}_0^+) \in S$ denote the "pre-impact" state at the end of the continuous-time phase starting from $\mathbf{x}_0^+$ and let $\mathbf{x_1}^+$ denote the "post-impact state" obtained after application of the reset map to $\mathbf{x}_0^-$, i.e. $\mathbf{x}_1^+ = \Delta(\mathbf{x}_0^-)$. The following Theorem uses the results of Lemma 1 and Lemma 2 to illuminate properties of hybrid executions of $\mathscr{H}_{\text{MBC}}$ starting from $\mathbf{x}_0^+$.

Theorem 2. *Consider a finite execution, $\chi = (\Lambda, \mathcal{I}, \mathcal{C})$, of a hybrid system under Mechanics-Based Control, $\mathscr{H}_{\mathrm{MBC}}$, of the form* (7.35)*, with the desired post-impact point (x_c^*, L^*). Let the initial condition of the execution be $\mathbf{x}_0^+ \in Z_{\mathrm{MBC}}$ as defined in Section 7.5.3 and assume that the robot's forward COM velocity is positive during all $N > 0$ steps in the finite execution χ, so that $\Lambda = \{0, 1, 2, \ldots, N\}$ and $I_{N-1} = [t_{N-1}, t_N]$. Then there exist constants $\beta_1, \beta_2, \beta_3 > 0$ such that for all $i \in \{1, 2, \ldots, N-1\}$*

$$\begin{bmatrix} \|\eta_{i+1}^+\| \\ \|\xi_{i+1}^+ - \xi^*\| \end{bmatrix} \leq A_i \begin{bmatrix} \|\eta_i^+\| \\ \|\xi_i^+ - \xi^*\| \end{bmatrix} + B, \tag{7.56}$$

where

$$A_i = \begin{bmatrix} L_{\Delta_\eta}(\varepsilon\sqrt{\frac{c_2}{c_1}}e^{-\frac{c_3}{2}\varepsilon\Delta T_i} + \beta_1) & L_{\Delta_\eta}e^{\beta_2\Delta T_i} \\ \beta_3\varepsilon\sqrt{\frac{c_2}{c_1}}e^{-\frac{c_3}{2}\varepsilon\Delta T_i} & 0 \end{bmatrix}, \tag{7.57}$$

$$B = \begin{bmatrix} \|\eta_1^+\| \\ 0 \end{bmatrix}., \tag{7.58}$$

and where $\Delta T_i = t_{i+1} - t_i$, and $\eta_1 = \eta(\mathbf{x}_1^+)$ with $\mathbf{x}_1^+$ as defined in Section 7.5.3 and L_{Δ_η} is the Lipschitz constant of the reset map for the outputs in $\mathscr{H}_{\mathrm{MBC}}$.

Proof. The proof begins with properties of the reset map. In particular, assuming a Lipschitz continuous reset map together with results from Lemma 2 due to the construction of the Mechanics-Based Outputs, it follows that

$$\|\eta_{i+1}^+ - \eta_1^+\| \leq L_{\Delta_\eta}\|\eta_i^-\| + L_{\Delta_\eta}\|\xi_i^- - \xi_0^-\|, \tag{7.59}$$

$$\|\xi_{i+1}^+ - \xi^*\| \leq \beta_3\|\eta_i^-\|, \tag{7.60}$$

where β_3 is obtained from (7.46) and (7.47) in Lemma 2. The next step in the proof is to use the exponential convergence property (4.10) of outputs in the closed-loop system under

RES-CLF based control, yielding

$$\|\eta_{i+1}^{+} - \eta_1^{+}\| \leq L_{\Delta_\eta}\varepsilon\sqrt{\frac{c_2}{c_1}}e^{-\frac{c_3}{2}\varepsilon\Delta T_i}\|\eta_i^{+}\| + L_{\Delta_\eta}\|\xi_i^{-} - \xi_0^{-}\| \tag{7.61}$$

$$\|\xi_{i+1}^{+} - \xi^{*}\|, \leq \beta_3\varepsilon\sqrt{\frac{c_2}{c_1}}e^{-\frac{c_3}{2}\varepsilon\Delta T_i}\|\eta_i^{+}\|. \tag{7.62}$$

The final step is to reason about the value of the uncontrolled states at the end of each step through construction of bounds on $\|\xi_i^{-} - \xi_0^{-}\|$ in (7.61). Using the Gronwall-Bellman method employed in the proof of Lemma 1 in [6] and assuming the zero dynamics is Lipschitz continuous with constant L_{f_Z}, it follows that there exists a $\beta_1 > 0$ such that

$$\|\xi_i^{-} - \xi_0^{-}\| \leq \beta_1\|\eta_i^{+}\| + e^{L_{f_Z}\Delta T_i}\|\xi_i^{+} - \xi^{*}\|. \tag{7.63}$$

for all $i \in \{1, 2, \ldots, N-1\}$ of the hybrid execution. Substituting the Gronwall-Bellman result into (7.61) and defining $\beta_2 := L_{f_Z}$ yields

$$\|\eta_{i+1}^{+} - \eta_1^{+}\| \leq L_{\Delta_\eta}\left(\varepsilon\sqrt{\frac{c_2}{c_1}}e^{-\frac{c_3}{2}\varepsilon\Delta T_i} + \beta_1\right)\|\eta_i^{+}\| + L_{\Delta_\eta}e^{\beta_2\Delta T_i}\|\xi_i^{+} - \xi^{*}\| \tag{7.64}$$

$$\|\xi_{i+1}^{+} - \xi^{*}\|, \leq \beta_3\varepsilon\sqrt{\frac{c_2}{c_1}}e^{-\frac{c_3}{2}\varepsilon\Delta T_i}\|\eta_i^{+}\|. \tag{7.65}$$

Noting that $\|\eta_{i+1}^{+}\| = \|\eta_{i+1}^{+} - \eta_1^{+} + \eta_1^{+}\| \leq \|\eta_{i+1}^{+} - \eta_1^{+}\| + \|\eta_1^{+}\|$ completes the construction of (7.57), (7.58) and (7.56). □

Theorem 2 provides insight into the behavior of the hybrid system under Mechanics-Based Control. Combining the results of Lemma 2 with the exponential convergence property of continuous-time control, shows that the post-impact values of the uncontrolled states ξ^{+} can be driven to arbitrarily close to the desired point ξ^{*} through choice of the controller convergence rate ε. The following Theorem uses this fact, together with an assumption of hybrid invariant outputs, to reason about the potential for exponentially stable periodic orbits in the closed-loop hybrid system under Mechanics-Based Control.

Theorem 3. *Consider a hybrid system under Mechanics-Based Control, $\mathscr{H}_{\mathrm{MBC}}$, of the form* (7.35)*, with desired post-impact values $\xi^* = (x_c^*, L^*)$ and let the corresponding state be $\mathbf{x}_0^+ \in Z_{\mathrm{MBC}}$ as defined in Section 7.5.3. If the outputs $\mathbf{y}_{\mathrm{MBC}}$ of $\mathscr{H}_{\mathrm{MBC}}$ are hybrid invariant, i.e. designed so that $\eta(\Delta(\phi_{T_I(\mathbf{x}_0^+)}(\mathbf{x}_0^+))) = 0$, then $\mathscr{H}_{\mathrm{MBC}}$ has a periodic orbit $\mathcal{O}$ with fixed point $\mathbf{x}^+ = \mathbf{x}_0^+$. Moreover, if there exists a $0 < \lambda_1 < \frac{1}{L_{\Delta_\eta}}$ and $\lambda_2 > 0$ such that*

$$\|\xi_i^- - \xi_0^-\| \leq \lambda_1 \|\eta_i^+\| + \lambda_2 \|\xi_i^+ - \xi^*\|. \tag{7.66}$$

then $\mathcal{O}$ is an exponentially stable hybrid periodic orbit.

Proof. Combining the results from Lemma 2 together with the forward velocity assumption and output invariance conditions establishes the existence of an orbit $\mathcal{O}$ in $\mathscr{H}_{\mathrm{MBC}}$. This is due to the fact that the Mechanics-Based Control outputs directly encode a desired transfer of forward COM position and angular momentum about the robot's support pivot, i.e. the outputs are designed to drive the uncontrolled states to the point (x_c^*, L^*) after each impact.

To establish exponential stability of $\mathcal{O}$, note that in the limit as $\varepsilon \to \infty$, the inequality (7.56) from Theorem 2 converges to

$$\begin{bmatrix} \|\eta_{i+1}^+\| \\ \|\xi_{i+1}^+ - \xi^*\| \end{bmatrix} \leq \begin{bmatrix} L_{\Delta_\eta}\beta_1 & L_{\Delta_\eta} e^{\beta_2 \Delta T_i} \\ 0 & 0 \end{bmatrix} \begin{bmatrix} \|\eta_i^+\| \\ \|\xi_i^+ - \xi^*\| \end{bmatrix} \tag{7.67}$$

The eigenvalues of the matrix in (7.67) are 0 and $L_{\Delta_\eta}\beta_1$ and therefore, for all $\beta_1 < \frac{1}{L_{\Delta_\eta}}$, the inequality (7.67) forms a contraction map with exponentially stable fixed point $(0, \xi^*)$. Equating coefficients in (7.66) and (7.63), which is used to form (7.56), it follows that $\beta_1 = \lambda_1$, and thus, for all $0 < \lambda_1 < \frac{1}{L_{\Delta_\eta}}$, the fixed point $(0, \xi^*)$ is exponentially stable. Moreover, by the results in [6, 34, 65, 97], exponential stability of the fixed point implies exponential stability of the orbit $\mathcal{O}$. □

7.6 Example Mechanics-Based Controller Construction and Simulation Results

This section presents an example of how to implement Mechanics-Based Control – through design of desired basis functions for (7.15), calculation of the dynamically updating coefficients $\mathbf{k_x}$, $\mathbf{k_z}$ and $\mathbf{k_c}$, and choice of fixed parameters – to drive a planar underactuated biped into a stable walking gait in simulation.

7.6.1 Desired Outputs

The following basis functions – for outputs of the form (7.15) – will be employed

$$x_s^d(x_c, \mathbf{k_x}(\mathbf{q}, \dot{\mathbf{q}})) = k_{x,1}x_c^3 + k_{x,2}x_c^2 + k_{x,3}x_c + k_{x,4}, \tag{7.68}$$

$$z_s^d(x_c, \mathbf{k_z}(\mathbf{q}, \dot{\mathbf{q}})) = z_s^{max}\sin(k_{z,1}x_c + k_{z,2}), \tag{7.69}$$

$$z_c^d(x_c, \mathbf{k_c}(\mathbf{q}, \dot{\mathbf{q}})) = z_0 + \delta_z\sin(k_{c,1}x_c + k_{c,2}), \tag{7.70}$$

$$\theta_t^d(x_c, \mathbf{k_t}(\mathbf{q}, \dot{\mathbf{q}})) = 0. \tag{7.71}$$

Recall that x_s^d, z_s^d, z_c^d and θ_t^d encode desired behaviors for the step-length, foot-height, COM height and torso orientation, respectively. The key to Mechanics-Based Control is encoding stable walking through dynamic computation of the coefficients $\mathbf{k_x} = (k_{x,1}, k_{x,2}, k_{x,3}, k_{x,4})$, $\mathbf{k_z} = (k_{z,1}, k_{z,2})$, $\mathbf{k_c} = (k_{c,1}, k_{c,2})$ which vary throughout the continuous-time phase of walking based on the evolution of x_c and L. As x_c is one the underactuated coordinates in MBC, we continuously estimate the pre-impact COM position, $\hat{x}_c^-$, using (7.19) and substitute this running estimate into boundary conditions to design continuously updating functions for the coefficients of (7.68)–(7.71).

Dynamically Updated Step Length Coefficients

In this example MBC construction, the basis function for the desired step length (7.68) is a cubic polynomial with independent variable x_c. The coefficients of this cubic can be

fully specified through four independent constraints. Here, we will use the step length constraints (7.25) – (7.26) encoding an initial step length x_s^+ and desired post-impact COM x_c^* (these are fixed parameters that will be specified later) together with the design choice that $\dot{x}_s^d = 0$ at the beginning and end of the step. The collection of constraints used to calculate $\mathbf{k_x}$ is given by the set of boundary conditions

$$x_s^d(x_c^+, \mathbf{k_x}(\mathbf{q}^+, \dot{\mathbf{q}}^+)) = x_s^+, \tag{7.72}$$

$$\dot{x_s^d}(x_c^+, \mathbf{k_x}(\mathbf{q}^+, \dot{\mathbf{q}}^+)) = 0, \tag{7.73}$$

$$x_s^d(\hat{x}_c^-, \mathbf{k_x}(\mathbf{q}^+, \dot{\mathbf{q}}^+)) = \hat{x}_c^- - x^*, \tag{7.74}$$

$$\dot{x_s^d}(\hat{x}_c^-, \mathbf{k_x}(\mathbf{q}^+, \dot{\mathbf{q}}^+)) = 0. \tag{7.75}$$

As mentioned, the endpoint of this function varies continuously based on the dynamic update of the pre-impact COM position, $\hat{x}_c^-$, as computed using (7.19). These equations can be solved symbolically – via a tool such as Mathematica – to obtain closed-form expressions for the coefficients $\mathbf{k_x}(\mathbf{q}, \dot{\mathbf{q}})$.

Dynamically Updated Foot Height and COM Height Coefficients

The desired foot height and COM height functions are designed to start and end at the same value at the beginning and end of a step. In particular, the frequency and phase shift of the sine functions (7.69) and (7.70) are chosen so that the sine functions complete one half of one period on the interval $[x_c^*, \hat{x}_c^-(\mathbf{q}, \dot{\mathbf{q}})]$, via

$$k_{z,1}(\mathbf{q}, \dot{\mathbf{q}}) = k_{c,1}(\mathbf{q}, \dot{\mathbf{q}}) = \frac{\pi x_c^*}{x_c^* - \hat{x}_c^-(\mathbf{q}, \dot{\mathbf{q}})}, \tag{7.76}$$

$$k_{z,2}(\mathbf{q}, \dot{\mathbf{q}}) = k_{c,2}(\mathbf{q}, \dot{\mathbf{q}}) = -\frac{k_{z,1}(\mathbf{q}, \dot{\mathbf{q}})}{\hat{x}_c^-(\mathbf{q}, \dot{\mathbf{q}})}. \tag{7.77}$$

Although it has been stated several times, it is worth reiterating that the endpoint of these desired functions varies based on the dynamic update $\hat{x}_c^-(\mathbf{q}, \dot{\mathbf{q}})$.

Center of Mass Height Oscillation

To encode an exact desired transfer of angular momentum from one step to the next, the oscillation of the COM height, δ_z, is calculated using the momentum-transfer mechanics boundary condition (7.18) applied to (7.70)

$$\delta_z(x_c, L) = \frac{L^* - \omega}{(\hat{x}_c - x^*)\cos(k_{c,1}x_c + k_{c,2})\left(\dot{k}_{c,1}x_c + k_{c,1}\dot{x}_c + \dot{k}_{c,2}\right)} \tag{7.78}$$

where $k_{c,1}$ and $k_{c,2}$ are given in (7.76) and (7.77), respectively. Note that in the case when the designed post-impact angular momentum is equal to the specified pre-impact value, i.e. when $L^* = \omega$, the desired COM oscillation (7.78) is zero and thus the desired COM function (7.70) becomes constant.

In practice, the desired COM height oscillation δ_z can be set to a constant value (rather than dynamically updating it through (7.78)). Often in walking controller design, the COM height oscillation is a parameter that needs to be directly tuned (for example, to ensure that the robot does not traverse through singular configurations). When designing δ_z in this manner, care has to be made to ensure that the resulting post-impact angular momentum returns to the region of the phase space corresponding to forward walking.

7.6.2 Fixed Parameter Choice

For the desired functions in this example, there are 5 fixed parameters that must be chosen. The specified value of the angular momentum at the end of the step, ω contributes to determination of the walking speed. The desired COM and angular momentum transfer, (x_c^*, L^*) must lie in the region of the LIP state space corresponding to Hybrid Periodic Walking, as defined by the set $\mathcal{X}_\omega$ in (6.44). As mentioned in the previous Section, the post-impact angular-momentum can be implicitly tuned through choice of fixed COM height oscillation δ_z. The maximum step-height z_s^{max} and nominal COM height z_0 depend on the mass and length distribution of the robot, and can be hand-tuned to produce desirable motions.

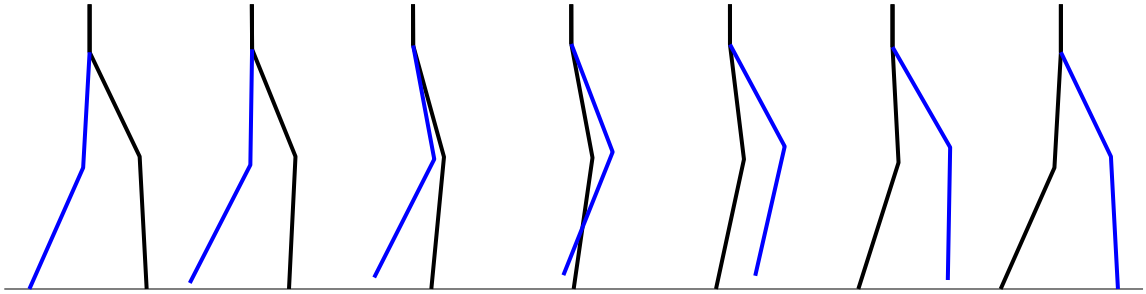

Figure 7.8: Snapshots depicting the planar underactuated walking gait obtained through the example Mechanics-Based Control implementation described in Section 7.6

7.6.3 Simulation Results

This section presents results from implementation of the example Mechanics-Based Controller construction in simulation of the AMBER 3M biped robot [79]. The rigid-body dynamics (3.12) and impact model (3.16) are computed for AMBER 3M and used to construct a hybrid control system of the form (7.30). Mechanics-Based Control is implemented via outputs of the form (7.31) wherein the desired outputs are constructed using the methods outlined in Section 7.6.1. To achieve forward walking in simulation of AMBER 3M, the fixed parameters listed in Table 7.1 are used in the desired outputs (7.68)–(7.71). These outputs, together with a linear feedback law $\mu = -2\varepsilon\dot{\mathbf{y}} - \varepsilon^2\mathbf{y}$ with gain $\varepsilon > 0$, are used to compute the Feedback Linearization control law (6.4) and thus, complete the closed-loop hybrid system under Mechanics-Based Control (7.35). To simulate walking, an initial condition $\mathbf{x}_0 = (\mathbf{q}_0, \dot{\mathbf{q}}_0)$ is chosen and the closed-loop dynamics are numerically integrated, starting from this initial condition, until the state reaches the guard (i.e. foot strike). The reset map is applied to the point on the guard to obtain the initial condition for the next step, and the process is repeated to obtain the hybrid execution. Figure 7.9 shows results from the simulation, wherein it can be observed that the closed-loop hybrid system converges to a periodic orbit, and thus AMBER 3M converges to a periodic gait. Snapshots from this gait are shown in Figure 7.8. To verify stability of the gait, the method described in Section 5.2 is used to approximate the eigenvalues λ_i Jacobian of the Poincaré map. For the non-unity eigenvalues, $\max(\mathrm{Re}(\lambda_i)) = 0.013$; thus the orbit is exponentially stable.

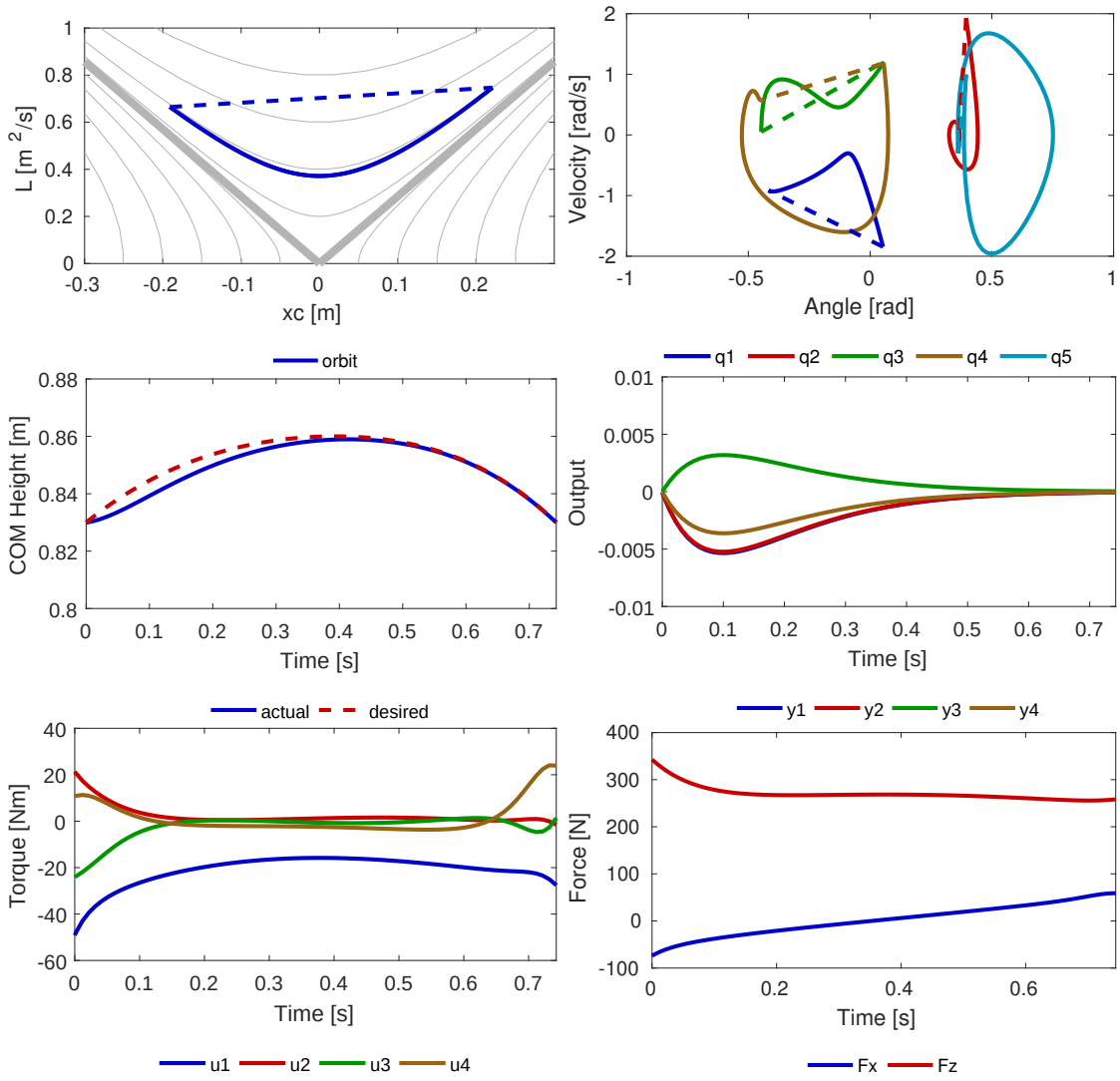

Figure 7.9: Simulation results for the example Mechanics-Based Control implementation described in Section 7.6. (Top Row) Shows the periodic orbit for the uncontrolled modes and the corresponding orbit in the robot's state space. (Middle Left) Shows the desired and actual COM height over on continuous-time phase on the orbit and (Middle Right) shows exponential convergence of the outputs. (Bottom Row) Shows joint torques and ground reaction forces over one complete step on the periodic orbit.

Parameter	x_c^*	ω	z_s^{max}	z_0	δ_z	ε
Value	-0.19	0.75	0.05	0.83	0.03	20

Table 7.1: Mechanics-Based Control parameters used in the planar underactuated walking simulation described in Section 7.6.3.

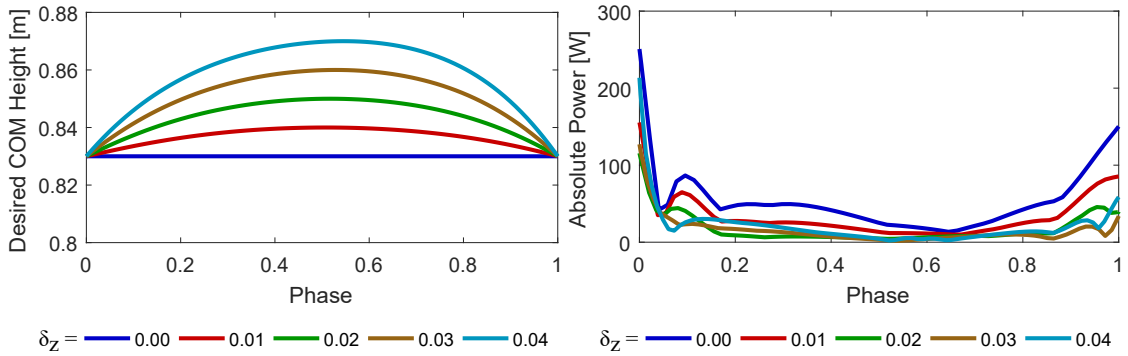

Figure 7.10: Comparison of data from orbits obtained through closed-loop Mechanics-Based Control for five choices of vertical COM oscillation (Left) and the corresponding power over one step (Right). Data is taken from one step on each orbit and is shown as a function of the continuous-time phase

7.6.4 Desired COM Height Oscillation and Gait Efficiency

Mechanics-Based Control is primarily focused on the *direct stabilization of underactuated walking* and as such, the prescribed output design method does not inherently address other practical implementation considerations, such as peak actuator requirements and gait efficiency. One means of addressing these design challenges would be to combine Mechanics-Based Control with nonlinear optimization; however, a simple heuristic for improving gait efficiency is to modify the desired COM height oscillation. Indeed, there is evidence from human walking data that gaits with minimal COM height movement – i.e. gaits that satisfy the Linear-Inverted Pendulum model conditions – are less efficient than gaits which have non-zero travel in the COM height [72].

The gait efficiency metric used in this work is the specific cost of mechanical transport [19], $MCOT_i$, which is calculated for each step i the robot takes, and is given by

$$MCOT_i = \frac{1}{Mgd_i} \int_0^{T_i} \sum_j^4 |\dot{q}_{j+1}(t) u_j(t)| dt, \tag{7.79}$$

where M is the total mass of the robot, d_i is the distance the COM traveled during the step, and T_i is the duration of the step. As the Mechanics-Based Control method directly drives the robot into a stable gait for each choice of controller parameters, several choices

δ_z [m]	0.00	0.01	0.02	0.03	0.04
$MCOT_i$	0.2660	0.1741	0.0986	0.0918	0.1394

Table 7.2: Mechanical Cost of Transport data – computed using (7.79) – for gaits obtained under closed-loop Mechanics-Based Control with various values for the desired COM height oscillation, δ_z.

for the desired COM height oscillation, δ_z, can be rapidly iterated through to find the one corresponding to the most efficient gait. For the current study, the nominal Mechanics-Based Control parameters listed in Table 7.1 are employed while the COM height δ_z is varied. For each value of δ_z the closed-loop hybrid system under Mechanics-Based Control is simulated until it converges to a periodic orbit and the specific cost of transport for each δ_z is then computed using data on the periodic orbit. Table 7.2 provides the specific cost of transport for a range of desired COM height oscillation values, and the on-orbit desired COM height profiles and power versus phase are shown in Figure 7.10. Among the set of COM height oscillations considered, $\delta_z = 0.03\mathrm{m}$ provides the most efficient gait with a mechanical cost of transport, $MCOT_i = 0.0918$.

CHAPTER 8

MECHANICS-BASED CONTROL IMPLEMENTATION AND EXTENSIONS

8.1 Experimental Implementation of Mechanics-Based Control Gaits

This section, as first published in [79], presents two strategies for designing underactuated, planar robotic walking gaits for the purpose of experimental implementation of Mechanics-Based Control. The methods draw upon insights gained the proposed Mechanics-Based Control method which leverages properties of the mechanics of the robot to design a controller that stabilizes walking by regulating the transfer of angular momentum about one support pivot to the next. One proposed gait design strategy is to simulate a closed-loop hybrid model of the robot under the action of the mechanics-based controller to produce an implicit periodic orbit for each set of controller parameters. The second design strategy modifies traditional usage of nonlinear optimization to produce parameterized outputs corresponding to a stable Hybrid Zero Dynamics. The novel approach is to reformulate the HZD stability constraint using the mechanics of the system and to propose an alternative to the periodic HZD orbit existence constraint through the use of an angular momentum variant of the Linear Inverted Pendulum. The two methods are used to design gaits that are implemented in experiments with the AMBER 3M robot.

Robot Parameters	AMBER 3M
Outputs	(1) Mechanics-Based Control Outputs and (2) Human-Inspired
Control Method	Embedded Position Control on Trajectories from Simulation
Highlight	First experimental realization of the Mechanics-Based Control principles.

Table 8.1: Summary of the Mechanics-Based Gait design and experimental implementation on AMBER 3M.

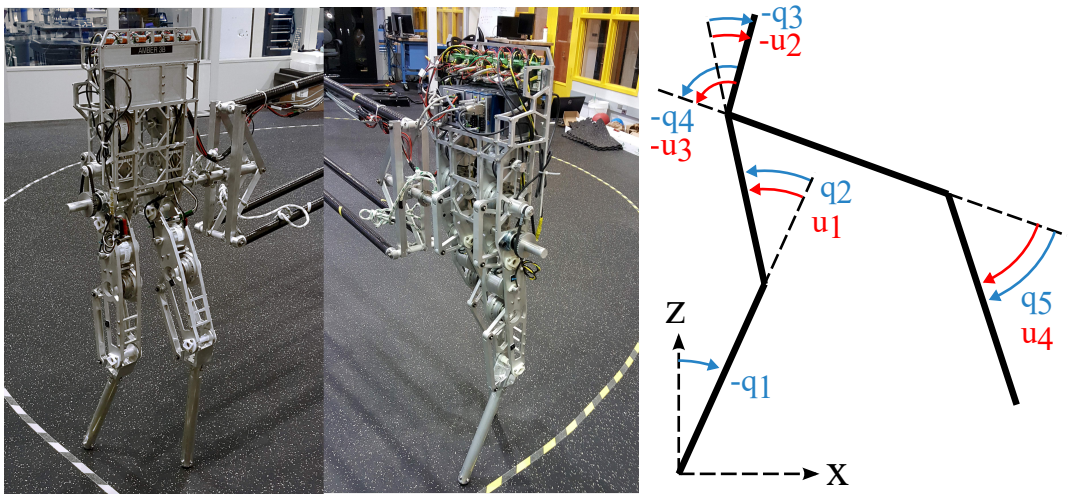

Figure 8.1: AMBER 3M: the modular bipedal robot custom-built by AMBER Lab. It has multiple leg configurations to test different walking types—in this case, the point-foot setup is considered.

AMBER 3M

The experiments in this research were performed on AMBER 3M, a planar bipedal robot developed at the Georgia Institute of Technology. A key component of the mechanical design that enabled this work is its *modularity*: AMBER 3M was designed with modular segments, such as calves and thighs, for the purpose of testing out a wide variety of behaviors. In this study, a pair of underactuated legs – each with a rounded bottom – are attached to the robot, resulting in a single point of contact with the ground. This robot-ground contact interface yields the underactuated angular momentum mechanics discussed in Section 3.5. The robot is connected to the world through a 3.35m radius circular boom which eliminates motion in the lateral direction. Shown in Figure 8.1, AMBER 3M has four actuators and five degrees of freedom. Thus, it is modeled using the planar, five-link articulated rigid body model presented in Chapter 3.

8.1.1 Implicit Gait Design

The first method of designing gaits for AMBER 3M is termed "implicit gait design" wherein gaits are obtained implicitly through simulation of the closed-loop hybrid walking model under the action of Mechanics-Based Control. In particular, the example Mechanics-Based Control implementation outlined in Section 7.6 is used to design controller outputs of the form (7.15). Given these outputs, a gait can be created by first choosing the fixed controller parameters, including x_c^* and L^*, then solving an inverse kinematics problem to obtain a initial condition $(\mathbf{q}(0), \dot{\mathbf{q}}(0))$ for the hybrid system simulation:

$$\begin{aligned} (\mathbf{q}(0), \dot{\mathbf{q}}(0)) &= (\mathbf{q}, \dot{\mathbf{q}}) \quad s.t. \\ \mathbf{y}(\mathbf{q}, \dot{\mathbf{q}}) = \dot{\mathbf{y}}(\mathbf{q}, \dot{\mathbf{q}}) &= 0,\ x_c(\mathbf{q}) = x_c^*,\ L(\mathbf{q}, \dot{\mathbf{q}}) = L^*. \end{aligned} \tag{8.1}$$

The gait is then obtained by simulating the closed loop hybrid system model of walking, starting from $(\mathbf{q}(0), \dot{\mathbf{q}}(0))$, under a controller that drives $\mathbf{y} \to 0$, e.g. Feedback Linearization (4.5) with linear feedback, until the hybrid system converges to a periodic orbit. If the robot falls over, the process is repeated for a new set of parameters.

Desired Functions and Adjustments for Experimental Use

The Mechanics-Based Control outputs (7.15) used in simulation of the rigid-body model of AMBER 3M are also used in the experimental deployment of the gait, however, the angular momentum computed on the measured encoder angles and velocities is currently unusable as a feedback signal. Thus in the experimental implementation, the dynamic update of the robot's center of mass $\hat{x}_c^-(\mathbf{q}, \dot{\mathbf{q}})$ (7.19) is disabled and a fixed value of x_c^- – obtained from simulation – is used in boundary conditions described in Section 7.4.1, resulting in a "feedforward" gait. Results from simulation and experimental implementation of a gait produced by this process are given in Section 8.1.3.

8.1.2 Optimized HZD Gait Design with Mechanics-Based Constraints

This section describes an alternative method of employing the insights gained from the mechanics of underactuated walking; here they are used to modify constraints in traditional optimization-based Hybrid Zero Dynamics gait design. The aim of the this proposed gait design approach is to use optimization to produce hybrid-invariant, efficient gaits while also exposing the mechanical structure of the constraints.

The traditional hybrid zero dynamics optimization approach to designing walking gaits ultimately results in the specification of outputs of the form

$$\mathbf{y}(\mathbf{q}) = \mathbf{y}^a(\mathbf{q}) - \mathbf{y}^d(\tau(\mathbf{q}), \alpha) \tag{8.2}$$

where for the model considered, $\mathbf{y}^d$ is a set of four basis functions that encode the desired behavior for the corresponding actual quantities $\mathbf{y}^a$, and $\tau(\mathbf{q})$ is a monotonically increasing function. Parameters α^* of the desired functions, and a fixed point $(\mathbf{q}(\alpha^*), \dot{\mathbf{q}}(\alpha^*))$ corresponding to a stable walking gait are obtained by solving a nonlinear optimization of the form

$$\alpha^* = \underset{\alpha \in \mathbb{R}^{n_\alpha}}{\operatorname{argmin}} \; J(\alpha) \tag{8.3}$$

$$\text{s.t.} \quad \Delta(S \cap Z(\alpha)) \subset Z(\alpha) \tag{8.4}$$

$$0 < \delta^2_{\text{zero}}(\alpha) < 1 \tag{8.5}$$

$$\frac{\delta^2_{\text{zero}}(\alpha)}{1 - \delta^2_{\text{zero}}(\alpha)} V_{\text{zero}}(\alpha) + K(\alpha) < 0 \tag{8.6}$$

$$C_p(\alpha) < 0. \tag{8.7}$$

In this paper $J(\alpha)$ is the mechanical cost of transport listed in [19], and $C_p(\alpha)$ are physical constraints, e.g. actuator limits. See [97] for definitions of Δ, S, Z, δ_{zero}, V, and K.

The constraint $\Delta(S \cap Z(\alpha)) \subset Z(\alpha)$ ensures that the zero dynamics surface, $Z(\alpha)$,

associated with the outputs $\mathbf{y}$ in (8.2) is invariant through intersection with the guard S and application of the reset map Δ. This *hybrid invariance* constraint reduces analysis of the stability of the walking gait to analysis of the stability of a two-dimensional hybrid system, with coordinates (ξ_1, ξ_2), termed the Hybrid Zero Dynamics. The Poincaré map for the Hybrid Zero Dynamics, with change of coordinates $\zeta_2 = \frac{1}{2}\xi_2^2$, is given in (53) of [97]

$$\zeta_2^-[k+1] = \delta_{\text{zero}}^2(\alpha)\zeta_2^-[k] - V_{\text{zero}}(\mathbf{q}^-(\alpha)) \tag{8.8}$$

The constraint $\frac{\delta_{\text{zero}}^2(\alpha)}{1-\delta_{\text{zero}}^2(\alpha)}V_{\text{zero}}(\alpha) + K(\alpha) < 0$ ensures existence of periodic orbits in the HZD. The constraint $0 < \delta_{\text{zero}}^2(\alpha) < 1$ implies stability of an HZD orbit, which further implies stability of the walking gait [97, 65].

A key observation connecting Hybrid Zero Dynamics and the mechanics of walking is that the coordinate ξ_2 is the angular momentum about the stance pivot, i.e. $\xi_2 \equiv L$ [17]. Thus, an alternative interpretation of Theorems in [34], [97] and [65] is that the stability of a walking gait can be established by creating a stable Poincaré map for the angular momentum. This interpretation motivates the following reformulation of (8.8) and (8.5) using the properties of the mechanics discussed in Chapter 6.

Mechanics Structure of the HZD Stability Constraint

As $\xi_2 \equiv L$, the mechanics of walking, namely (6.29) and (6.32), can be used to construct a Poincaré map analogous to (8.8) for the angular momentum

$$L^-[k+1] = L^-[k] + x_s^-[k]\dot{z}_c^-[k] + \int_0^{T[k]} g x_c(t) dt. \tag{8.9}$$

Inverse kinematics on $Z(\alpha)$ can be used to further expose the structure of (8.9). In particular, the angles and velocities of the robot at impact on $Z(\alpha)$ can be expressed as functions

of α and L^- as in the following equations:

$$\mathbf{q}^-(\alpha) = \mathbf{q} \quad \text{s.t.} \begin{bmatrix} \mathbf{y}(\mathbf{q}) \\ z_s(\mathbf{q}) \end{bmatrix} = \begin{bmatrix} \mathbf{0} \\ 0 \end{bmatrix}, \tag{8.10}$$

$$\dot{\mathbf{q}}^-(\alpha, L^-) = \dot{\mathbf{q}} \quad \text{s.t.} \begin{bmatrix} \frac{\partial \mathbf{y}}{\partial \mathbf{q}}(\mathbf{q}^-(\alpha)) \\ -MD_{1,:}(\mathbf{q}^-(\alpha)) \end{bmatrix}^{-1} \begin{bmatrix} \mathbf{0} \\ 1 \end{bmatrix} L^-, \tag{8.11}$$

where $D_{1,:}(\mathbf{q})$ is the row of the inertia matrix corresponding to the angular momentum of the robot about the stance pivot, i.e. here $L = -(1/M)D_{1:}(\mathbf{q})\dot{\mathbf{q}}$ [97]. Defining

$$w(\alpha) = x_s(\mathbf{q}^-(\alpha))\frac{\partial z_c}{\partial \mathbf{q}}(\mathbf{q}^-(\alpha)) \begin{bmatrix} \frac{\partial \mathbf{y}}{\partial \mathbf{q}}(\mathbf{q}^-(\alpha)) \\ -MD_{1,:}(\mathbf{q}^-(\alpha)) \end{bmatrix}^{-1} \begin{bmatrix} \mathbf{0} \\ 1 \end{bmatrix}$$

and substituting into (8.9) yields a form analogous to (8.8)

$$L^-[k+1] = (1 + w(\alpha))L^-[k] + \int_0^{T[k]} g x_c(t) dt. \tag{8.12}$$

Using a change of variables $\zeta_2 := \frac{1}{2}L^2$ presented in (45)-(46) of [97], it can be shown that on $Z(\alpha)$, the integral term in (8.12) is independent of L and thus the momentum Poincaré map is exponentially stable if

$$-1 < w(\alpha) < 0. \tag{8.13}$$

This constraint will be used to replace (8.5) in (8.3).

Mechanics-Based Forward Walking Constraint

As the angular momentum is uncontrollable in continuous-time, proper gait design must ensure that the post-impact L along the gait is sufficiently high for the robot to complete the next step. This is reflected in the HZD constraint (8.6). For an alternative to (8.6), we

propose to enforce that the initial x_c and L_y are sufficiently within the region of the LIP phase space corresponding to forward walking, through

$$a(z_0)x_c(\mathbf{q}^+(\alpha)) + b(z_0)d < L^+. \tag{8.14}$$

where $a = -z_0\sqrt{g/z_0}$, $b = \sin(\tan^{-1}(z_0\sqrt{g/z_0}))$, and $d > 0$. This constrains the post-impact x_c and L to lie at least a distance d further in the interior of the upper (walking) quadrant of the LIP phase space, and is used to replace (8.6) in (8.3).

Optimized Gait Design Process

The HZD optimization (8.3) – with (8.13) in place of (8.5) and (8.14) in place of (8.6) – can be used to generate stable, hybrid invariant walking gaits that also correspond to a local maximum in gait efficiency. The process of designing a gait through this method consists of configuring the initial condition and the specific values of the constraints. The next section presents experimental results from implementation of a gait produced by this and the implicit gait design processes.

8.1.3 Experimental Implementation on AMBER 3M

This section presents results from implementation of the two mechanics-based gait design strategies, discussed in Sections 8.1.1 and 8.1.2, that produce parameterized functions and corresponding fixed points encoding the respective gaits; inverse kinematics on these functions and joint-level position control is used to experimentally realize the gaits.

Implicit MBC Gait Design

The first experimental gait was designed via the method described in Section 8.1.1, which generates a gait by simulating the closed-loop hybrid walking model under the action of the mechanics-based controller. The following describes the specific choice of MBC parameters and the rationale behind each choice: $x_c^* = -0.12\mathtt{m}$ provides a relatively "conservative" stride length, $L^* = 0.6$ provides a conservative forward walking speed for the choice of x_c^*, $z_s^{max} = 0.08\mathtt{m}$ results in large foot clearance, $z_0 = 0.87\mathtt{m}$ results in a "high" nominal center of mass height and reduces knee flexion and $\delta_z = 0.03\mathtt{m}$ results in lower joint velocities than other values of δ_z for a fixed choice of the previous parameters.

Optimized Gait Design

The second experimental gait was designed via the method described in Section 8.1.2. For this work, we employed a collocation based optimization algorithm, based on [42], to solve the nonlinear programming problem (8.3) with the mechanics-based HZD stability constraint (8.13) and forward walking constraint (8.14). In particular, due to the complex nonlinearity of the robot dynamics and constraints, we employed a *pseudospectral method* [31] to boost the efficiency and robustness of optimization process. The core idea of this approach is to numerically approximate the solution of a dynamical system by trigonometric or orthogonal polynomials at special collocation points. The resulting nonlinear program is solved after `84` iterations and `0.54` seconds with a constraint violation $6e^{-11}$ via IPOPT [1] using the linear solver `ma57`.

Experiment Method and Results

To deploy a gait on the robot hardware, the robot is first position controlled to the gait's initial angles $\mathbf{q}^*$ as it is suspended in air, and then lowered to the ground while holding these positions. The control mode is switched to a state-based position controller which solves an inverse kinematics problem on the designed gait functions together with an auxiliary function, $\tau(\mathbf{q}^{\text{meas}})$, computed on the measured joint angles $\mathbf{q}^{\text{meas}}$, that is monotonic and used to provide a state-based substitution for time in the system [61]. For the mechanics-based control outputs, $\tau(\mathbf{q}) = (x_c(\mathbf{q}) - x_c^+)/(x_c^- - x_c^+)$. For both gaits, τ progresses from $0 \to 1$ and when τ reaches 1, the controller switches the stance and nonstance labeling of the left and right legs. To start the motion, an operator pushes the robot and the inherent hybrid momentum transfer encoded in each gait results in sustained walking.

Results from experiments with the implicit MBC gait are shown in the left column of Fig 8.2 and similarly, the optimized gait experiment results are shown in the right column of Fig 8.2. Note that the observed joint velocities in experiments, shown in the phase portraits in the top row, are much higher than the velocities in the simulated gaits. The leading hypothesis for this discrepancy is that the slope of the lab floor varies around the circular walking path, and as both gaits are designed for flat ground, the robot tends to gain and lose speed on different parts of the track. The joint angle tracking, shown in the third row, shows good agreement between the measured and the commanded signals. Joint torques from selected steps in experiment are shown in the second row of Fig. 8.2 and the mechanical cost of transport is shown in the bottom row; this is calculated via

$$MCOT_i = \frac{1}{Mgd_i} \int_0^{T_i} \sum_j \dot{q}_j(t) u_j(t) | dt \tag{8.15}$$

where d_i and T_i are the distance traveled and duration of the ith step. Snapshots from the experimental and simulated gaits are shown in Fig. 8.3 and Fig. 8.4, and a movie of the experiments is available online [2].

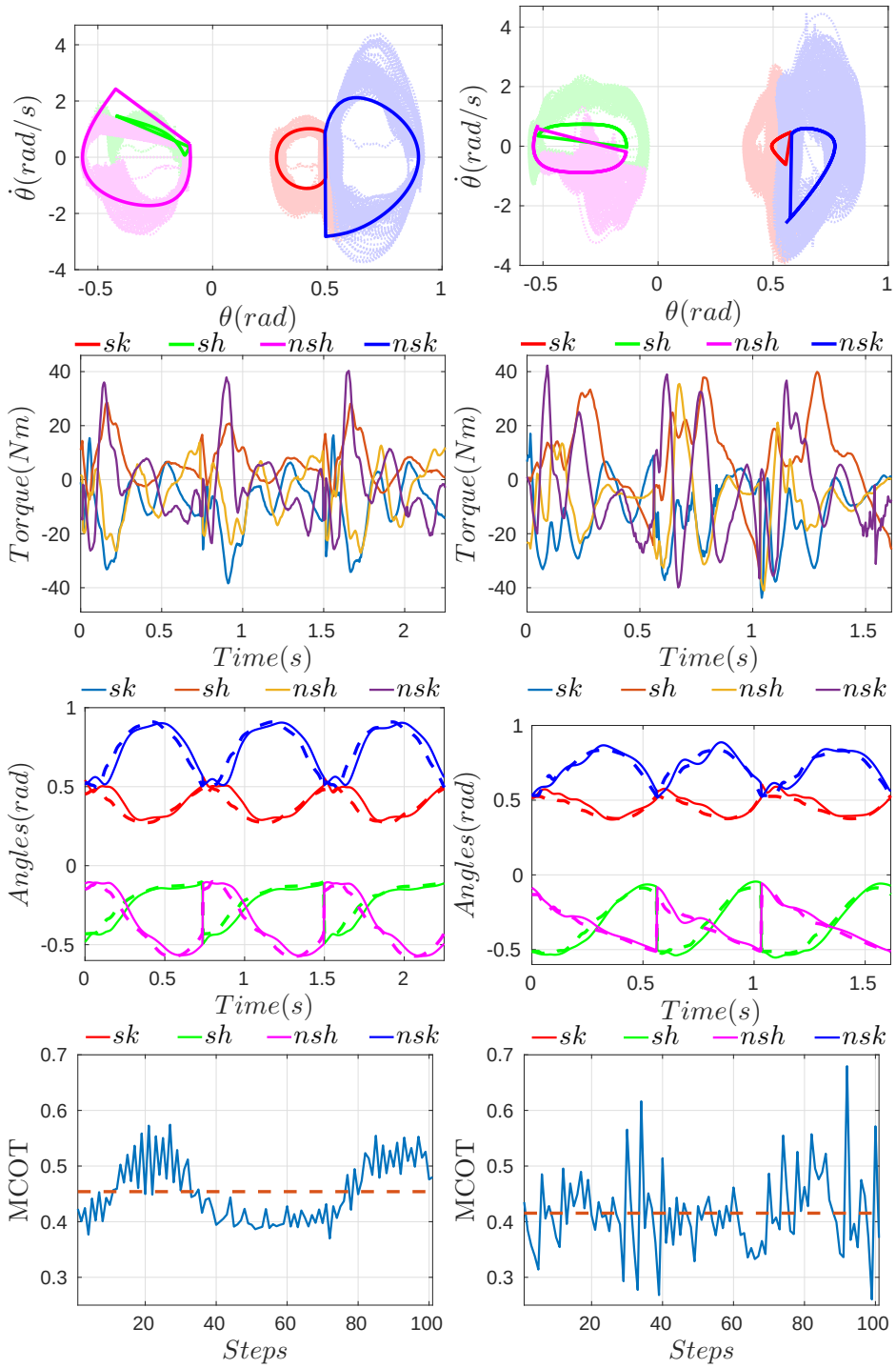

Figure 8.2: Experimental results from implementation of the Mechanics-Based Control gait design strategies on AMBER 3M. (Left Column) Implicit MBC gait experiments. (Right Column) Optimized gait experiments. (Top row) Experimental and simulated phase portraits. (Second row) Experimental torques for selected steps. (Third row) Desired and actual angles for selected steps in the experiments. (Bottom row) Mechanical cost of transport over several steps in each experiment.

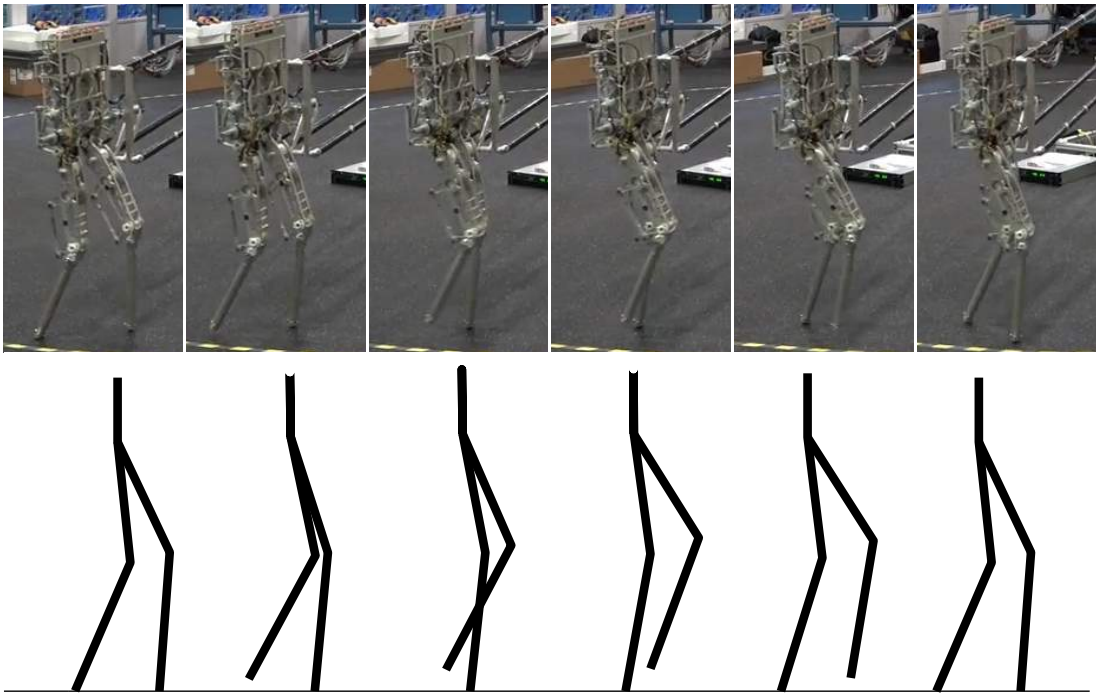

Figure 8.3: Snapshots from experiment and simulation implementation of the Implicit Mechanics-Based Gait produced by the methods described in Section 8.1.1.

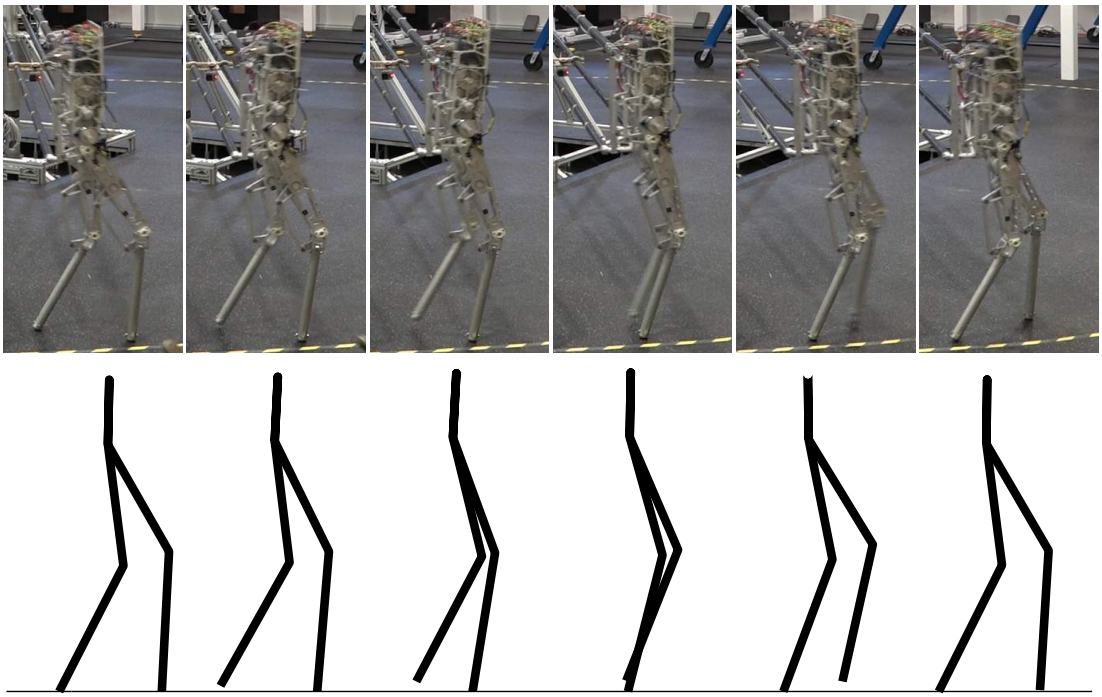

Figure 8.4: Snapshots from experiment and simulation implementation of the optimized gait with mechanics-based constraints produced by the method in Section 8.1.2.

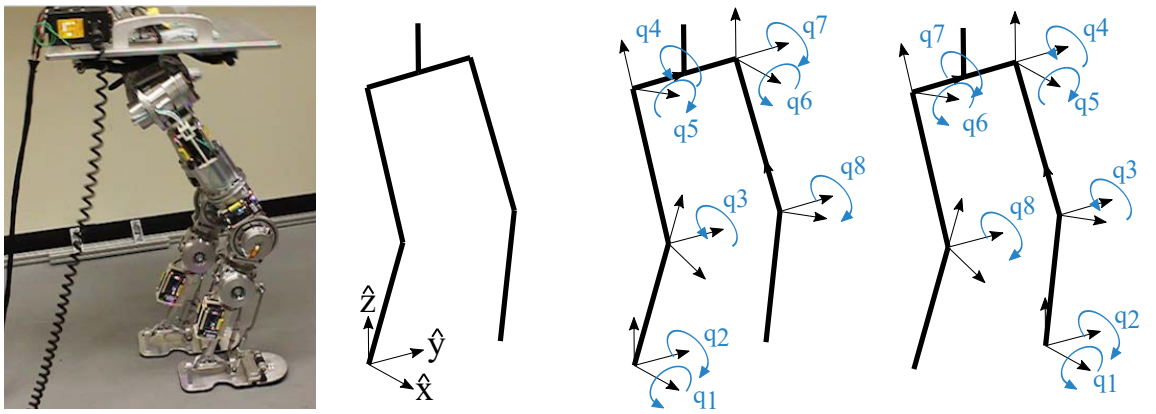

Figure 8.5: (Left) The Leg Testbed Robot. (Second from Left) Articulated 3D rigid-body model of an underactuated version of the Leg Testbed. The base of the kinematic chain is currently located at the end of the right leg. (Third from Left) shows the coordinates used in the underactuated biped robot when the right leg is the support leg and (Right) shows coordinates when the left leg is the support leg .

8.2 Mechanics-Based Control of Torque-Limited, Underactuated 3D Walking

This section, as first published in [76], presents a method of extending Mechanics-Based Control to 3D Underactuated Walking under the presence of non-trivial actuator torque constraints. Whereas underactuation corresponds to two locally uncontrollable states in the planar model, there are four uncontrollable states in the underactuated 3D robot model. Newton's second law dictates that two of these states correspond to the forward and the lateral components of angular momentum about the robot's support pivot. Thus, the strategy in Mechanics-Based Control of 3D underactuated walking is to drive the hybrid walking model into a periodic gait by regulating the transfer of both components of angular about one support pivot to the next.

Robot Parameters	The Leg Testbed
Outputs	Mechanics-Based Control Outputs Extended to 3D
Control Method	Model-Predictive Control
Challenges	Torque Constraints and 2 Degrees of Underactuation.

Table 8.2: Summary of the Mechanics-Based Control implementation for underactuated 3D walking under torque constraints.

8.2.1 Underactuated 3D Robot Model

The 3D robot, shown in Fig. 8.5, is modeled as a rigid-body tree comprised of five links and six actuators. The base of the tree is located at the bottom of the support leg; it is assumed that sufficient friction prevents the support leg from sliding on the ground and from rotating about the axis perpendicular to the ground (the $\hat{z}$ axis). Two rotations, $\mathbf{q_u} = (q_1, q_2)^T$, are used to describe the rotation of the support calf about the world $\hat{x}$ and $\hat{y}$ axes; and six relative (intrinsic) rotations, $\mathbf{q_a} = (q_3, q_4, \ldots, q_8)^T$, are used to describe the actuated joint angles, which are acted upon by joint torques $\mathbf{u} = (u_1, u_2, \ldots, u_6)^T$, in order. The collection of unactuated and actuated angles is $\mathbf{q} = (q_1, q_2, \ldots, q_8)^T$.

As in the planar model described in Chapter 3, the equations of motion for the underactuated 3D biped can be obtained through the Euler-Lagrange method. Letting $\mathbf{x} = (\mathbf{q}, \dot{\mathbf{q}})$, the equations of motion can be written

$$\dot{\mathbf{x}} = f(\mathbf{x}) + g(\mathbf{x})\mathbf{u}, \tag{8.16}$$

where f and g are constructed analogously to (4.3). The impact model is obtained through the methods described in Section 3.4, resulting and can be expressed as

$$\dot{\mathbf{q}}^+ = \Delta(\mathbf{q}^-)\dot{\mathbf{q}}^-, \tag{8.17}$$

see [36] for a definition of $\Delta(\mathbf{q}^-)$. A key property of this impact model is that the forward and lateral components of angular momentum about the point of impact are conserved. This fact is exploited in the development of the Mechanics-Based Control strategy which regulates the hybrid evolution of the angular momentum about the support pivot.

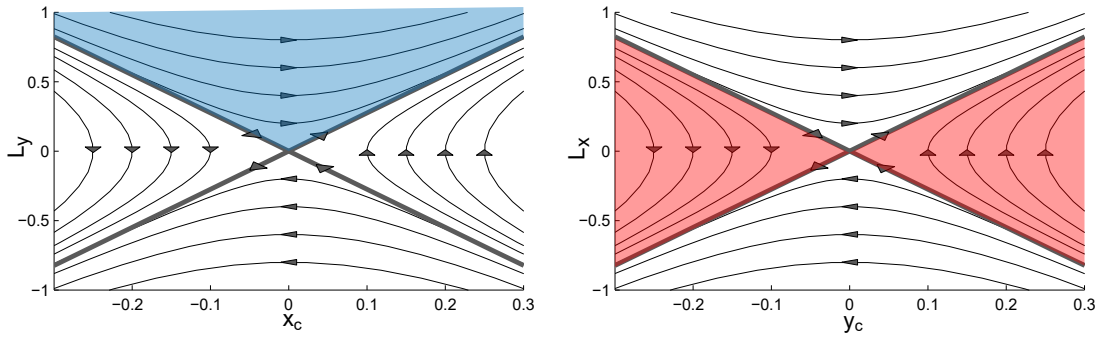

Figure 8.6: Angular momentum variants of the LIP phase space corresponding to (Left) the forward $(\hat{x}, \hat{z})$ plane angular momentum and (Right) the lateral $(\hat{y}, \hat{z})$ plane angular momentum about the support pivot. The highlighted regions show the quadrants of the phase spaces corresponding to nominal, periodic 3D walking.

8.2.2 Underactuated 3D Walking Mechanics

Angular Momentum

The (mass-normalized) angular momentum about the support pivot in the 3D underactuated robot biped is a vector quantity given by $\mathbf{L} = \mathbf{r_c} \times \mathbf{v_c} + \mathbf{H}$ where $\mathbf{r_c} = (x_c, y_c, z_c)^T$ and $\mathbf{v_c} = (\dot{x}_c, \dot{y}_c, \dot{z}_c)^T$ are the center of mass position and velocity relative to the support foot, and $\mathbf{H} = (H_x, H_y, H_z)^T$ is the (mass-normalized) centroidal angular momentum. As mentioned, the rotation about the vertical, $\hat{z}$, axis is constrained (through sufficient friction) to be constant. However, the robot is free to pivot about the forward, $\hat{x}$, and lateral, $\hat{y}$, axes corresponding to respective components of angular momentum L_x and L_y given by

$$\begin{pmatrix} L_x \\ L_y \end{pmatrix} = \begin{pmatrix} y_c \dot{z}_c - z_c \dot{y}_c + H_x \\ z_c \dot{x}_c - x_c \dot{z}_c + H_y \end{pmatrix}. \tag{8.18}$$

The instantaneous rate of change of angular momentum about the support pivot point

$$\begin{pmatrix} \dot{L}_x \\ \dot{L}_y \end{pmatrix} = \begin{pmatrix} -g y_c \\ g x_c \end{pmatrix} \tag{8.19}$$

where g is the constant acceleration due to gravity.

Forward and Lateral Angular Momentum Characterization

Under the Linear Inverted Pendulum constraints, namely constant height of the center of mass $z_c \equiv z_0$ and zero centroidal angular momentum, the momentum mechanics (8.19) become linear, decoupled functions of the forward and lateral positions of the COM relative to the support pivot. Thus we can construct two linear systems to characterize the evolution of the angular momentum about the support pivot in underactated 3D walking

$$\begin{array}{ll} \overbrace{\dot{x}_c = \frac{1}{z_0} L_y}^{\text{Forward Plane}} & \overbrace{\dot{y}_c = -\frac{1}{z_0} L_x,}^{\text{Lateral Plane}} \\ \dot{L}_y = g x_c & \dot{L}_x = -g y_c. \end{array} \tag{8.20}$$

The phase spaces for these two linear systems are shown in Figure 8.6. Note that the angular momentum about the $\hat{y}$ axis, L_y, is characterized through the methods used in planar walking, as described in Section 6.1.2, wherein the top quadrant of the phase space corresponds to forward walking. In 3D walking, additional motion occurs in the lateral direction. As such, the phase space for the lateral plane angular momentum, shown in the right side of Figure 8.6, is used to characterize this lateral movement. Note that nominal walking takes place in the left and right quadrants of the phase space of the lateral angular momentum variant of the LIP. This corresponds to the natural side-to-side sway of walking and the relabeling of the definition of the COM position based on change of support pivot.

Angular Momentum Transfer in 3D

Let $\mathbf{r_s} = (x_s, y_s, z_s)^T$ denote the vector from the support pivot to the swing foot. When the swing foot impacts the ground, support of the robot transfers from the current support pivot to the point of impact. The corresponding transfer of angular momentum about the current pivot, $\mathbf{L}[k]$, $k \in \mathbb{N}_0$, to angular momentum about the next, $\mathbf{L}[k+1]$, can be obtained

through direct computation

$$\mathbf{L}[k+1] = \mathbf{L}[k] - \mathbf{r_s}[k] \times \mathbf{v_c}[k]. \tag{8.21}$$

Furthermore, as angular momentum is conserved about the point of impact in the model of interest, (8.21) can be used to obtain the post-impact angular momentum about the new pivot as a function of the pre-impact state. This fact, together with the fact that the center of mass relative to the support foot undergoes a discrete change at impact due to support change results in a useful representation of the discrete mechanics in underactuated walking

$$\mathbf{r_c}^+[k+1] = \mathbf{r_c}^-[k] - \mathbf{r_s}^-[k], \tag{8.22}$$

$$\mathbf{L}^+[k+1] = \mathbf{L}^-[k] - \mathbf{r_s}^-[k] \times \mathbf{v_c}^-[k]. \tag{8.23}$$

For flat ground walking, (8.22) and (8.23) restricted to the forward $(\hat{x}, \hat{z})$ plane are

$$x_c^+[k+1] = x_c^-[k] - x_s^-[k], \tag{8.24}$$

$$L_y^+[k+1] = L_y^-[k] + x_s^-[k]\dot{z}_c^-[k]. \tag{8.25}$$

which is equivalent to the discrete-mechanics of the planar underactuated biped (6.31)–(6.32). The restrictions of (8.22) and (8.23) to the $(\hat{y}, \hat{z})$ plane are

$$y_c^+[k+1] = y_c^-[k] - y_s^-[k], \tag{8.26}$$

$$L_x^+[k+1] = L_x^-[k] - y_s^-[k]\dot{z}_c^-[k]. \tag{8.27}$$

Mechanics-Based Control of 3D underactuated walking dictates continuous-time controllers for x_s and z_c designed to achieve pre-impact values, $x_s^-[k]$ and $\dot{z}_c^-[k]$, corresponding to desired $(x_c^+[k+1], L_y^+[k+1])$ using (8.24) and (8.25). And similarly, continuous-time control of y_s is designed to stabilize $(y_c^+[k+1], L_x^+[k+1])$ using (8.26) and (8.27).

8.2.3 Mechanics-Based Control of Underactuated 3D Robotic Walking

This section presents a controller that stabilizes 3D underactuated robotic walking by operating on the transfer of angular momentum from one leg to the next. The goal will be to construct continuous-time desired trajectories for the robot's swing leg and vertical center of mass – which update continuously as the center of mass and angular momentum evolve – to effect a desired transfer of angular momentum through foot impact and then stabilize to these trajectories – in the presence of actuation limits – via Model Predictive Control.

The final form of the outputs to be constructed is

$$\mathbf{y}(\mathbf{q},\dot{\mathbf{q}}) = \begin{bmatrix} x_s(\mathbf{q}) \\ y_s(\mathbf{q}) \\ z_s(\mathbf{q}) \\ z_c(\mathbf{q}) \\ \theta_x(\mathbf{q}) \\ \theta_y(\mathbf{q}) \end{bmatrix} - \begin{bmatrix} x_s^d(x_c(\mathbf{q}),\mathbf{k_x}(\mathbf{q},\dot{\mathbf{q}})) \\ y_s^d(x_c(\mathbf{q}),\mathbf{k_y}(\mathbf{q},\dot{\mathbf{q}})) \\ z_s^d(x_c(\mathbf{q}),\mathbf{k_z}(\mathbf{q},\dot{\mathbf{q}})) \\ z_c^d(x_c(\mathbf{q}),\mathbf{k_c}(\mathbf{q},\dot{\mathbf{q}})) \\ 0 \\ 0 \end{bmatrix}, \tag{8.28}$$

where $x_s^d(x_c,\mathbf{k_x})$, $y_s^d(x_c,\mathbf{k_y})$, and $z_s^d(x_c,\mathbf{k_z})$ are desired trajectories for the horizontal, lateral, and vertical components of the swing foot, and $z_c^d(x_c,\mathbf{k_c})$ is a desired trajectory for the vertical center of mass. Coefficients $\mathbf{k}_\square(\mathbf{q},\dot{\mathbf{q}})$ of the desired trajectories in (7.15) will be designed to connect initial values for the swing leg and vertical center of mass to desired pre-impact values of these quantities corresponding to a prescribed transfer of angular momentum using the COM and momentum transfer equations (8.24)–(8.26). These coefficients are continuously updated based on a future horizon estimate of the pre-impact COM and momentum. The final two outputs encode the auxiliary goal of maintaining an upright torso by driving $\theta_x = q_1 + q_5$ and $\theta_y = q_2 + q_3 + q_4$ to zero.

8.2.4 Desired Pre-Impact Kinematics

To stabilize walking, the proposed mechanics-based control approach dictates desired values for the post-impact horizontal $x_c^+[k+1] = x_c^*$ and lateral $y_c^+[k+1] = y_c^*$ components of the center of mass and forward $L_y^+[k+1] = L_y^*$ and lateral $L_x^+[k+1] = L_x^*$ components of the angular momentum. The desired x_c^* and y_c^* are realized through the use of (8.24) and (8.26) in the construction of desired trajectories for the swing leg that satisfy the following conditions when the robot reaches pre-impact values x_c^- and y_c^-

$$x_s^d(x_c^-, \mathbf{k_x}) = x_c^- - x_c^*, \tag{8.29}$$

$$y_s^d(y_c^-, \mathbf{k_y}) = y_c^- - y_c^*, \tag{8.30}$$

$$z_s^d(x_c^-, \mathbf{k_z}) = 0. \tag{8.31}$$

Similarly, a desired transfer of forward momentum from a pre-impact value L_y^- to the desired post-impact value L_y^* is realized using (8.25) via the following condition on the desired trajectory for the vertical center of mass

$$\dot{z}_c^d(x_c^-, \mathbf{k_c}) = \frac{L_y^* - L_y^-}{x_c^- - x_c^*}. \tag{8.32}$$

Note that these "boundary conditions" are functions of (x_c^-, y_c^-, L_y^-), which are unknown in general; however, the following section describes a method of continuously estimating (x_c^-, y_c^-) for a fixed L_y^- using the LIP.

8.2.5 Forward Horizon Center of Mass and Momentum

Given the current horizontal center of mass $x_c(\mathbf{q})$ and forward angular momentum, $L_y(\mathbf{q}, \dot{\mathbf{q}})$, the LIP solution described in (6.22) and (6.25) can be used to obtain the time T required

for the LIP to reach to a future state (x_L^-, L_y^-)

$$T(\mathbf{q}, \dot{\mathbf{q}}) = -\frac{1}{\lambda} \ln \left(\frac{x_L^- \sqrt{g z_0} - L_y^-}{x_c(\mathbf{q}) \sqrt{g z_0} - L_y(\mathbf{q}, \dot{\mathbf{q}})} \right). \tag{8.33}$$

Substituting (8.33) for t in the center of mass component of the LIP solution (6.22) yields

$$x_L^-(\mathbf{q}, \dot{\mathbf{q}}) = \sqrt{\frac{\left(L_y^-\right)^2}{g z_0} - \frac{L_y(\mathbf{q}, \dot{\mathbf{q}})^2}{g z_0} + x_c^2(\mathbf{q})}. \tag{8.34}$$

Thus the horizontal center of mass component of the LIP, x_L^-, corresponding to a specific future value of the angular momentum, L_y^-, can be obtained as a function of the state of the robot on the flow $(\mathbf{q}(t), \dot{\mathbf{q}}(t))$. This motivates the development of a controller which drives the height of the swing foot to zero when the forward momentum $L_y(\mathbf{q}, \dot{\mathbf{q}})$ reaches L_y^-, resulting in an impact occurring at $x_c^- = x_L^-(\mathbf{q}, \dot{\mathbf{q}})$. This provides a moving estimate of the value of the pre-impact center of mass that can be used in (7.16) and (7.18) to dynamically produce desired pre-impact values for the horizontal swing leg position and the vertical COM velocity.

Similarly, an estimate of the pre-impact lateral component of the center of mass can be obtained using (8.33) in the solution to the lateral plane variant of the LIP dynamics

$$\begin{aligned} y_L^-(\mathbf{q}, \dot{\mathbf{q}}) = &\left(\frac{y_c(\mathbf{q})}{2} + \frac{L_x(\mathbf{q}, \dot{\mathbf{q}})}{2 \lambda z_0} \right) e^{\lambda T(\mathbf{q}, \dot{\mathbf{q}})} \\ &+ \left(\frac{y_c(\mathbf{q})}{2} - \frac{L_x(\mathbf{q}, \dot{\mathbf{q}})}{2 \lambda z_0} \right) e^{-\lambda T(\mathbf{q}, \dot{\mathbf{q}})}. \end{aligned} \tag{8.35}$$

This provides an estimate $y_L^-(\mathbf{q}, \dot{\mathbf{q}})$ of y_c^- which can be used in conjunction with (8.30) to dynamically update a desired pre-impact value for the step length in the lateral direction. The following section presents the construction of a desired trajectory for the height of the swing foot which renders (8.34) and (8.35) viable moving estimates of the pre-impact center of mass.

8.2.6 Height of the Swing Foot Output Construction

The desired trajectory for the height of the swing foot is designed to keep the foot above the ground until the angular momentum reaches a specified value, L_y^-, at which point the foot is forced to impact the ground. Here, we use a quadratic

$$z_s^d(x_c, \mathbf{k_z}) = k_{z,1}x_c^2 + k_{z,2}x_c + k_{z,3}. \tag{8.36}$$

The coefficients of (8.36) are updated at each $(\mathbf{q}, \dot{\mathbf{q}})$ by solving

$$z_s^d(x_c^+, \mathbf{k_z}) = 0, \tag{8.37}$$

$$z_s^d(x_L^-(\mathbf{q}, \dot{\mathbf{q}}), \mathbf{k_z}) = 0, \tag{8.38}$$

$$z_s^d(x_c^+ + (x_L^-(\mathbf{q}, \dot{\mathbf{q}}) - x_c^+)/2, \mathbf{k_z}) = z_s^{\max}, \tag{8.39}$$

where $z_s^{\max} > 0$ is a parameter encoding the maximum height of the foot. Note that these coefficients are dynamically updated in continuous-time; as the pre-impact center of mass estimate $x_L^-(\mathbf{q}, \dot{\mathbf{q}})$ is a function of the current state, the coefficients $\mathbf{k_z}(\mathbf{q}, \dot{\mathbf{q}})$ are likewise a function of the state.

8.2.7 Continuous-Time Control

Similar to the height of the swing foot, desired outputs for the forward, x_s^d, and lateral, y_s^d, components of the swing foot and for the height of the center of mass, z_c^d, are constructed to effect the desired transfer of angular momentum described in (8.29) – (8.32) using (8.34) and (8.35). The resulting output vector (8.28) has relative degree two [86] along the rigid body dynamics (8.16), as the dependence on $\dot{\mathbf{q}}$ appears via the angular momentum and the time-derivative of the angular momentum is independent of the joint torques. The partial

feedback linearization control law [86] is given by

$$\mathbf{u}(\mathbf{q}, \dot{\mathbf{q}}) = L_g L_f \mathbf{y}^{-1}(\mathbf{q}, \dot{\mathbf{q}}) \left(-L_f^2 \mathbf{y}(\mathbf{q}, \dot{\mathbf{q}}) + \mu \right), \tag{8.40}$$

where $L_g L_f \mathbf{y}$ and $L_f^2 \mathbf{y}$ are Lie derivatives of the (relative degree two) outputs along the rigid body dynamics and $L_g L_f \mathbf{y}$ is invertible. As described in the following, Model Predictive Control is used to produce a stabilizing μ consistent with torque limits and momentum transfer constraints.

8.2.8 Model Predictive Control

Applying partial feedback linearization (8.40) to the rigid body dynamics (8.16) results in a linear control system on the outputs and their derivatives $\eta = (\mathbf{y}, \dot{\mathbf{y}})$; discretization of this control system yields

$$\eta_{k+1} = \underbrace{\begin{bmatrix} 1 & \Delta T \\ 0 & 1 \end{bmatrix}}_{F_{\Delta T}} \eta_k + \underbrace{\begin{bmatrix} 0 \\ \Delta T \end{bmatrix}}_{G_{\Delta T}} \mu_k. \tag{8.41}$$

for a discrete time-step $\Delta T > 0$. Given an initial condition, $\eta_0(\mathbf{q}, \dot{\mathbf{q}})$, and a sequence of control inputs, $\bar{\mu} = \{\mu_0, \mu_1, \mu_2, \ldots, \mu_{k-1}\}$, the value of η after k time-steps, denoted η_k, can be obtained by successively computing (8.41).

Model Predictive Control [64, 77] is used to obtain the sequence of control inputs $\bar{\mu}^*(\mathbf{q}, \dot{\mathbf{q}})$ that minimizes the future values of the outputs η_k subject to torque and momentum transfer constraints, over a future time-horizon of length $T(\mathbf{q}, \dot{\mathbf{q}})$ seconds, where $T(\mathbf{q}, \dot{\mathbf{q}})$ is the time-to-impact estimate provided by the LIP (8.33). This horizon results in $N = \text{ceiling}\left(T(\mathbf{q}, \dot{\mathbf{q}})/\Delta T\right)$ discrete time-steps. The MPC problem is implemented as a Quadratic Program (QP) which provides an implicit definition of a feedback control law $\bar{\mu}^*(\mathbf{q}, \dot{\mathbf{q}})$ to be used in (8.40). In particular, the MPC-QP for Mechanics-Based Control of

3D underactuated walking is given by

$$\bar{\mu}^*(\mathbf{q}, \dot{\mathbf{q}}) = \underset{\bar{\mu}}{\operatorname{argmin}} \, \eta_N^T P_\varepsilon \eta_N + \sum_{k=0}^{N-1} \eta_k^T P_\varepsilon \eta_k + \mu_k^T R \mu_k \tag{8.42}$$

$$\text{s.t.} \quad A_k \mu_k \leq b_k, \;\; k \in \{0, 1, 2, \ldots, N\}$$

$$A_{eq,k} \mu_k = b_{eq,k}, k \in \{0, 1, 2, \ldots, N\}.$$

Here $P_\varepsilon > 0$, $R > 0$ encode the goal of minimizing future values of the controller outputs. The inequalities A_k and b_k enforce torque constraints $|u_k| \leq u^{max}$ and $A_{eq,k}$ and $b_{eq,k}$ enforce the transfer of momentum described in (8.32). The constraints can be estimated over a forward horizon using the solution of the angular momentum LIP, together with inverse kinematics on the zero dynamics surface associated with $\mathbf{y}, \dot{\mathbf{y}}$. The proceeding simulation example simply uses $A_k = A_0(\mathbf{q})$ and $b_k = b_0(\mathbf{q}, \dot{\mathbf{q}})$ for the torque constraints. The first six entries in $\bar{\mu}^*(\mathbf{q}, \dot{\mathbf{q}})$ are used in the feedback linearization control law (8.40) to obtain the joint torque-control law $\mathbf{u}(\mathbf{q}, \dot{\mathbf{q}})$.

8.2.9 Desired Momentum Transfer for Forward Walking

To achieve forward walking, the desired (x_c^*, L_y^*) and the desired L_y^- are chosen using the planar methods described in Sections 6.3 and 7.4.1. The current lateral control solution is to pick reference values y_c^d and L_x^d and use the angular momentum LIP forward horizon estimate to update the corresponding desired post-impact, lateral component of the center of mass

$$y_c^*(\mathbf{q}, \dot{\mathbf{q}}) = \pm(y_c^d - \rho((L_x^-(\mathbf{q}, \dot{\mathbf{q}}))^2 - (L_x^d)^2)) \tag{8.43}$$

with $\rho > 0$. The change in sign reflects the alternation of the support foot between the left and right legs. The sequence $y_c^*(\mathbf{q}^-[k], \dot{\mathbf{q}}^-[k]), \; k = \{1, 2, \ldots\}$ converges to a fixed point for the simulation and controller configuration considered.

8.2.10 Simulation Results

The proposed mechanics-based control method is implemented in simulation of the 67.7kg underactuated 3D robot shown in Fig. 8.5. The equations of motion (8.16) are computed using a MATLAB implementation of Spatial Vector Algebra [25] and numerically integrated using MATLAB's `ode45` function. The Mathematica package [67] is used to generate kinematics expressions for the controller.

Mechanics-Based Control Setup

The nominal walking height is chosen to be $z_0 = 0.7$m. Forward walking is encoded through a desired post-impact COM, $x^* = -0.18$m, $y_c^d = 0.12$m, and normalized angular momentum values $L_y^* = 0.7$, $L_y^- = 0.75$ and $L_x^d = 0.26$. The desired post-impact lateral center of mass converges to $y_c^* = \pm 0.1$m with $\rho = 0.75$. In this example, the desired forward and lateral step lengths, x_s^d and y_s^d, are linear functions of the horizontal center of mass, x_c, the desired height of the swing foot z_s^d is given in (8.36), and the desired vertical center of mass is z_0. The MPC is configured with $\varepsilon = 100$ and $R = 0.001I$, $u^{max} = 250$ N-m and time step $\Delta T = 0.02s$.

Results

The proposed control method under the given parameters drives the system into a periodic orbit, shown in the middle column of Fig. 8.7. The maximum magnitude of the real part of the eigenvalues of a numerical approximation of the Jacobian of the Poincaré map for the orbit is $0.85 < 1$, which indicates that the orbit, and thus the walking is locally asymptotically stable [34]. The left column shows the corresponding prescribed transfer of angular momentum in the forward and lateral planes, and convergence to these orbits in a simulation starting from perturbed initial conditions. A movie of the simulations can be found online [3].

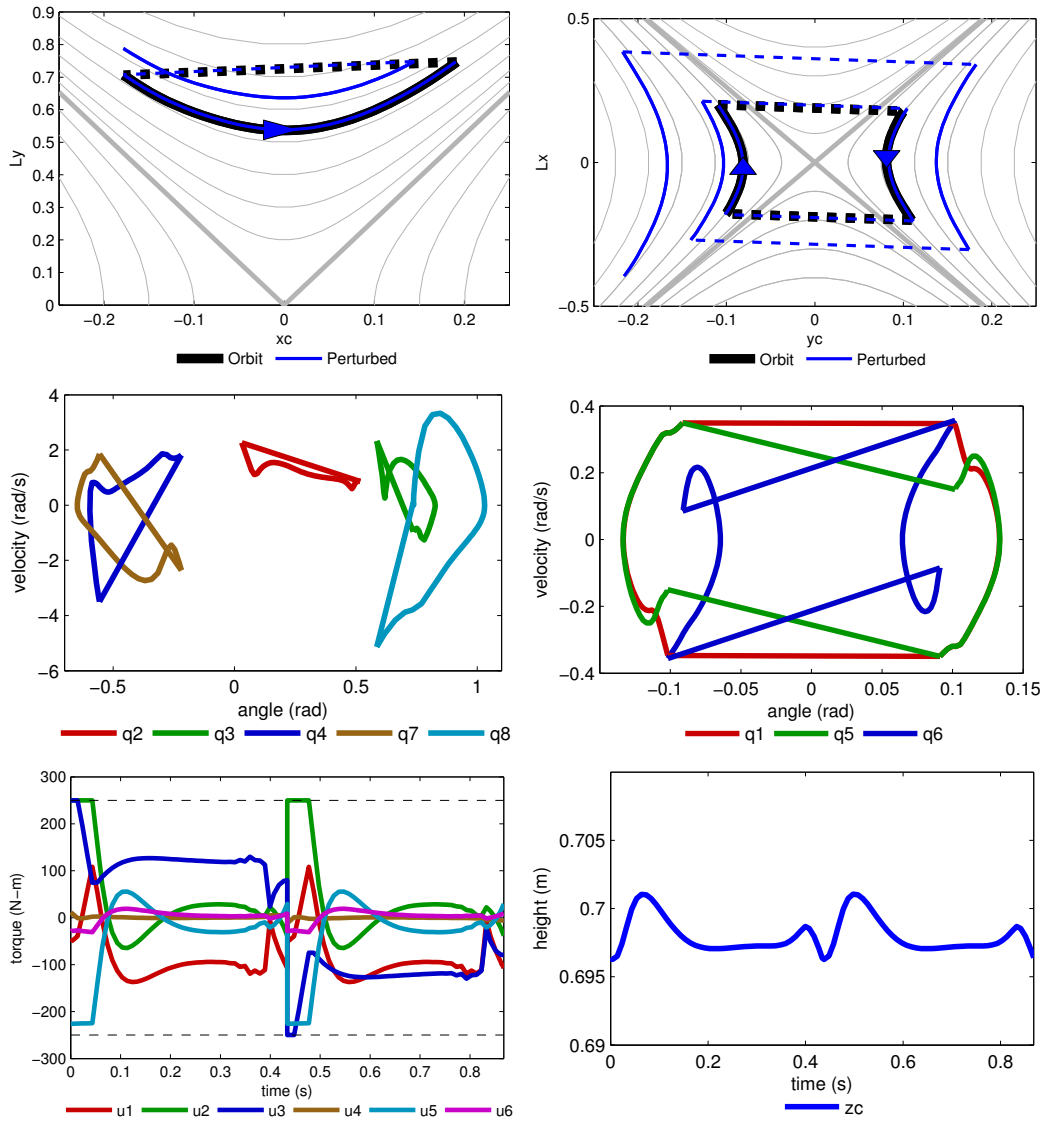

Figure 8.7: Simulation results from the application of proposed mechanics-based control approach to underactuated 3D walking. (Top Row) The robot's post-impact angular momentum and center of mass are driven into regions of a variant of the LIP phase space corresponding to forward walking. Exact expressions for the transfer of angular momentum (8.24)–(8.26) allow for the incorporation of discrete effects in the LIP model. (Blue) The flows starting from perturbed initial states converge to the (black) flows along the orbit. (Middle Row) The method results in stable periodic orbits for the (middle-left) pitch angles and (middle-right) roll angles. (Bottom-left) The torques obtained through Model Predictive Control (8.42) satisfy limits $u^{max} = 250$N-m; data is shown for two steps on the orbit (an impact occurs at 0.43 seconds). (Bottom-right) The vertical center of mass is nominally driven to a constant, however, conditions on the pre-impact velocity (7.18) are enforced via equality constraints in the MPC-QP (8.42) to achieve a desired transfer of angular momentum.

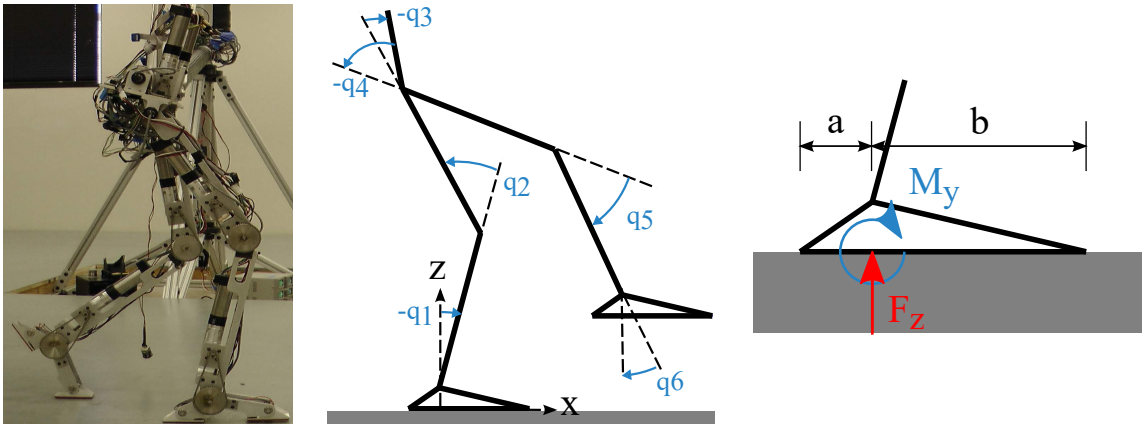

Figure 8.8: (Left) The AMBER 2 robot, (middle) the corresponding articulated rigid-body model and (right) the Zero-Moment Point constraints required for flat-foot balance are expressed in terms of the normal force F_z and moment M_y acting on the support foot.

8.3 Planar Flat-Foot Walking: Satisfying ZMP Bounds

The particular articulated-rigid body model considered is the planar, seven-link biped shown in the middle of Figure 8.8, that has six motors which actuate the ankle, knee and hip joints. The goal will be to drive this model into a "flat-foot" walking gait, wherein the robot's support foot remains flat on the ground at all times. Under these conditions, the robot is fully actuated: it has six degrees of freedom corresponding to the six actuated joints. The primary challenge associated with flat-foot walking is satisfying the well-known Zero Moment Point (ZMP) [95] constraints which ensure that robot's support foot remains flat on the ground. The strategy for extending Mechanics-Based Control to this model is to add an additional output to (7.15) which zeros the orientation of the swing foot and to set the support ankle torque to zero. In doing so, the ZMP constraints are naturally satisfied.

Robot Parameters	AMBER 2
Outputs	Mechanics-Based Control Outputs Extended to Feet
Control Method	Input/Output Linearization and Linear Feedback
Challenge	Satisfying Zero-Moment Point Constraints.

Table 8.3: Summary of the Mechanics-Based Control implementation for planar walking with flat feet.

8.3.1 Rigid Body Model and ZMP Constraints

The seven-link biped is modeled as an articulated rigid-body, and as such, the equations of motion and impact model are constructed through the methods described in Chapter 3. Control will be used to ensure that the robot's swing foot lands flat on the ground, and by doing so, the resulting walking gait can be modeled using a simple hybrid system. In order to ensure that the support foot remains flat at all times, the following constraints on the normal reaction, F_z, and moment acting on the support foot, M_y, must be satisfied

$$-aF_z < M_y < bF_z, \tag{8.44}$$

where a is the distance between the heel and point of application of the force F_z, and b is the distance between the toe and point of application of F_z, as depicted in Figure 8.8. The inequalities (8.44) correspond to having the Zero Moment Point lie within base of support and when satisfied, prevent the support foot from rotating [36].

8.3.2 Mechanics-Based Control of Flat-Foot Walking

A perk of the ability to design underactuated walking gaits is that it is relatively simple to extend them to flat-foot walking. In in underactuated walking, the robot's actuators are not capable of applying a moment about the support pivot. Thus, forward motion of the limbs must be obtained without "help" from the ankle joint and below. As seen in the simulation results to follow, these gaits can be immediately applied to flat-foot walking by setting the robot's ankle torque to zero which results in a relatively small magnitude reaction moment acting on the support pivot – and thus no additional computation is needed to ensure that the Zero Moment Point constraints (8.44) are satisfied.

In addition to setting the support ankle torque to zero, another output is defined which encodes the goal of keeping the swing foot parallel to the ground at all times. Thus, the five outputs used in Mechanics-Based Control of flat-foot walking are the four outputs (7.15)

used for underactuated walking, as described in Section 7.4, and an additional output for the orientation of the swing foot, $\theta_s(\mathbf{q})$. The final form of the outputs is

$$\mathbf{y}(\mathbf{q},\dot{\mathbf{q}}) = \begin{bmatrix} x_s(\mathbf{q}) \\ z_s(\mathbf{q}) \\ z_c(\mathbf{q}) \\ \theta_T(\mathbf{q}) \\ \theta_s(\mathbf{q}) \end{bmatrix} - \begin{bmatrix} x_s^d(x_c(\mathbf{q}), \mathbf{k_x}(\mathbf{q},\dot{\mathbf{q}})) \\ z_s^d(x_c(\mathbf{q}), \mathbf{k_z}(\mathbf{q},\dot{\mathbf{q}})) \\ z_c^d(x_c(\mathbf{q}), \mathbf{k_c}(\mathbf{q},\dot{\mathbf{q}})) \\ 0 \\ 0 \end{bmatrix} \tag{8.45}$$

where $x_s^d(x_c, \mathbf{k_x})$ and $z_s^d(x_c, \mathbf{k_z})$ are desired trajectories for the horizontal and vertical components of the swing foot, and $z_c^d(x_c, \mathbf{k_c})$ is a desired trajectory for the vertical center of mass. Coefficients $\mathbf{k}_\square(\mathbf{q},\dot{\mathbf{q}})$ of the desired trajectories in (7.15) are designed to connect initial values for the swing leg and vertical center of mass to desired pre-impact values of these quantities corresponding to a prescribed transfer of angular momentum using the methods described in Section 7.4. The fourth output encodes the auxiliary goal of keeping an upright torso by driving θ_T to zero. For the purposes of flat-foot walking, a fifth output is employed to drive the rotation of the swing foot relative to the world frame, $\theta_s = -q_1 - q_2 - q_3 + q_4 + q_5 + q_6$, to zero and thereby keep the swing foot parallel to the ground at all times. Feedback linearization of the form (7.32), together with a linear feedback, is used to drive the outputs to zero in the continuous-time evolution of the system. Here, the first input – corresponding to the ankle actuator – is set to zero, and the corresponding decoupling matrix $L_g L_f \mathbf{y}$ is computed accordingly. The final form of the torque control law used in flat-foot walking is

$$\mathbf{u}(\mathbf{q},\dot{\mathbf{q}}) = \begin{bmatrix} 0 \\ L_g L_f \mathbf{y}^{-1} \left(-L_f^2 \mathbf{y} - 2\varepsilon L_f \mathbf{y} - \varepsilon^2 \mathbf{y} \right) \end{bmatrix}, \tag{8.46}$$

where $\varepsilon > 0$ dictates the output convergence rate, and where dependence on the states, i.e. $\mathbf{y} = \mathbf{y}(\mathbf{q},\dot{\mathbf{q}})$ has been suppressed for brevity.

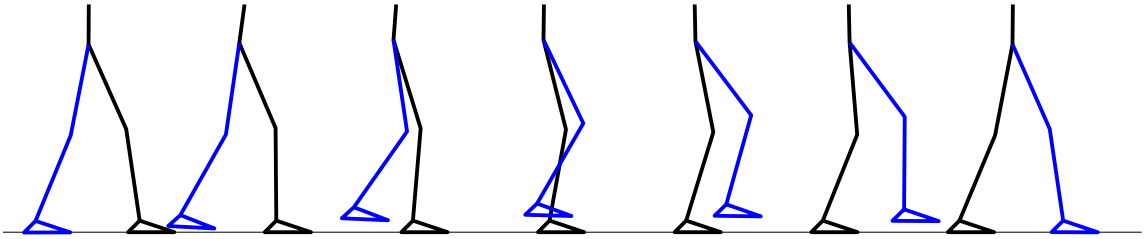

Figure 8.9: Snapshots from one step flat-foot walking under Mechanics-Based Control.

8.3.3 Nominal Footed Walking Simulation Setup and Results

This section presents results from simulation of a hybrid model of flat-footed robotic walking, under the action of Mechanics-Based Control with desired outputs (8.45), as designed in the preceding section. The mass, length and inertia parameters used are those of the AMBER 2 robot, shown in Figure 8.8. Torques $u(q, \dot{q})$ obtained through (8.46) are applied to the rigid-body dynamics of the robot model to exponentially stabilize the outputs in continuous-time. Table 8.4 lists the fixed Mechanics-Based Control parameters used in this simulation. The resulting evolution of the hybrid walking model converges to a periodic orbit, which is shown in the top right of Figure 8.10. A depiction of the corresponding walking gait is shown in Figure 8.9. As shown in the bottom left of Figure 8.9, the ground reach wrench acting on the support pivot satisfies the inequalities (8.44) required to keep the foot flat on the ground – a result of applying zero torque with the support ankle actuator. Note that this is a strong constraint on the motion; future research should be devoted to understanding how to use non-zero ankle actuation to manipulate the general mechanics of walking, and to stabilize walking with foot rotation as in [58].

Parameter	Value	Units
x_c^*	-0.2	$[m]$
L^*	0.7	$[m^2/s]$
ω	0.8	$[m^2/s]$
z_s^{max}	0.08	$[m]$
z_0	0.6	$[m]$

Table 8.4: Parameters chosen for the nominal planar footed walking example.

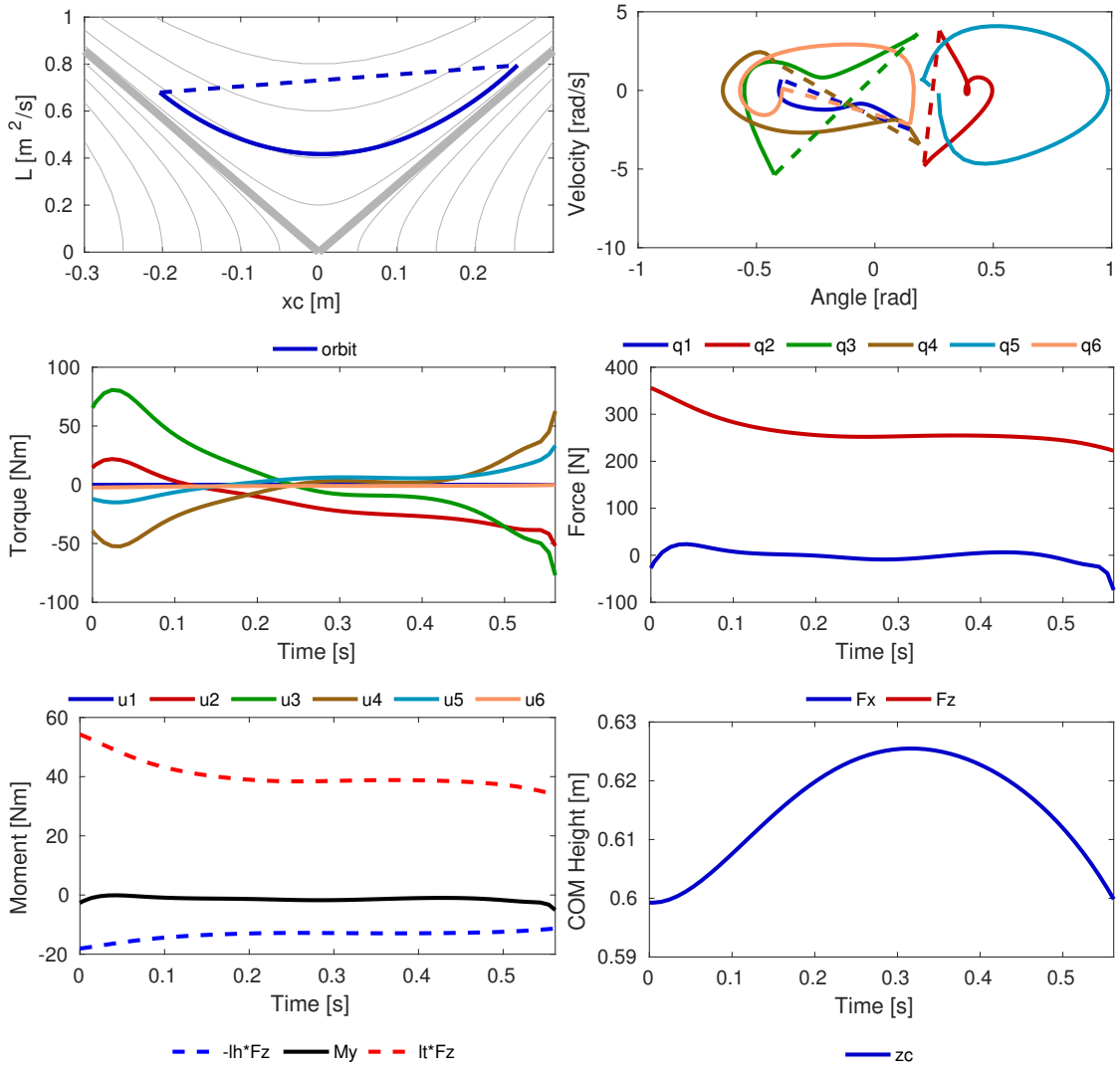

Figure 8.10: Simulation results from the Mechanics-Based Control implementation for flat-foot walking described in Section 8.3. (Top Left) The angular momentum is computed about the support ankle in flat foot walking. Mechanics-Based Control ensures that the post impact angular momentum and center of mass relative to the support ankle return to the quadrant of the LIP phase space corresponding to forward walking. (Top Right) The states in the hybrid system ultimately converge to a periodic orbit. (Middle Row) Shows torques and reaction forces over the course of one step during the flat-foot walking gait. (Bottom Left) The Zero Moment Point constraints are satisfied naturally by zeroing the torque applied by the ankle actuator. (Bottom Right) The actual COM height over one step during flat foot walking.

CHAPTER 9
CONCLUSION

This Dissertation addresses the challenge of handling phases of underactuation during robot locomotion. The primary philosophy is to uncover the general mechanics associated with underactuated walking and then to exploit these mechanics via control. The result is the proposed Mechanics-Based Control approach: a method of stabilizing underactuated walking by regulating the transfer of the center of mass and angular momentum about the robot's support pivot. Whereas underactuated walking control design has historically required usage of nonlinear programming to search for stable gaits, Mechanics-Based Control directly embeds stability in the design of continuous-time outputs which effect the angular momentum transfer strategy. A major takeaway from this Dissertation is that **the primary feedback mechanism needed to stabilize underactuated walking is the regulation of the transfer of angular momentum and forward center of mass from one support pivot to the next**. To conclude the Dissertation, we revisit the list of contributions set forth in Section 1.2 and expound upon them with details discussed in the interim chapters.

9.1 Summary of the Contributions in this Dissertation

1. **Structure in the Hybrid Walking Mechanics.** In underactuated walking, and particularly in the five-link planar underactuated biped considered in this Dissertation, existing hybrid systems methods stabilize walking by stabilizing the locally uncontrollable modes in the system. This Dissertation leverages the fact – from classical mechanics – that one of the uncontrolled modes in underactuated walking is the the angular momentum about the robot's support pivot. This novel insight into the structure of underactuated walking – the Hybrid Walking Mechanics – illuminates a novel feedback mechanism for stabilizing underactuated walking.

2. **Novel Feedback Mechanism for Stabilizing Underactuated Walking.** Combining existing results which relate the stability of a walking gait to the stability of the hybrid evolution of the uncontrolled modes in the system, with the fact that one of the uncontrolled modes is the angular momentum about the support pivot, reveals a new strategy for stabilizing walking: regulating the transfer of angular momentum from one support pivot to the next. This Dissertation uses a representative hybrid model of walking to illustrate the power of this hybrid angular momentum feedback, and then illustrates how to implement the feedback strategy on the full-dimensional robot model via Mechanics-Based Control.

3. **Mechanics-Based Control.** Using properties of the mechanics of the robot, the transfer of angular momentum from one support pivot to the next can be expressed as functions of the robot's controllable kinematics. Thus, this Dissertation presents Mechanics-Based Control: a method of designing continuous-time outputs which simultaneously correspond to a desired continuous-time walking behavior while also encoding a desired transfer of angular momentum. Stabilization of these outputs via standard nonlinear control drives the robot into a stable gait. Historically, stabilization of underactuated walking has required use of nonlinear programming to search for stable periodic orbits; however, by augmenting these methods with properties of the mechanics of the system, Mechanics-Based Control encodes stability directly.

4. **Applications and Extensions.** This Dissertation shows a number of ways Mechanics-Based Control can be implemented and extended to achieve robotic walking. The method is applied in the design of experimental walking gaits for the AMBER 3M robot. Mechanics-Based Control is also extended to 3D underactuated walking under torque constraints, and planar footed walking under Zero-Moment Point constraints.

9.2 Future Directions for Mechanics-Based Control

The developments in this Dissertation focus on manipulating the mechanics of the underactuated, planar five-link biped. It is shown that the Mechanics-Based Control principles can be extended to the case of walking with flat feet and underactuated walking in 3D; however, it is not immediately clear how to treat the mechanics of general legged locomotion. One open challenge is transitioning into and out-of phases of double support – phases where both feet are in contact with the ground. In double support, the robot is overactuated, and the angular momentum about support points can be instantaneously influenced by the robot's actuators. Combining double and single support results a "non-simple" hybrid system model; regulating the mechanics of this system would require a controller that manages both the underactuated and the overactuated domains to ensure the hybrid evolution of the uncontrolled modes is stable. Adding feet and allowing them to rotate results in an even more complicated hybrid system with three or more domains characterized by heel and toe making and breaking contact. Additional properties of the mechanics of these hybrid models are needed to augment the angular-momentum transfer strategy to achieve general, multi-domain walking.

Another open area of research is manipulating the height of the center of mass and the centroidal angular momentum to influence the continuous-time mechanics of walking [23, 57]. While the Linear Inverted Pendulum assumptions provide a useful starting point for prescribing a nominal forward walking behavior, adding nonlinearities improve efficiency of walking [72]. Moreover, allowing for non-zero centroidal angular momentum and vertical COM velocity provides greater control authority over the continuous-time evolution of the system. Recent work shows one such way of realizing this control authority through manipulation of the COM height to bring the robot to rest [53]. The future of Mechanics-Based Control lies in further exploitation of the COM and centroidal momentum mechanics and in the management of the mechanics during transitions in multi-domain walking.

REFERENCES

[1] https://projects.coin-or.org/ipopt.

[2] https://youtu.be/xw8jaDz8XTc.

[3] https://youtu.be/kIuuBMWYljM.

[4] A. D. Ames, "Human-inspired control of bipedal walking robots," *IEEE Transactions on Automatic Control*, vol. 59, no. 5, pp. 1115–1130, 2014.

[5] A. D. Ames, K. Galloway, and J. W. Grizzle, "Control Lyapunov functions and hybrid zero dynamics," in *IEEE Conference on Decision and Control*, 2012, pp. 6837–6842.

[6] A. D. Ames, K. Galloway, K. Sreenath, and J. W. Grizzle, "Rapidly exponentially stabilizing control Lyapunov functions and hybrid zero dynamics," *IEEE Transactions on Automatic Control*, vol. 59, no. 4, pp. 876–891, 2014.

[7] A. D. Ames, "Characterizing knee-bounce in bipedal robotic walking: A zeno behavior approach," in *ACM International Conference on Hybrid Systems: Computation and Control*, 2011, pp. 163–172.

[8] A. D. Ames, P. Tabuada, B. Schürmann, W.-L. Ma, S. Kolathaya, M. Rungger, and J. W. Grizzle, "First steps toward formal controller synthesis for bipedal robots," in *ACM International Conference on Hybrid Systems: Computation and Control*, 2015, pp. 209–218.

[9] M. Azad and R. Featherstone, "A new nonlinear model of contact normal force," *IEEE Transactions on Robotics*, vol. 30, no. 3, pp. 736–739, 2014.

[10] J. Baillieul, A. Bloch, P. Crouch, and J. Marsden, *Nonholonomic Mechanics and Control*. Springer New York, 2007.

[11] P. Bézier, *Numerical control: mathematics and applications*. J. Wiley, 1972.

[12] A. V. Birn-Jeffery, C. M. Hubicki, Y. Blum, D. Renjewski, J. W. Hurst, and M. A. Daley, "Don't break a leg: Running birds from quail to ostrich prioritise leg safety and economy on uneven terrain," *Journal of Experimental Biology*, vol. 217, no. 21, pp. 3786–3796, 2014.

[13] R. Blickhan, "The spring-mass model for running and hopping," *Journal of Biomechanics*, vol. 22, no. 11, pp. 1217 –1227, 1989.

[14] B. G. Buss, K. A. Hamed, B. A. Griffin, and J. W. Grizzle, "Experimental results for 3D bipedal robot walking based on systematic optimization of virtual constraints," in *American Control Conference*, 2016, pp. 4785–4792.

[15] K. Byl and R. Tedrake, "Metastable walking machines," *The International Journal of Robotics Research*, vol. 28, no. 8, pp. 1040–1064, 2009.

[16] C. Chevallereau, G. Bessonnet, G. Abba, and Y. Aoustin, *Bipedal Robots: Modeling, Design and Walking Synthesis*. Wiley, 2013.

[17] C. Chevallereau, J. W. Grizzle, and C. H. Moog, "Nonlinear control of mechanical systems with one degree of underactuation," in *IEEE International Conference on Robotics and Automation*, vol. 3, 2004, pp. 2222–2228.

[18] C. Chevallereau, J. W. Grizzle, and C.-L. Shih, "Asymptotically stable walking of a five-link underactuated 3-D bipedal robot," *IEEE Transactions on Robotics*, vol. 25, no. 1, pp. 37–50, 2009.

[19] E. Cousineau and A. D. Ames, "Realizing underactuated bipedal walking with torque controllers via the ideal model resolved motion method," in *IEEE International Conference on Robotics and Automation*, 2015, pp. 5747–5753.

[20] B. Dadashzadeh, H. R. Vejdani, and J. Hurst, "From template to anchor: A novel control strategy for spring-mass running of bipedal robots," in *IEEE/RSJ International Conference on Intelligent Robots and Systems*, 2014, pp. 2566–2571.

[21] H. Dai and R. Tedrake, "Optimizing robust limit cycles for legged locomotion on unknown terrain," in *IEEE Conference on Decision and Control*, 2012, pp. 1207–1213.

[22] H. Dai, A. Valenzuela, and R. Tedrake, "Whole-body motion planning with centroidal dynamics and full kinematics," in *2014 IEEE-RAS International Conference on Humanoid Robots*, 2014, pp. 295–302.

[23] J. Englsberger and C. Ott, "Integration of vertical COM motion and angular momentum in an extended capture point tracking controller for bipedal walking," in *IEEE-RAS International Conference on Humanoid Robots*, 2012, pp. 183–189.

[24] J. Englsberger, C. Ott, M. A. Roa, A. Albu-Schffer, and G. Hirzinger, "Bipedal walking control based on capture point dynamics," in *IEEE/RSJ International Conference on Intelligent Robots and Systems*, 2011, pp. 4420–4427.

[25] R. Featherstone, http://royfeatherstone.org/spatial/v2/index.html.

[26] ——, *Rigid Body Dynamics Algorithms*. Springer US, 2014.

[27] R. Full and D. Koditschek, "Templates and anchors: Neuromechanical hypotheses of legged locomotion on land," *Journal of Experimental Biology*, vol. 202, no. 23, pp. 3325–3332, 1999.

[28] G. Garofalo, C. Ott, and A. Albu-Schffer, "Walking control of fully actuated robots based on the bipedal SLIP model," in *IEEE International Conference on Robotics and Automation*, 2012, pp. 1456–1463.

[29] H. Geyer, A. Seyfarth, and R. Blickhan, "Compliant leg behaviour explains basic dynamics of walking and running," *Proceedings of the Royal Society B: Biological Sciences*, vol. 273, no. 1603, pp. 2861–2867, 2006.

[30] H. Goldstein, C. Poole, and J. Safko, *Classical Mechanics*. Addison Wesley, 2002.

[31] D. Gottlieb and S. Orszag, *Numerical Analysis of Spectral Methods*. Society for Industrial and Applied Mathematics, 1977.

[32] B. Griffin and J. Grizzle, "Nonholonomic virtual constraints for dynamic walking," in *IEEE Conference on Decision and Control*, 2015, pp. 4053–4060.

[33] J. W. Grizzle, C. Chevallereau, and C. Shih, "HZD-based control of a five-link underactuated 3D bipedal robot," in *IEEE Conference on Decision and Control*, Cancún, 2008.

[34] J. W. Grizzle, F. Plestan, and G. Abba, "Poincare's method for systems with impulse effects: Application to mechanical biped locomotion," in *IEEE Conference on Decision and Control*, vol. 4, 1999, 3869–3876 vol.4.

[35] J. W. Grizzle, C. Chevallereau, R. W. Sinnet, and A. D. Ames, "Models, feedback control, and open problems of 3D bipedal robotic walking," *Automatica*, vol. 50, no. 8, pp. 1955 –1988, 2014.

[36] J. Grizzle, C. Chevallereau, A. D. Ames, and R. W. Sinnet, "3D bipedal robotic walking: Models, feedback control, and open problems," *International Federation of Automatic Control*, vol. 43, no. 14, pp. 505 –532, 2010.

[37] W. Haddad, V. Chellaboina, and S. Nersesov, *Impulsive and Hybrid Dynamical Systems: Stability, Dissipativity, and Control*. Princeton University Press, 2014.

[38] K. A. Hamed, B. G. Buss, and J. W. Grizzle, "Continuous-time controllers for stabilizing periodic orbits of hybrid systems: Application to an underactuated 3D bipedal robot," in *IEEE Conference on Decision and Control*, 2014, pp. 1507–1513.

[39] A. Hereid, E. A. Cousineau, C. M. Hubicki, and A. D. Ames, "3D dynamic walking with underactuated humanoid robots: A direct collocation framework for optimizing hybrid zero dynamics," in *IEEE International Conference on Robotics and Automation*, 2016, pp. 1447–1454.

[40] A. Hereid, C. M. Hubicki, E. A. Cousineau, J. W. Hurst, and A. D. Ames, "Hybrid zero dynamics based multiple shooting optimization with applications to robotic walking," in *IEEE International Conference on Robotics and Automation*, 2015, pp. 5734–5740.

[41] A. Hereid, M. J. Powell, and A. D. Ames, "Embedding of SLIP dynamics on underactuated bipedal robots through multi-objective quadratic program based control," in *IEEE Conference on Decision and Control*, 2014, pp. 2950–2957.

[42] A. Hereid, S. Kolathaya, and A. D. Ames, "Online optimal gait generation for bipedal walking robots using legendre pseudospectral optimization," in *IEEE Conference on Decision and Control*, 2016, pp. 6173–6179.

[43] A. Hereid, S. Kolathaya, M. S. Jones, J. Van Why, J. W. Hurst, and A. D. Ames, "Dynamic multi-domain bipedal walking with ATRIAS through SLIP based human-inspired control," in *ACM International Conference on Hybrid Systems: Computation and Control*, 2014, pp. 263–272.

[44] D. G. E. Hobbelen and M. Wisse, "A disturbance rejection measure for limit cycle walkers: The gait sensitivity norm," *IEEE Transactions on Robotics*, vol. 23, no. 6, pp. 1213–1224, 2007.

[45] J. K. Hodgins and M. N. Raibert, "Adjusting step length for rough terrain locomotion," *IEEE Transactions on Robotics and Automation*, vol. 7, no. 3, pp. 289–298, 1991.

[46] C. Hubicki, J. Grimes, M. Jones, D. Renjewski, A. Sprwitz, A. Abate, and J. Hurst, "ATRIAS: Design and validation of a tether-free 3D-capable spring-mass bipedal robot," *The International Journal of Robotics Research*, vol. 35, no. 12, pp. 1497–1521, 2016.

[47] Y. Hurmuzlu and D. B. Marghitu, "Rigid body collisions of planar kinematic chains with multiple contact points," *The International Journal of Robotics Research*, vol. 13, no. 1, pp. 82–92, 1994.

[48] S. Kajita, M. Morisawa, K. Miura, S. Nakaoka, K. Harada, K. Kaneko, F. Kanehiro, and K. Yokoi, "Biped walking stabilization based on linear inverted pendulum tracking," in *IEEE/RSJ International Conference on Intelligent Robots and Systems*, 2010, pp. 4489–4496.

[49] S. Kajita and K. Tani, "Study of dynamic biped locomotion on rugged terrain-derivation and application of the linear inverted pendulum mode," in *IEEE International Conference on Robotics and Automation*, 1991, pp. 1405–1411.

[50] S. Kajita, T. Yamaura, and A. Kobayashi, "Dynamic walking control of a biped robot along a potential energy conserving orbit," *IEEE Transactions on Robotics and Automation*, vol. 8, no. 4, pp. 431–438, 1992.

[51] S. Kajita *et al.*, "Biped walking pattern generation by using preview control of zero-moment point," in *IEEE International Conference on Robotics and Automation*, 2003, pp. 1620–1626.

[52] S. Kolathaya and A. D. Ames, "Achieving bipedal locomotion on rough terrain through human-inspired control," in *IEEE International Symposium on Safety, Security, and Rescue Robotics*, 2012, pp. 1–6.

[53] T. Koolen, M. Posa, and R. Tedrake, "Balance control using center of mass height variation: Limitations imposed by unilateral contact," in *IEEE-RAS International Conference on Humanoid Robots*, 2016, pp. 8–15.

[54] T. Koolen, T. de Boer, J. Rebula, A. Goswami, and J. Pratt, "Capturability-based analysis and control of legged locomotion, part 1: Theory and application to three simple gait models," *The International Journal of Robotics Research*, vol. 31, no. 9, pp. 1094–1113, 2012.

[55] S. Kuindersma, F. Permenter, and R. Tedrake, "An efficiently solvable quadratic program for stabilizing dynamic locomotion," in *International Conference on Robotics and Automation*, 2014, pp. 2589–2594.

[56] S. Kuindersma, R. Deits, M. Fallon, A. Valenzuela, H. Dai, F. Permenter, T. Koolen, P. Marion, and R. Tedrake, "Optimization-based locomotion planning, estimation, and control design for the ATLAS humanoid robot," *Autonomous Robots*, vol. 40, no. 3, pp. 429–455, 2016.

[57] J. Lack, "Integrating the effects of angular momentum and changing center of mass height in bipedal locomotion planning," in *IEEE-RAS International Conference on Humanoid Robots (Humanoids)*, 2015, pp. 651–656.

[58] J. Lack, "Planar multicontact locomotion using hybrid zero dynamics," Master's thesis, Texas A&M Univeristy, 2013.

[59] Y. Liu, P. M. Wensing, D. E. Orin, and Y. F. Zheng, "Dynamic walking in a humanoid robot based on a 3D actuated dual-SLIP model," in *IEEE International Conference on Robotics and Automation*, 2015, pp. 5710–5717.

[60] Y. Liu, P. M. Wensing, J. P. Schmiedeler, and D. E. Orin, "Terrain-blind humanoid walking based on a 3-D actuated dual-SLIP model," *IEEE Robotics and Automation Letters*, vol. 1, no. 2, pp. 1073–1080, 2016.

[61] W. L. Ma, H. H. Zhao, S. Kolathaya, and A. D. Ames, "Human-inspired walking via unified PD and impedance control," in *IEEE International Conference on Robotics and Automation*, 2014, pp. 5088–5094.

[62] J. Marsden and T. Ratiu, *Introduction to Mechanics and Symmetry: A Basic Exposition of Classical Mechanical Systems*. Springer New York, 2002.

[63] A. E. Martin, D. C. Post, and J. P. Schmiedeler, "Design and experimental implementation of a hybrid zero dynamics-based controller for planar bipeds with curved feet," *The International Journal of Robotics Research*, vol. 33, no. 7, pp. 988–1005, 2014.

[64] D. Q. Mayne, J. B. Rawlings, C. V. Rao, and P. O. M. Scokaert, "Survey constrained model predictive control: Stability and optimality," *Automatica*, vol. 36, no. 6, pp. 789–814, 2000.

[65] B. Morris and J. W. Grizzle, "A restricted Poincaré; map for determining exponentially stable periodic orbits in systems with impulse effects: Application to bipedal robots," in *IEEE Conference on Decision and Control*, 2005, pp. 4199–4206.

[66] B. Morris and J. Grizzle, "Hybrid invariance in bipedal robots with series compliant actuators," in *IEEE Conference on Decision and Control*, 2006, pp. 4793–4800.

[67] R. M. Murray, Z. Li, and S. S. Sastry, *Robotlinks Mathematica package*, `http://www.cds.caltech.edu/~murray/mlswiki/index.php/Software`, Accessed 01-Oct-2013.

[68] R. M. Murray, J. Hauser, A. Jadbabaie, M. B. Milam, N. Petit, W. B. Dunbar, and R. Franz, "Online control customization via optimization-based control," in *In Software-Enabled Control: Information Technology for Dynamical Systems*, Wiley-Interscience, 2002.

[69] R. Murray, Z. Li, S. Sastry, and S. Sastry, *A Mathematical Introduction to Robotic Manipulation*. Taylor & Francis, 1994.

[70] G. Nelson, A. Saunders, N. Neville, B. Swilling, J. Bondaryk, D. Billings, C. Lee, R. Playter, and M. Raibert, "PETMAN: A humanoid robot for testing chemical pro-

tective clothing," *Journal of the Robotics Society of Japan*, vol. 30, no. 4, pp. 372–377, 2012.

[71] D. E. Orin and A. Goswami, "Centroidal momentum matrix of a humanoid robot: Structure and properties," in *IEEE/RSJ International Conference on Intelligent Robots and Systems*, 2008, pp. 653–659.

[72] J. D. Ortega and C. T. Farley, "Minimizing center of mass vertical movement increases metabolic cost in walking," *Journal of Applied Physiology*, vol. 99, no. 6, pp. 2099–2107, 2005.

[73] T. Parker and L. Chua, *Practical numerical algorithms for chaotic systems*. Springer Verlag, 1989.

[74] M. Posa, C. Cantu, and R. Tedrake, "A direct method for trajectory optimization of rigid bodies through contact," *The International Journal of Robotics Research*, vol. 33, no. 1, pp. 69–81, 2014.

[75] I. Poulakakis and J. W. Grizzle, "The spring loaded inverted pendulum as the hybrid zero dynamics of an asymmetric hopper," *IEEE Transactions on Automatic Control*, vol. 54, no. 8, pp. 1779–1793, 2009.

[76] M. J. Powell and A. D. Ames, "Mechanics-based control of underactuated 3D robotic walking: Dynamic gait generation under torque constraints," in *IEEE/RSJ International Conference on Intelligent Robots and Systems*, 2016, pp. 555–560.

[77] M. J. Powell, E. A. Cousineau, and A. D. Ames, "Model predictive control of underactuated bipedal robotic walking," in *IEEE International Conference on Robotics and Automation*, 2015, pp. 5121–5126.

[78] M. J. Powell, A. Hereid, and A. D. Ames, "Speed regulation in 3D robotic walking through motion transitions between human-inspired partial hybrid zero dynamics," in *IEEE International Conference on Robotics and Automation*, 2013, pp. 4803–4810.

[79] M. J. Powell, W. L. Ma, E. R. Ambrose, and A. D. Ames, "Mechanics-based design of underactuated robotic walking gaits: Initial experimental realization," in *IEEE-RAS International Conference on Humanoid Robots*, 2016, pp. 981–986.

[80] M. J. Powell, H. Zhao, and A. D. Ames, "Motion primitives for human-inspired bipedal robotic locomotion: Walking and stair climbing," in *IEEE International Conference on Robotics and Automation*, 2012, pp. 543–549.

[81] J. Pratt, J. Carff, S. Drakunov, and A. Goswami, "Capture point: A step toward humanoid push recovery," in *IEEE-RAS International Conference on Humanoid Robots*, 2006, pp. 200–207.

[82] J. Pratt, P. Dilworth, and G. Pratt, "Virtual model control of a bipedal walking robot," in *IEEE International Conference on Robotics and Automation*, vol. 1, 1997, pp. 193–198.

[83] J. Pratt and R. Tedrake, "Velocity-based stability margins for fast bipedal walking," in *Fast Motions in Biomechanics and Robotics: Optimization and Feedback Control*, M. Diehl and K. Mombaur, Eds. Berlin, Heidelberg: Springer Berlin Heidelberg, 2006, pp. 299–324.

[84] J. Pratt, T. Koolen, T. de Boer, J. Rebula, S. Cotton, J. Carff, M. Johnson, and P. Neuhaus, "Capturability-based analysis and control of legged locomotion, part 2: Application to M2V2, a lower-body humanoid," *The International Journal of Robotics Research*, vol. 31, no. 10, pp. 1117–1133, 2012.

[85] H. Razavi, A. Bloch, X. Da, and A. Ijspeert, "Symmetric virtual constraints for periodic walking of legged robots," in *IEEE Conference on Decision and Control*, 2016, pp. 7520–7526.

[86] S. Sastry, *Nonlinear Systems: Analysis, Stability, and Control*. Springer New York, 1999.

[87] R. W. Sinnet and A. D. Ames, "Energy shaping of hybrid systems via control Lyapunov functions," in *American Control Conference*, 2015, pp. 5992–5997.

[88] R. W. Sinnet, M. J. Powell, R. P. Shah, and A. D. Ames, "A human-inspired hybrid control approach to bipedal robotic walking," *International Federation of Automatic Control*, vol. 44, no. 1, pp. 6904 –6911, 2011.

[89] M. W. Spong and M. Vidyasagar, *Robotic Dynamics and Control*. New York, NY: John Wiley and Sons, 1989.

[90] K. Sreenath, H.-W. Park, I. Poulakakis, and J. W. Grizzle, "A compliant hybrid zero dynamics controller for stable, efficient and fast bipedal walking on mabel," *The International Journal of Robotics Research*, vol. 30, no. 9, pp. 1170–1193, 2011.

[91] B. J. Stephens and C. G. Atkeson, "Push recovery by stepping for humanoid robots with force controlled joints," in *IEEE-RAS International Conference on Humanoid Robots*, 2010, pp. 52–59.

[92] W. J. Stronge, *Impact Mechanics*. Cambridge: Cambridge University Press, 2000.

[93] P. Tabuada, *Verification and Control of Hybrid Systems: A Symbolic Approach*. Springer US, 2009.

[94] H. R. Vejdani, A. Wu, H. Geyer, and J. W. Hurst, "Touch-down angle control for spring-mass walking," *IEEE International Conference on Robotics and Automation*, pp. 5101–5106, 2015.

[95] M. Vukobratović and B. Borovac, "Zero-moment point–thirty-five years of its life," *International Journal of Humanoid Robotics*, 2005.

[96] P. M. Wensing and D. E. Orin, "Generation of dynamic humanoid behaviors through task-space control with conic optimization," in *IEEE International Conference on Robotics and Automation*, 2013, pp. 3103–3109.

[97] E. R. Westervelt, J. W. Grizzle, and D. E. Koditschek, "Hybrid zero dynamics of planar biped walkers," *IEEE Transactions on Automatic Control*, vol. 48, no. 1, pp. 42–56, 2003.

[98] E. Westervelt, J. Grizzle, C. Chevallereau, J. Choi, and B. Morris, *Feedback Control of Dynamic Bipedal Robot Locomotion*. CRC Press, 2007.

[99] P.-B. Wieber, R. Tedrake, and S. Kuindersma, "Modeling and control of legged systems," in *Springer Handbook of Robotics, 2nd Ed*, B. Siciliano and O. Khatib, Eds. Springer, 2016.

[100] M. Zamani, G. Pola, M. Mazo, and P. Tabuada, "Symbolic models for nonlinear control systems without stability assumptions," *IEEE Transactions on Automatic Control*, vol. 57, no. 7, pp. 1804–1809, 2012.